TITLE:

Studies on Physicochemical Properties of Porous Coordination Polymers(Dissertation_全文)

AUTHOR(S):

Bureekaew, Sareeya

CITATION:

Bureekaew, Sareeya. Studies on Physicochemical Properties of Porous Coordination Polymers. 京都大学, 2009, 博士(工学)

ISSUE DATE:

2009-11-24

URL:

https://doi.org/10.14989/doctor.k15007

RIGHT:

京都大学学術情報リポジトリ
KURENAI 紅
Kyoto University Research Information Repository

Studies on Physicochemical Properties of Porous Coordination Polymers

Sareeya Bureekaew

2009

Preface

The study presented in this thesis has been carried out under the direction of Professor Susumu Kitagawa during April 2006 – October 2009 at the Department of Synthetic Chemistry and Biological Chemistry, Graduate School of Engineering, Kyoto University.

The author is greatly indebted to Professor Susumu Kitagawa for his significant guidance, continuous encouragement, and valuable discussion. The author also wishes to express his sincere gratitude to Associate Professor Masaaki Ohba for his kind suggestion and discussion. The author is grateful to Research Associate Takashi Uemura, and Dr. Satoshi Horike for their hearty encouragements, and kind advices.

The author is thankful to Professor Motohiro Mizuno (Kanazawa University) and Professor Hiroshi Nakatsuji (Quantum Chemistry Research Institute), Professor Takashi Kawamura (Gifu University), Professor Masahiro Ehara (Insititute for Molecular Science) and Lecturer Jun-ya Hasegawa (Kyoto University) for their kind suggestions and helpful discussions.

The author expresses his gratitude to Association Professor Ho-Chol Chang (Hokkaido University), Associate Professor Ryotaro Matsuda (ERATO Kitagawa Integrated Pores Project), Associate Professor Shuhei Furukawa (ERATO Kitagawa Integrated Pores Project), Assistant Professor Sujit K. Ghosh (Indian Institute of Science Education and Research), Dr. Masakazu Higuchi (The University of Tokyo), Dr. Daisuke Tanaka (…..), Mr. Hirotoshi Sakamoto, Mr. Shinpei Hasegawa, Mr. Shinji Kato, Ms. Kana Kitagawa, Mr. Keiji for their informative discussion, and kind advice on the studies of porous coordination polymers.

The author is thankful to Ms. Hiroko Hirohata and Ms. Kiyo Yamashita for her secretarial works and warm encouragement. Acknowledgement is to all other members of the group of Professor Kitagawa for their hearty encouragements and friendship during his time in the laboratory.

The author is much indebted for the financial support of Research Fellowships of the Japan Society for the Promotion of Science for Young Scientists.

Sareeya Bureekaew

Department of Synthetic Chemistry and Biological Chemistry
Graduate School of Engineering, Kyoto University

March, 2009

Contents

General Introduction

Porous Coordination Polymers

Porous coordination polymers (PCPs), also known as metal-organic frameworks (MOFs),[1-7] are porous crystalline organic–inorganic hybrid–compounds, extending infinitely into one, two or three dimensions (1D, 2D or 3D, respectively). They are built up through metal-ligand coordination bonding or other weaker forces such as hydrogen bonds, π–π stacking or van der Waals interactions under the self-assembly processes, therefore the handling to get PCPs is usually simple. The metal cations have guided the direction of coordination geometries while the bridging organic ligands give the building components with variety of sizes and shapes. The ligands used in the construction of coordination polymers have to bridge between metal ions. This requires usually multidentate ligands with two or more donor atoms. Such bridging ligands are called di-, tri-, tetratopic depending on the number of donor atoms[8]. Thanks to the variety of combination between metal ions and organic ligands, the structure architectures and properties are possibly designed. The pore surface can be engineered by, for example, functionalization of the organic ligand, immobilization of the open metal sites. By carefully selecting the organic ligand one also aims to tune the physical properties and, thus, realize various applications, such as gas storage[9-11], catalysis,[12] , ion exchange[13], catalysis, separation[14-16], electrical conductivity, luminescence, magnetism, non-linear optics or zeolitic behavior.

Synthesis of PCPs

Usually, the structures of PCPs are obtained by characterization of single crystal. Thus, an improvement of synthesis is essential in order to get good quality enough for doing the X-ray measurement. To obtain the desired PCPs, metal ion and ligand, solvent, and counterions must be carefully considered. Rigid or semi-rigid ligands are usually used because the product complexes obtained from too much flexible ligands tend to be amorphous or low stability. Aromatic ligands are usually employed because an aromatic part is more rigid than aliphatic one. The PCPs are generally synthesized in the liquid phase by using solvent as a medium to induce the self assembly of a regular framework. Main synthetic methods of PCPs are shown below[17]. It is important to remember that several processes with the same starting materials lead sometimes to different products:

Saturated methods allow the crystal formation from a mixture of the different reagents. Molecular recognition permits the construction of products following pre-determined rules. This technique can carried out by *slow evaporation* of the mother liquor or *cooling* the of the mother liquor which is heated into increase the solubility.

Diffusion methods. The principle of this method is to slowly bring into contact the different species. The reactants are dissolved each separately in one of the two solutions. The separation between both solutions can be a solution layer and/or physical barriers. The reactant slowly diffuses into the separate layer and crystal growth occurs at the interface.

Hydro(solvo)thermal methods. The running temperature range is usually 100–260 °C

inside a closed space (autoclave) under autogenous pressure. This method can be a good alternative as solubility of starting materials can be increased.

One of key obstacles to overcome in the synthesis of nanoporous materials is

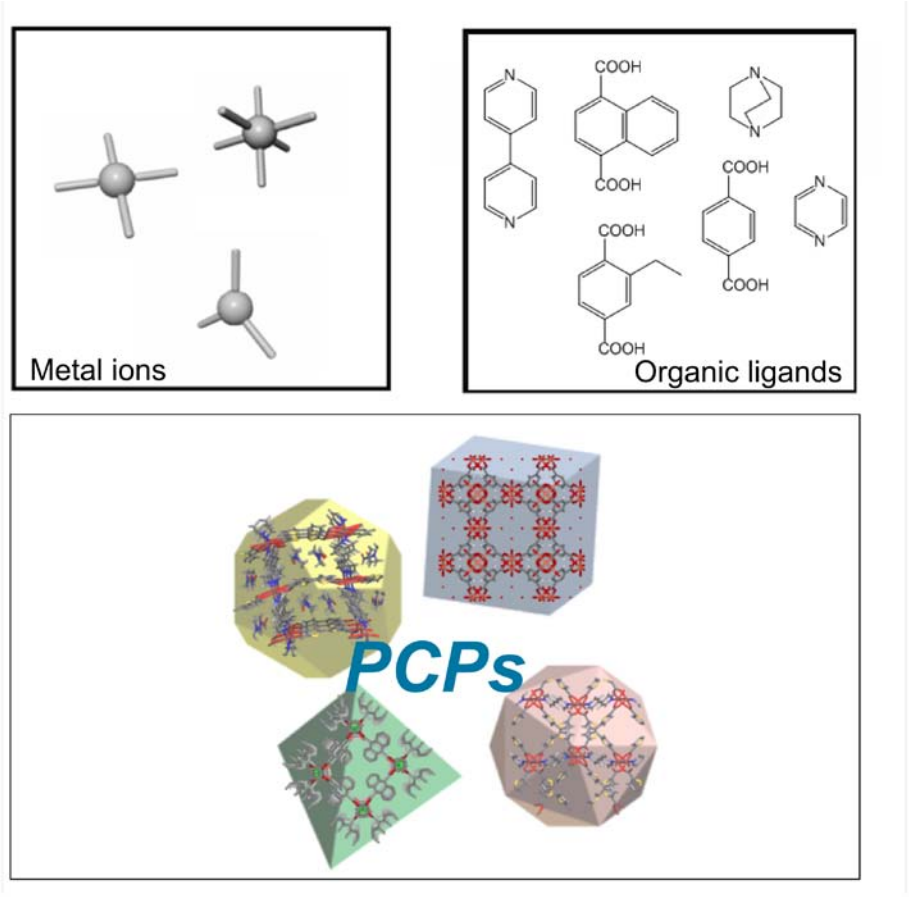

Figure 1. Schematic representation of crystalline porous coordination polymers (PCPs).

interpenetration because of the reduction of working space. However, the interpenetration of PCPs results in the higher stability compared with the non-interpenetrate isostructure. In this thesis, Chapter 2 describes how to take advantage from synthesis method to control the interpenetration, and consequently tuning of the physical characteristic such as flexibility, sorption property and stability.

Flexibility

Recently, the flexible PCPs have attracted the interest because these PCPs possibly undergo the spontaneous arrangement of structure into the appropriate spatial orientation responding to the external stimuli.[18-21] This would be a key principle for high selectivity recognition, accommodation, and separation of a target molecule. The structures of such crystalline frameworks might be rearranged by a balance of attractive and repulsive forces between host and guest.

The guest-responsive propertied of some flexible PCPs show unusual adsorption properties that are not observed in robust frameworks or other conventional porous solids due to the strong confinement effect for specific guest molecules by shrinking or expanding in different guest-inclusion states[21]. The flexibility is associated with (i) the flexible ligands used in the constructing of frameworks, (ii) the weaker interactions, including coordination bonds, H-bonds, π-electron stacking and van der Waals interactions. We can classify the dynamics of PCPs as show below.

1. Framework softness: Flexibility of bridging ligands and/or coordination geometry of metal ion

The organic ligands used in the construction of coordination polymers provide building components of various sizes and shapes. Use of flexible ligands[22, 23] should offer a greater degree of structural diversity, consequently flexible PCPs. This softness may come from the rotation, or expansion/contraction of ligand which might affect the pore shape/size (Figure 2). The flexibility is possibly from the metal ion part. Some PCPs, containing metal ions with versatile coordination geometry, undergo structural transformation corresponding to external stimuli.[24,25]

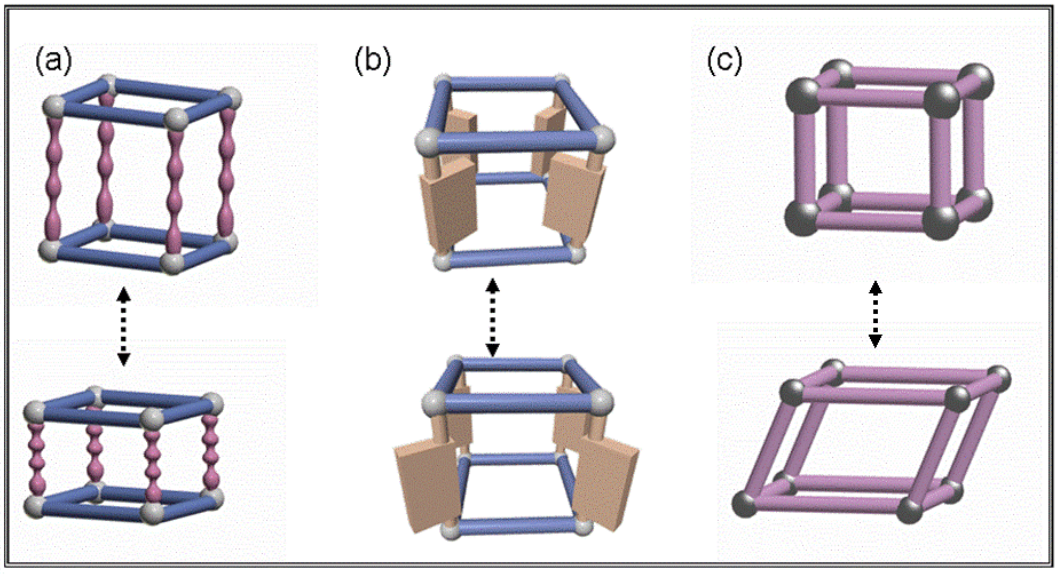

Figure 2. View of flexibility of PCPs induced by ligands (expansion/contraction (a) and rotation (b) of ligands) and metal clusters (c).

2. Slipping motion of framework

In the case of interpenetrated and interdigitated frameworks, even though the singular framework is rigid, the dynamics can arise from the slipping motion of the interpenetrated layers[24,26,27] (Figure 3). In this case, the interaction between frameworks, degree of interpenetration and their topology strongly affect the flexibility.

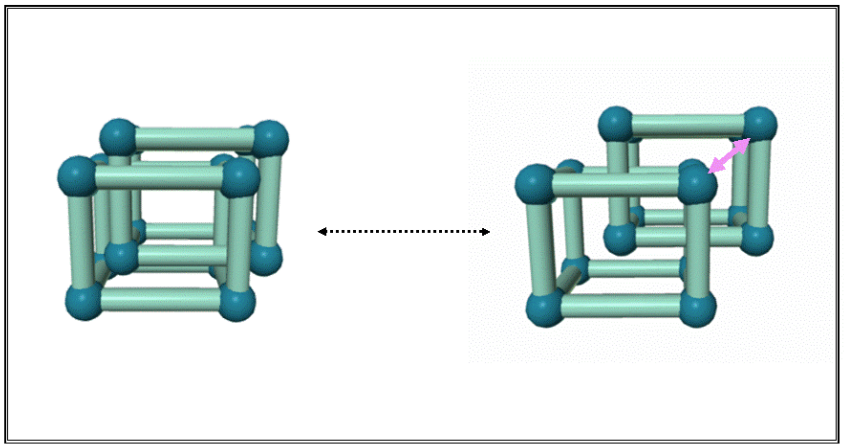

Figure 3. Mutual sliding of interpenetrating frameworks.

Nanospace and Properties

Porosity and high surface area (a few thousand $m^2\ g^{-1}$), flexibility, together with the rational synthesis are the merit of PCPs as the porous materials. In gas storage application, basically, PCPs with the large void volume and high surface area are the main target. However, an efficiency of some applications for instance, separation, the efficiency directly depends on the communication between host framework and guest molecules. Even in the case of no specific chemical interaction of host and guest, if the pore size and shape is fitted with guest molecules, the frameworks could control the nature of accommodated molecules. If the host-guest interaction can be tuned properly, the orientation or position of guests installed in nanochanel is controlled, and we can achieve the unusual property from them. For example, the oxygen molecules (O_2) with spin S = 1 adsorbed in CPL-1 form the 1D ladder array, and the unusual magnetic property of O_2 was observed in this case. An explosive acetylene gas (C_2H_2) can be safely stored in CPL-1, because it was stabilized by the basic oxygen sites in the host framework[28, 29].

The PCP frameworks probably function by themselves due to the using of reactive ligands metal clusters. Some PCPs, the frameworks themselves are functionless, but when hybrid with the active molecules as the guest, it is possible to observe the interesting properties. With the restricted space and host-guest interaction, the nanospace in PCPs might influence the unusual but valuable properties. For instance, the $[Mn_3\text{-}(HCOO)_6]$ presents the high dielectric constant after the accommodation of high dielectric constant water and methanol as the guest molecules[30].

Ionic conductivity

Ionic conductive solids or solid electrolytes have attracted particular interest such as batteries, fuel cell, electrochromic, chemical sensors (e.g., for H_2, O_2, NH_3, CO, CO_2, NO_x, SO_x, CH_4 , C_nH_{2n+2},etc.), and photogalvanic solar cells. According to the Nernst – Einstein law,[31]

$$\sigma = (DCe^2)/kT$$

The ionic conductivity (σ) is the product of carrier mobility (D) and their concentration (C), high concentration of ions and their mobility are needed to provide good proton conductivity. The second factor is determined by the nature of the mobile ion and the matrix of the compound in which the ion transport occurs. The progresses in the field of proton conductor modification are increasing carrier concentration and improvement the ion mobility in the matrix of a material.

Structural flexibility, void space and functional pore surface of porous coordination polymers might support the mobility of ionic species. However, it is difficult to load mobile ionic species in framework, because basically, ionic species are found in term of counter ions, therefore, it is difficult to separate the ion pairs due to strong columbic interaction. This problem might be resolved by tethering ionic species on dynamic ligands. Some porous coordination polymers provide rotation property[32, 33]. This dynamic property may act as one of driving force of ionic conduction. The second strategy is using guest molecules as mobile matrix in ion migration by taking advantages of porosity and guest accommodation property.

Thermal conductivity

Heat conduction in PCPs is one of important physical properties because in some applications, for instance, catalytic reaction, gas storage, thermal property directly affect the efficiency of PCPs. Even though PCPs are porous materials and constructed from weak interaction which cause PCPs are categorized in the low thermal conductive material[34-36]. Difference from dense crystalline solid, PCPs can show flexibility of structures as described before. Herein, the effect of rotation of bridging ligand on thermal conductivity is focused. Until now, crystal data and solid state NMR have been used for probing this rotational mode. However, after study the thermal conductivity, based on the assumption that the rotation of ligands decelerates heat transfer process, we might detect or investigate the rotation of ligands by checking thermal conductivity.

Computational chemistry

Because the interaction between host and guest is one of key role in some applications for instance the catalysis and separation, thus the design and selection of chemical component to construct PCPs which served the target properties have to be considered carefully. Recently, computational chemistry is rapidly applied in various chemistry fields. It focuses on solving chemically related problems (energy, structure, reaction path and properties) by calculation. This computational chemistry may help us to design the PCPs frameworks and interpret their properties.

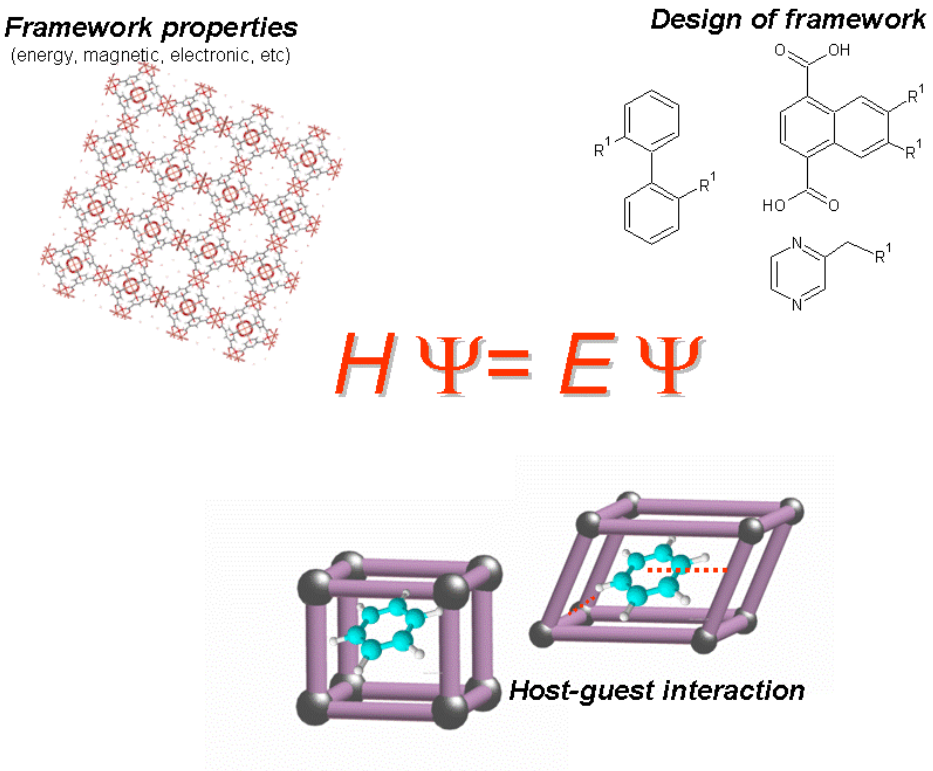

Figure 4. The uses of computational chemistry to investigate the properties if ligand, PCPs, and interaction between host and guest.

In Latin, *"ab Initio"* means "from the beginning"[37]. This name is given to computations which are derived directly from theoretical principles, with no inclusion of experimental data. Most of the time, this is refers to an approximate quantum mechanical calculation. We can calculate the molecular properties such as geometry, dipole moment, energy, spectroscopy, magnetism, electronic structure and so on. By taking advantage of this computational method, we can design what kind of ligand or metal ions we should use to achieve PCPs with target properties.

The good point of *ab initio* methods is that they eventually converge to the exact solution, once all of the approximations are made sufficiently small in magnitude[38]. The

electronic structure of an infinite crystalline PCP is defined by a band structure plot, which gives energies of electron orbitals. Since *ab initio* calculations yield orbital energies, they can be applied to band structure calculations. It is time consuming to calculate the energy for whole molecule. However, it is useful tool to predict or interpret the small fraction of PCPs. In this thesis, the low-cost computing Hartree-Fock (HF)[38-40] method was applied to calculate the hydrophilicity of aluminium PCPs in chapter 1, and the high accuracy SAC–CI (Symmetry Adapted Cluster–Configuration Interaction)[41 42] method was applied to calculated the electronic structures of small organic molecules in chapter 5.

Thesis outline

The outline of this thesis is as follows:

Chapter 1 explains the use of PCPs as host framework for creating the new hybrid materials with proton conductivity. Two aluminium frameworks $[Al(OH)(ndc)]_n$ (ndc = 1,4-naphthalenedicarboxylic acid) which has hydrophobic pore surface and $[Al(OH)(bdc)]_n$ (ndc = 1,4-benznedicarboxylic acid) which has hydrophilic pore surface were applied as host, while amphoteric imidazole was used as guest molecules. Basically, the dynamics of ionic carriers (imidazole) is an important factor in the proton transferring process. The interaction between aluminium frameworks and imidazole both of are different. The hydrophilic host decelerates the mobility of imidazole by trapping on its hydrophilic part; therefore it presents lower conductivity than hydrophobic system. The hydrophilicities of both host frameworks are also calculated by ab initio method. The dynamics of accommodated imidazole was investigated by solid state NMR.

Chapter 2 describes the synthesis and dynamic property of two isomeric interpenetrating PCPs, 2-fold and 3-fold. These two compounds can be selectively synthesized based on the template effect. According to the difference in degree of interpenetration, they show difference in the framework flexibility which confirmed by CO_2 sorption profile and in situ X-ray diffraction technique. The denser packing of frameworks of 3-fold interpenetrate compound does not present the structural transformation during the CO_2 sorption process, and the X-ray powder diffractions (XRPD) patterns during the sorption remain almost unchanged. On the other hand, the 2-fold interpenetration has

looser packing; therefore, the structural transformation potentially occurs. The hysteresis loop of CO_2 sorption profile and the change of XRPD patterns during sorption can be observed.

Chapter 3 describes about two isomorphous sponge-like flexible 3D porous frameworks providing the hydrophilic channel surface, by using a flexible ligand with the secondary functional group (C=O) were synthesized. The frameworks show size and affinity based selective sorption *via* dynamic structural transformation visualized by the single-crystal-to single-crystal structural analysis.

Chapter 4 explains the thermal conductivity of the 3D Cu^{II} frameworks, $[Cu_2(R)_2(dabco)]_n$ with variation of R ligands. In insulators, normally, heat transfers by the vibrational mode of the atomic lattices, so-called phonon. PCPs are categorized in materials with low thermal conductivity due to the low density. Theoretically, heat transferred by phonon can be decelerated by the lattice vibration-rotation interaction. Some of these Cu^{II} compound series, ligands L can rotate freely; therefore, the heat transfer in such PCPs is less than compound with non-rotating ligands. Based on this observation, the thermal conductivity is possibly use as the new indicator for the observation of ligand rotation or dynamics in PCPs

Four Chapters above described the synthesis and properties of PCPs in the experimental aspect. However, to achieve the PCPs with expected properties, we have to concern about the chemicals we use in the synthesis, such as; the organic ligands should provide the target properties. Moreover, the explanations of framework

properties, host-guest interaction, etc. are needed to fulfill our study. Theoretical calculation is one option to solve these problems. Chapter 5 describes the theoretical study of electronic structure of organic chromophore (lumiflavin), focused on electronic excited states by using ab initio method. This can be examples to explore the electronic properties of ligand, especially in the excited state which is probably useful in the design of PCPs which are active in electronic ground or/and excited states.

Chapter 5 describes the study of ground and excited (lowest singlet and triplet) states of flavin-related compound, lumiflavin by the symmetry-adapted cluster (SAC)-configuration interaction (CI) method. The structures of in first excited states (singlet; S1 and Triplet; T1) are also optimized by SAC-CI method and found that there is no significant change in the bond lengths. The electronic transition is mainly from bonding to non-bonding orbitals. The solvation effect on the absorption energy in aqueous solution was investigated using polarizable continuum model (PCM) and by including water molecules into the computational model.

References

[1] O. M. Yaghi, M. O'Keeffe, N. W. Ockwig, H. K. Chae, M. Eddaoudi, J. Kim, *Nature* **2003**, *423*, 705.

[2] S. Kitagawa, R. Kitaura, S.-i. Noro, *Angew. Chem., Int. Ed.* **2004**, *43*, 2334.

[3] G. Ferey, *Chem. Soc. Rev.* **2008**, *37*, 191.

[4] M. Eddaoudi, J. Kim, N. Rosi, D. Vodak, J. Wachter, M. O'Keeffe, O. M. Yaghi, *Science* **2002**, *295*, 469.

[5] K. Ariga, A. Vinu, J. P. Hill, T. Mori, *Coor. Chem. Rev.* **2007**, *251*, 2562.

[6] S. L. James, *Chem Soc Rev* **2003**, *32*, 276.

[7] U. Mueller, M. Schubert, F. Teich, H. Puetter, K. Schierle-Arndt, J. Pastre, *J. Mater. Chem.* **2006**, *16*, 626.

[8] C. Janiak, *Dalton. Trans.* **2003**, 2781.

[9] N. L. Rosi, J. Eckert, M. Eddaoudi, D. T. Vodak, J. Kim, M. O'Keeffe, O. M. Yaghi, *Science* **2003**, *300*, 1127.

[10] Y. S. Nechaev, O. K. Alexeeva, *Intl. J. Hydrogen Energy* **2003**, *28*, 1433.

[11] S. Ma, D. Sun, M. Ambrogio, J. A. Fillinger, S. Parkin, H.-C. Zhou, *J. Am. Chem. Soc.* **2007**, *129*, 1858.

[12] S. Hasegawa, S. Horike, R. Matsuda, S. Furukawa, K. Mochizuki, Y. Kinoshita, S. Kitagawa, *J. Am. Chem. Soc.* **2007**, *129*, 2607.

[13] K. S. Min, M. P. Suh, *J Am Chem Soc* **2000**, *122*, 6834.

[14] L. Pan, D. H. Olson, L. R. Ciemnolonski, R. Heddy, J. Li, *Angew. Chem., Int. Ed.* **2006**, *45*, 616.

[15] S. Horike, D. Tanaka, K. Nakagawa, S. Kitagawa, *Chem. Commun.* **2007**, 3395.

[16] K. Uemura, S. Kitagawa, M. Kondo, K. Fukui, R. Kitaura, H.-C. Chang, T.

Mizutani, *Chem. Euro. J.* **2002**, *8*, 3586.

[17] A. Y. Robin, K. M. Fromm, *Coord. Chem. Rev.* **2006**, *250*, 2127.

[18] K. Barthelet, J. Marrot, D. Riou, G. Férey, *Angew. Chem. Int. Ed.* **2002**, *41*, 281.

[19] E. J. Cussen, J. B. Claridge, M. J. Rosseinsky, C. J. Kepert, *J. Am. Chem. Soc.* **2002**, *124*, 9574.

[20] D. N. Dybtsev, H. Chun, K. Kim, *Angew. Chem. Inter. Ed.* **2004**, *43*, 5033.

[21] A. J. Fletcher, E. J. Cussen, D. Bradshaw, M. J. Rosseinsky, K. M. Thomas, *J. Am. Chem. Soc.* **2004**, *126*, 9750.

[22] S. M. Hawxwell, G. M. Espallargas, D. Bradshaw, M. J. Rosseinsky, T. J. Prior, A. J. Florence, J. v. d. Streek, L. Brammer, *Chem. Commun.* **2007**, 1532.

[23] P. Horcajada, C. Serre, G. Maurin, N. A. Ramsahye, F. Balas, M. Vallet-Regi, M. Sebban, F. Taulelle, G. Ferey, *J. Am. Chem. Soc.* **2008**, *130*, 6774.

[24] S. Kitagawa, K. Uemura, *Chem. Soc. Rev.* **2005**, *34*, 109.

[25] R. Matsuda, R. Kitaura, S. Kitagawa, Y. Kubota, T. C. Kobayashi, S. Horike, M. Takata, *J. Am. Chem. Soc.* **2004**, *126*, 14063.

[26] J. L. Rowsell, O. M. Yaghi, *Angew. Chem. Int. Ed. Engl* **2005**, *44*, 4670.

[27] K. Seki, *Phys. Chem. Chem. Phys.* **2002**, *4*, 1968.

[28] A. Matsuo, T. C. Kobayashi, M. Suzuki, K. Kindo, R. Kitaura, R. Matsuda, H. C. Chang, S. Kitagawa, *J. Magnetism Magnetic Mater.* **2004**, *272-276*, E643.

[29] R. Kitaura, S. Kitagawa, Y. Kubota, T. C. Kobayashi, K. Kindo, Y. Mita, A. Matsuo, M. Kobayashi, H.-C. Chang, T. C. Ozawa, M. Suzuki, M. Sakata, M. Takata, *Science* **2002**, *298*, 2358.

[30] C. Heng-Bo, T. Kazuyuki, O. Yoshinori, K. Hayao, W. Zheming, K. Akiko, *Angew. Chem. Inter. Ed.* **2005**, *44*, 6508.

[31] C. Kittel, *Introduction to Solid State Physics* Wiley, **1995**.

[32] K. Yamada, S. Yagishita, H. Tanaka, K. Tohyama, K. Adachi, S. Kaizaki, H. Kumagai, K. Inoue, R. Kitaura, H. C. Chang, S. Kitagawa, S. Kawata, *Chem. Eur. J.* **2004**, *10*, 2647.

[33] T. Yamada, M. Sadakiyo, H. Kitagawa, *J. Am. Chem. Soc.* **2009**, *131*, 3144.

[34] B. L. Huang, A. J. H. McGaughey, M. Kaviany, *Int. J. Heat Mass Transfer* **2007**, *50*, 393.

[35] B. L. Huang, Z. Ni, A. Millward, A. J. H. McGaughey, C. Uher, M. Kaviany, O. Yaghi, *Int. J. Heat Mass Transfer* **2007**, *50*, 405.

[36] T. M. Tritt, *Thermal Conductivity: Theory, Properties, and Applications* Springer, **2005**.

[37] H. F. Schaefer, *Quantum Chemistry: The Development of Ab Initio Methods in Molecular Electronic Structure Theory*, Dover Publications, **2004**.

[38] F. Jensen, *Introduction to Computational Chemistry* John Wiley & Sons, **1998**.

[39] A. Leach, 2 ed., Prentice Hall, **2001**.

[40] A. Szabo, N. S. Ostlund, *Modern Quantum Chemistry: Introduction to Advanced Electronic Structure Theory* Dover Publications, **1996**.

[41] N. Nakatsuji, *Chem. Phys. Letter.* **1978**, *59*, 362.

[42] H. Nakatsuji, *Chem. Phys. Letter.* **1979**, *67*, 334.

Chapter 1

One-Dimensional Imidazole Aggregate in Aluminum Porous Coordination Polymers with High Proton Conductivity

ABSTRACT: A new approach to prepare anhydrous proton−conducting materials is proposed. Imidazole molecules isolated in nanochannels of porous coordination polymers behave as good proton carriers. Spectroscopic studies showed that the mechanism of conductance is closely related to the pore environment and guest properties.

Introduction

Anhydrous proton–conducting solids that are able to operate at high temperature (~120 °C) are required in fuel cell technology.[1,2] Heterocyclic organic molecules such as imidazole or benzyl imidazole have attracted considerable attention for this purpose because they are nonvolatile molecules with high boiling points, and they can exist in two tautomeric forms with respect to a proton that moves between the two nitrogen atoms, which supports a proton transport pathway.[3,4] The protonic defect may cause local disorder by forming protonated and unprotonated imidazoles. In such materials the proton transport may occur through structure diffusion which involves proton transfer between the imidazole and the imidazolium ion through the hydrogen–bonded chain, including the molecular reorientation process for subsequent intermolecular proton transfer.[1] Theoretically, the magnitude of the ionic conductivity is given as

$$\sigma(T) = \sum n_i q_i \mu_i \qquad (1)$$

where n_i is the number of carriers, and q_i and μ_i are the charge and mobility of the carriers, respectively.[5] Both a large amount and a high mobility of ion carriers are required to provide good proton conductivity. Hence it is important to find suitable materials that meet these requirements. For instance, solid imidazole has a low conductivity (~10^{-8} S cm^{-1}) at ambient temperature[6] although the imidazole density (n_i) is adequately high. This is because the dense packing of imidazole, with strong hydrogen bonding in the solid state, decreases the mobility of each molecule (μ_i).

The main goal of proton conductor modification should therefore be an improvement of the mobility of proton carriers. It is known that local and translational motion of proton carriers strongly affect the proton transfer rate.[1] In order to control the mobility of proton carriers, additional support matrices such as flexible organic

polymers or high-porosity solids that afford movable space for a carrier are considered promising.

Porous coordination polymers (PCPs) or metal organic frameworks constructed from transition metal ions and organic ligands have received much attention over the past few years because of their promising applications, such as in gas storage,[7-11] separation,[12-17] catalysis,[18-26] and conductivity.[27,28] Recent developments in approaches to combine PCP frameworks and functional guests such as polymers,[29,30] metals,[22,31-33] or small organic molecules[34-36] on a molecular scale have prompted us to create hybrid materials with novel performance based on the feature that crystalline nanochannels can afford a unique assembly field for functional guests with specific host–guest interactions. The guests in the nanospace of PCPs exhibit unusual behavior compared to in the bulk phase because each manner of assembly is heavily dependent on the nature of the PCP channels, such as their size, shape and chemical environment. Hence, we propose the use of PCPs for incorporation with proton carrier molecules because they can contribute to provide desirable working space for carrier molecules, with high mobility, and show an appropriate packing structure, for improved proton conductivities at high temperatures and under anhydrous conditions (Scheme 1).

In this study we focused on two types of PCPs with 1D channels and high thermal stability (~400 °C), and imidazole as the guest proton carrier molecule. Taking the size and shape of imidazole (4.3 × 3.7 $Å^2$) into consideration, we chose to use the aluminum compounds $[Al(\mu_2\text{-OH})(1,4\text{-ndc})]_n$ (**1**; 1,4-ndc = 1,4-naphthalenedicarboxylate)[37] and $[Al(\mu_2\text{-OH})(1,4\text{-bdc})]_n$ (**2**; 1,4-bdc = 1,4-benzenedicarboxylate),[9,38] both of which have pore dimensions of ca. 8 Å, but different pore shapes and surface potential, and installed imidazole in each host material. We found that the nanochannels potentiated the

different packing of imidazole, compared with the bulk solid imidazole. Conductivity measurements for each of the PCP–imidazole composites at various temperatures and under anhydrous condition presented different profiles because of the different characteristics of the channels of the respective PCPs, resulting in different host–guest interactions, and **1**⊃Im had a conductivity of 2.2×10^{-5} S cm^{-1} at 120 °C. We investigated the behavior of absorbed imidazole in the micropores by means of the solid-state NMR technique, and succeeded in determining a good correlation between the features of the host channels, guest mobility and proton conductivity.

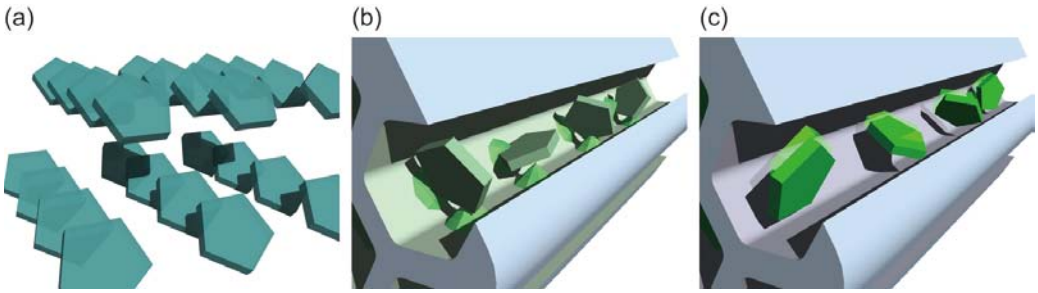

Scheme 1. Imidazole molecules are densely packed with low mobility that adversely affects proton transport process. This occurs in the bulk solid (a). Imidazole accommodated in nanochannel containing the active site with a high affinity to imidazole. The strong host–guest interaction retards the mobility of

Results and discussion

Structural information of 1 and 2

The structures of **1** and **2** comprise an infinite number of chains of corner–sharing $AlO_4(\mu_2\text{-}OH)_2$ interconnected by the dicarboxylate ligand, resulting in a 3D framework containing 1D channels. The guest–free structures of **1** and **2** are shown in Figure 1. Crystallographic structures show that the pore surfaces of **1** and **2** are composed of hydrophobic (aromatic naphthalene and benzene ring) and hydrophilic ($AlO_4(\mu_2\text{-}OH)_2$) parts. The principal difference between the two aluminum frameworks arises from the difference in ligands 1,4-ndc and 1,4-bdc. Because of asymmetric bridging ligand, **1** consists of two kinds of rectangular channels with dimensions of 7.7 × 7.7 $Å^2$ and 3.0 × 3.0 $Å^2$ running along the *c* axis (Figure 2a). This compound shows the property of a rigid framework. Figure 1b shows that steric hindrance arising from the bulky naphthalene ring of the 1,4-ndc ligand of **1** induces restriction of interaction between the polar guest molecule and μ_2-OH and/or carboxylate group of the framework. Because of the absence of an accessible hydrophilic pore surface the hydrophobic character from the aromatic part of the naphthalene ring of the ligand is dominant. In other words, **1** provides two types of microchannels with hydrophobic pore surfaces.

In the case of **2** the framework exhibits only 1D diamond–shaped channels composed of the smaller benzene moieties of 1,4-bdc, with dimensions 8.5 × 8.5 $Å^2$, running along the *a* axis. Eventually, the polar sites on the surface are exposed to guest molecules, which enhances guest–induced structural transformation of **2,** with the aid of the interaction between the imidazoles and μ_2-OH and/or a carboxylate groups.[39] Thus, it is intriguing that a simple modification on the organic moiety produces channels with

different nature, hydrophobic and hydrophilic for **1** and **2,** respectively. [38]

Hydrophillicity

The hydrophilicity of both **1** and **2** were calculated by ab initio calculation method. The structures of all calculations are taken from crystal data with the optimization of only position of hydrogen atoms. The hydrophilicity can be determined by calculating the stabilization energy of water accommodated system. Because the calculation of the whole periodic system takes enormous amount of computer times, memory, and disk space, only small fraction of the system is chosen and water molecule are far apart because of the bulky of naphthalene ligand. The distance between O_{water} and O_{OH} is ca 5.1 Å. From the calculation using HF with 3-21G basis set, the hydrated state is less stable than degassed state with the energy of 49.4 kJ/mol, indicative of the hydrophobic **1**. In contrast, the interaction between 2 and water takes place easily. The distance between O_{water} and O_{OH} is ca 2.7 Å. The stabilization energy of hydration of **2** is -54.7 kJ/mol, confirmed the hydrophilic characteristic of **2**.

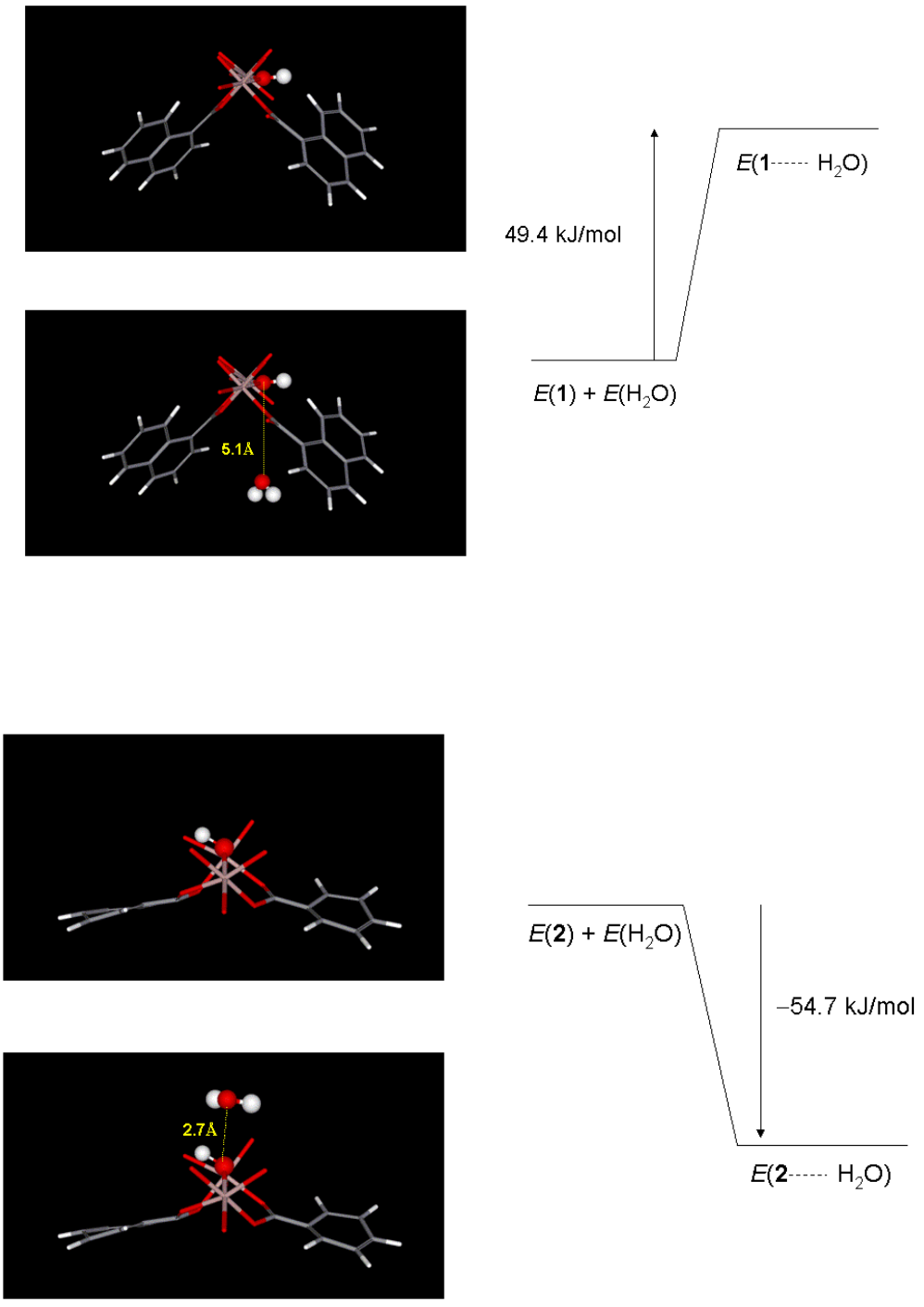

Figure 1. Models for study of hydrophilic properties of 1 and 2 calculated by HF method using 3-21G basis functions.

Properties of the inclusion compounds

The thermogravimetric (TG) profiles of **1**⊃Im and **2**⊃Im are shown in Figure 3. Note that**1**⊃Im and **2**⊃Im indicate the imidazole hybrid compound of **1** and **2**, respectively. The existence of imidazole in **1** and **2** was confirmed by thermogravimetry/mass spectrometry (TG–MS). The TG profile of **1**⊃Im shows 14% weight imidazole loading or 0.6 imidazole/1 Al ion. The release of accommodated imidazole commences at 160 °C and completes at 225 °C. In

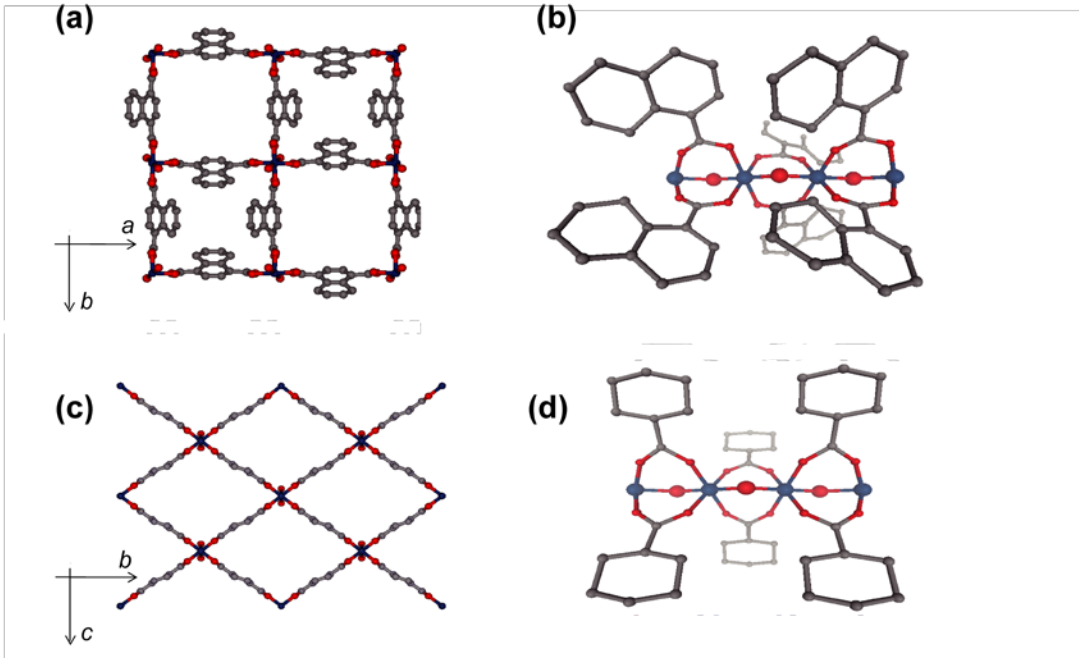

Figure 2. 3D structures of **1** (a) and **2** (c). Al, C, and O are represented in blue, gray, and red, respectively. H atoms are omitted for clarification. (b) and (d) show comparison of ligand size effect on μ_2-OH group of **1** and **2** respectively.

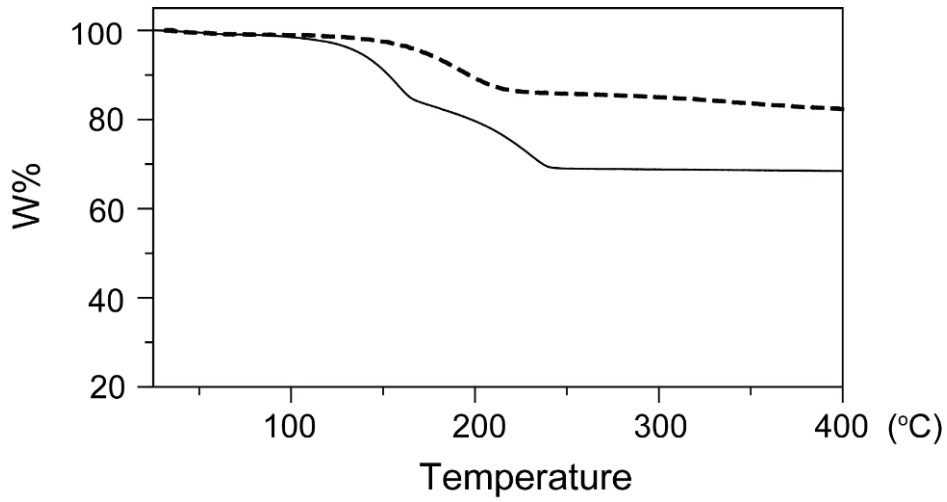

Figure 3. TGA curves for **1**⊃Im (dash line) and **2**⊃Im (solid line) over the temperature range from 25 – 400 ^{o}C at heating rate 10 ^{o}C min^{-1} under N_2 atmosphere. The guest release of **1**⊃Im occurs in one single step that clues the homogeneous installation of imidazole in **1**, whereas of **2**⊃Im occurs in two steps, indicating two types of imidazole (strongly and weakly interacts with **2**).

the case of **2,** the loaded imidazole amounts to 30% weight or 1.3 imidazole/1 Al ion, which is twice as much as in **1**. The TG curve shows that the loss of imidazole molecules in **2**⊃Im occurs in two steps: in the first step, the release of imidazole commences at 130 °C and is completed by approximately 160 °C and in the second step it commences at 160 °C and is completed by 240 °C. The percentage imidazole loss is half the amount of the imidazole, followed by the residual in the second step.

The one single step mass loss in **1**⊃Im is indicative of uniformly accommodated imidazole molecules. On the other hand, based on the TG curve of **2**⊃Im, there are two types of imidazole molecules installed in the channel. According to the amphiphilic nature of the surface of the channel, the imidazoles with strong interaction with the

hydrophilic sites of a μ_2-OH or a carboxylate group are released at higher temperature (160 – 240 °C), correlated to the weight loss in second step, whereas the imidazoles which have less interaction with pore surface are removed in the first step (below 160 °C).

The crystal structures of **1** and **2** (Figure 2) reveal the following. Compound **1** consists of two types of 1D channels, namely small channels with dimensions 3.0 × 3.0 $Å^2$ in which imidazole is unable to be installed: only large channels with dimensions of 7.7 × 7.7 $Å^2$ can install the guest. Compared with **2**⊃Im, half the amount of accommodating imidazole per one Al is reasonable from crystal structures.

Considering that the dispersion of imidazole is uniform in the crystalline channel we could calculate the density of imidazole in the larger channels of **1** (443 $Å^3$) and channels of **2** (750 $Å^3$). This was calculated from the void space of the guest–free state by using the PLATON software package.[40] The values were about 0.15 and 0.19 g cm^{-3}, respectively. However, as the structure of **2** changes after accommodation of imidazole and it is difficult to determine the density of imidazole in **2**⊃Im. The density of imidazoles in **1**⊃Im and **2**⊃Im are much smaller than that of solid bulk imidazole, which is 1.23 g cm^{-3} at ambient temperature.[41] This evidence indicates that the behaviors of imidazoles loaded to the framework considerably differ from bulk imidazole resulting from the space effect.

The X–ray powder diffraction (XRPD) patterns shown in Figure 3 show that the diffraction pattern of **1**⊃Im is the same as that of apohost **1**, corresponding to the robustness of **1**. Conversely, the peak positions and pattern of **2**⊃Im are different from those of apohost **2** and the shrinkage after installation of imidazole is observed. This is

because of strong interaction between the polar imidazole and hydrophilic pore surface of flexible **2**.

Conductivity of 1⊃Im and 2⊃Im

We aimed to achieve proton conductivity at temperatures around 100 °C, and hence to design composites that are stable at the target temperatures. We already confirmed that the prepared composites **1**⊃Im and **2**⊃Im are stable up to 130 °C without any loss from TG. Conductivities of **1**⊃Im and **2**⊃Im were measured by AC impedance spectroscopy, which is a versatile electrochemical tool to characterize intrinsic electrical properties of materials. Figure 4 shows Nyquist plots (Z' versus Z'') of the complex impedance measured on **1**⊃Im and **2**⊃Im under a nitrogen atmosphere at 120 °C.

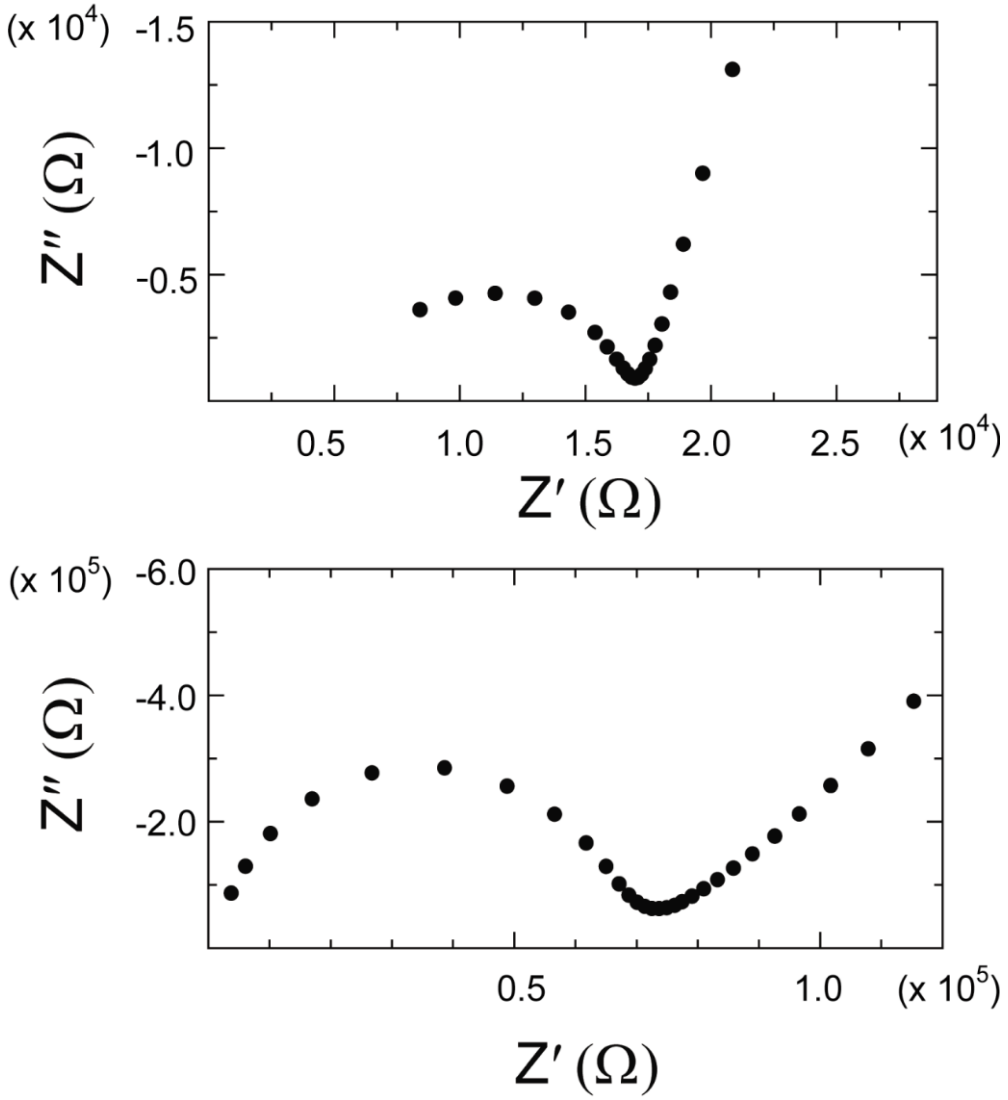

Figure 4. Nyquist diagrams of **1**⊃Im (above) and **2**⊃Im (below) at temperature of 120 ^{o}C.

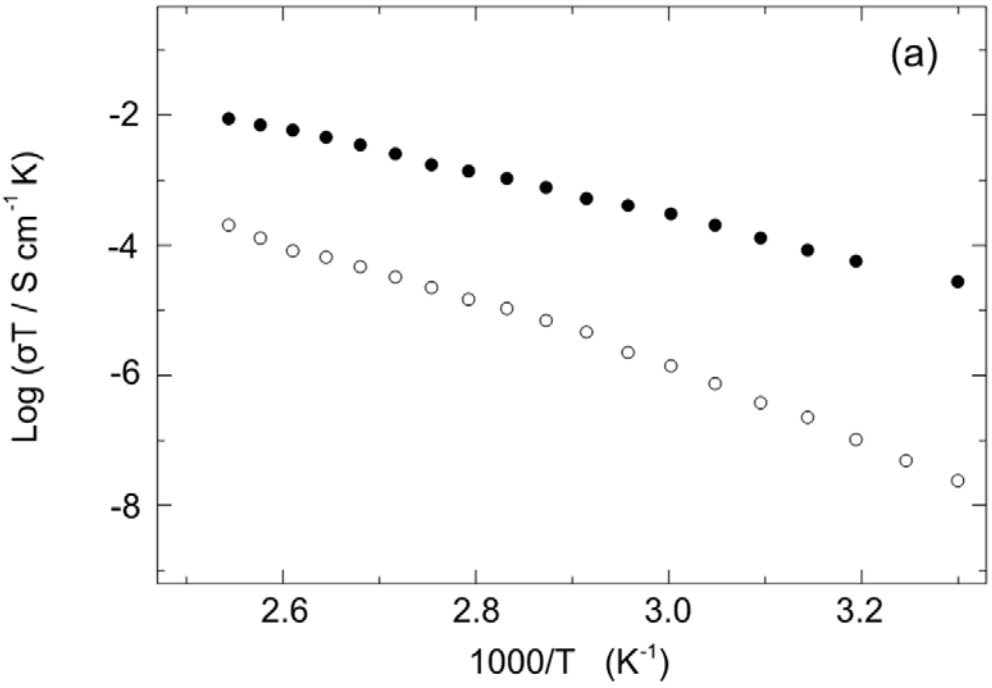

Figure 5. Proton conductivity of **1**⊃Im (filled dots), and **2**⊃Im (empty dots) under anhydrous condition performed by A.C. impedance analyzer.

The impedance plots of the two complexes are typical of materials with predominant ionic conductivity. They show one semicircle with a characteristic spur at low frequencies, which indicates blocking of H^+ ions at the gold electrodes. The magnitude of Z' decreased with an increase in temperature. The conductivity of the samples was calculated from the impedance value using the following equation

$$\sigma = \frac{L}{Z \cdot A} \tag{2}$$

where σ is the conductivity (S cm^{-1}), L is the measured sample thickness (cm), A is the electrode area (cm^2) and Z is the impedance (Ω).

The temperature dependence of proton conductivities of **1**⊃Im and **2**⊃Im, measured under anhydrous conditions at temperatures ranging from 25 to 120 °C, are shown in Figure 5. Guest–free **1** exhibits a conductivity less than 10^{-11} S cm^{-1}, which is indicative of negligible proton conductivity for this apohost framework. An increase in conductivity could not be observed even at high temperature. After installation of imidazole the proton conductivity of **1**⊃Im is 5.5×10^{-8} S cm^{-1} at room temperature. Although the mole fraction of imidazole in **1**⊃Im is much smaller than that of bulk imidazole, the proton conductivity of **1**⊃Im is of the same order as that of solid bulk imidazole. This is possibly because of the effect of the nanospace on the dynamic motion of imidazole. The proton conductivity of **1**⊃Im improves significantly as the temperature increases: at 120 °C the proton conductivity reaches 2.2×10^{-5} S cm^{-1}. Note that bulk imidazole at this temperature is no longer in the solid phase. This increase in the temperature dependent conductivity of **1**⊃Im, compared with the conductivity profile of apohost **1**, indicates that a significant improvement in the conductivity arises directly from the accommodated imidazole. Furthermore, the conductivity of **1**⊃Im continuously increases with an increase in temperature. This result indicates that phase transition does not take place. The mobile imidazole induces high temperature (> 100 °C) proton conductivity in **1**⊃Im. We can improve the mobility of imidazole by taking advantage of the isolating effect of PCPs.

In order to improve proton conductivity we increased the amount of loaded imidazole (the number of charge carriers, n_i) by using **2**, which has twice the amount of accessible space for imidazole as the supporting framework. However, the proton conductivity of **2**⊃Im at ambient temperature is about 10^{-10} S cm^{-1}, which is lower than that of **1**⊃Im. As in the case of **1**⊃Im, the conductivity of **2**⊃Im increases as the

temperature increases, and it reaches 1.0 × 10^{-7} S cm^{-1} at 120 °C. The proton conductivity of **2**⊃Im is about two orders of magnitude lower than that of **1**⊃Im, although the amount of loaded imidazole is higher than that of **1**⊃Im. This is also possibly because of the difference in dynamic motion of the guest, which is based on the interaction between guest and host. Microchannels in compound **1** have nonpolar potential surface and polar imidazole does not interact strongly with the host framework; therefore, it can move freely in this channel. Nonetheless, in the case of polar surface microchannels in **2**, the half amount of imidazole interact strongly with the hydrophilic sites of host framework. The strong host–guest interactions give rise to the shrinkage of the framework, eventually of a unit cell, resulting in the different environment of imidazole accommodated in **2**, compared to in **1**. Therefore, because of strong host–guest interaction and dense packing, the imidazoles with strong interaction with the μ_2-OH and/or carboxylate group of **2** are not allowed to move or rotate freely in the framework. Consequently, the conductivity in **1**⊃Im is larger than in **2**⊃Im.

Direct observation of dynamics of imidazoles in 1⊃Im and in 2⊃Im

Solid-state ^{2}H NMR spectroscopy is suitable for examining the dynamics of target molecules selectively.[42-44] We therefore used this analytical technique to determine the mobility and its correlation with the conductivity of adsorbed imidazole in **1** and **2.** The ^{2}H NMR powder line shapes are sensitive to motion and are characterized in terms of both the time scale and the mode of the motion.[45,46] We introduced imidazole-d_4 for each host instead of nondeuterated imidazole and checked that the adsorbed amount for each guest was identical to that in the normal hosts. The ^{2}H NMR spectra of **1**⊃Im and **2**⊃Im recorded at different temperatures are shown in Figure 7. In the case of **2**⊃Im, at the lowest measured temperature of 20 °C, we observed a clear Pake-type doublet

pattern with a splitting width of 120 kHz, indicating that the adsorbed imidazole-d_4 behave totally anisotropically and does not show any effective mobility in the ^{2}H NMR spectrum time scale. As the temperature increases, a narrow Lorentzian-type peak appears in the middle of the anisotropic powder pattern, corresponding to the emergence of isotropic imidazole by thermal activation. There are two possible explanations for the spectrum: the first is that free motional imidazole with low frequency shows a narrow peak and the second is the simultaneous coexistence of frequencies of slow and fast imidazole. Nonetheless, the spectrum at 40 °C indicates the existence of activated guests in pores, and the relative intensity of the activated species increases as the temperature increases to 80 °C.

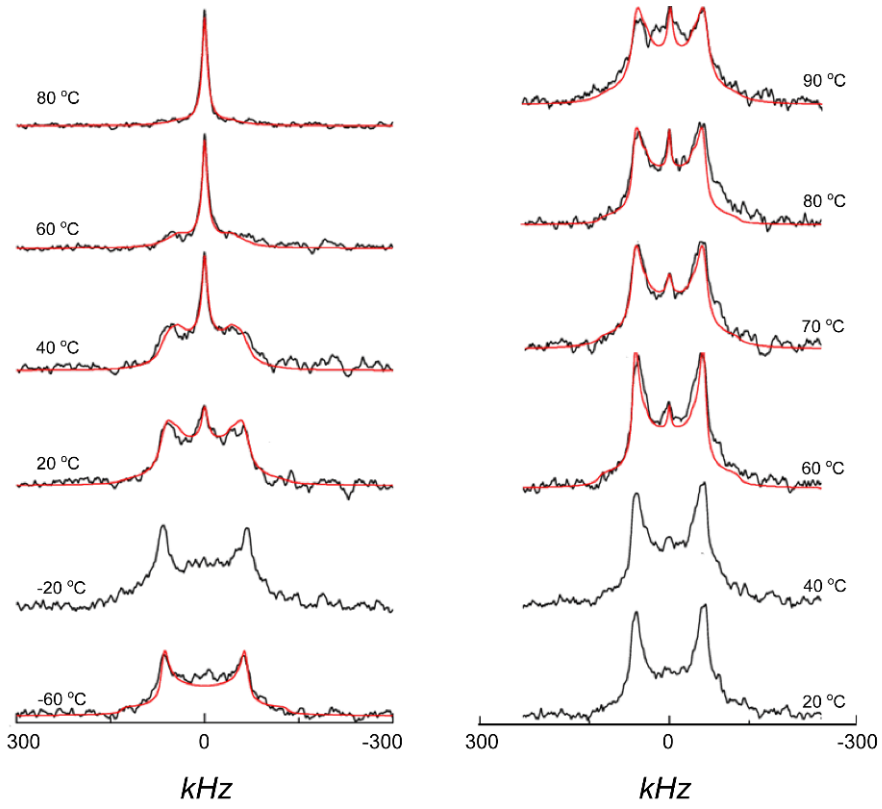

Figure 6. ^{2}H solid state NMR spectra of **1**⊃Im-d_4 (left) and **2**⊃Im-d_4 (right). The simulation results are shown in red lines.

Although it is difficult to assign a suitable motional model for the adsorbed imidazole, we tried to simulate the ^{2}H NMR spectra with a free rotation model (tetrahedral orientation model), using the assumption that all adsorbed imidazole shows uniform activation. As shown in Figure S1, we obtained simulated patterns from 60 to 90 °C and determined the activation energy for modeled motion to be 19 (±0.19) kJ mol^{-1}. In the case of **1**⊃Im, spectra also show doublet powder patterns at low temperatures (–20 and –60 °C) with the same splitting width as in **2**⊃Im at temperatures lower than 30 °C. However, a narrow Lorentzian-type peak starts to appear at 20 °C. This clearly indicates that at ambient temperature the imidazole in **1** can show isotropic

motion with a larger frequency than **2**. The fraction of isotropic imidazole becomes dominant at 40 °C, and at 80 °C we can no longer observe any Pake-doublet pattern at all. This suggests that all adsorbed imidazole within the pores of **1** has a fast isotropic motion. By applying the tetrahedral orientation model, we simulated the powder patterns for each temperature. We succeeded in obtaining theoretical patterns from 20 to 80 °C, as shown in Figure 6, and calculated the activation energy to be 16 (±0.16) kJ mol^{-1}, which is lower than in the case of **2**. Consequently, we are able to conclude that the degree of motional behavior of the accommodated imidazole of **1** is greater than in the case of **2**, which is consistent with the results of conductivity. Conductivities of both compounds **1** and **2** continuously increase linearly as a function of temperature, and **1**⊃Im shows higher conductivity than **2**⊃Im in all temperature ranges studied.

We have presented a new approach to create proton transportation space based on the use of proton carrier organic molecules to enhance the proton conductivity of solid materials under anhydrous conditions at high temperature. The different values of conductivity of imidazole in compounds **1** and **2** are consistent with the dynamic properties of imidazole adsorbed in the pores. The hydrophilic microporous surface of **2** results in strong interaction with even the half amount the adsorbed imidazoles and significantly decelerates their mobility, resulting in a poor proton transfer rate. On the other hand, because of the hydrophobic and flat pore surface of **1**, adsorbed imidazole can move more freely than in **2** and than bulk phase, and we eventually observe higher proton conductivity, which is comparable to that of a conventional organic polymer conductor such as poly(4-vinylimidazole).[47] PCP can provide an appropriate pore environment and size for target proton carrier by the fine–tuning of their components. In the other word, the optimum mobility and density of proton carriers can be reached by

taking advantage of the designability of PCPs. The strategy would be considered significant to prepare hybrid materials high proton–conductive.

Experimental section

Materials

Aluminium(III) nitrate nanohydrate $Al(NO_3)_3 \cdot 9H_2O$ (WAKO, 99.9%); terephthalic acid $HO_2C–(C_6H_4)–CO_2H$ (WAKO, 95%); 1,4-naphthalene dicarboxylic acid $HO_2C–(C_{10}H_8)–CO_2H$ (WAKO, 95%); imidazole (WAKO, 99%) and imidazole (D–4, CIL, 98%) were used as received. Distilled water was used.

Synthesis of {Al(μ_2-OH)(1,4-ndc)}$_n$ (1)

A mixture of $Al(NO_3)_3 \cdot 9H_2O$ (0.375 g, 1.0 mmol); 1,4-naphthalene dicarboxylic acid (0.108 g, 0.5 mmol) and deionized water (10 mL) was placed in a 23 mL Teflon autoclave and heated at 180 °C for one day. The initial pH of the reaction mixture was 2.5 and the final pH was 2.0. After filtering and washing the crude product with distilled water, a pure, light-yellow powder of **1**·$2H_2O$ was obtained (yield 80%). The sample was evacuated at 150 °C for 12 hours to afford the guest-free compound **1**.

Synthesis of {Al(μ_2-OH)(1,4-bdc)}$_n$ (2)

The synthesis of **2** was carried out under hydrothermal conditions using $Al(NO_3)_3 \cdot 9H_2O$ (1.30 g, 3.5 mmol); 1,4-benzenedicarboxylic acid (0.288 g, 2.5 mmol) and distilled water (10 mL). The reaction was performed in a 23 mL Teflon autoclave. The reaction mixture was heated at 220 °C for three days. After filtering and washing with distilled water, a white powder was obtained. It was identified by powder X-ray diffraction analysis. The excess terephthalic acid in the pores was removed by high-temperature treatment at 330 °C for three days. X-ray powder diffraction (XRPD) analysis revealed that the material was the guest-free compound **2**.

Preparation of imidazole-loaded frameworks

Products **1** and **2** were again degassed by heating to 120 °C under reduced pressure

for 12 h to remove guest molecules. Imidazole was vaporized into guest-free **1** and **2** at 120 °C, overnight, to yield **1**⊃Imi and **2**⊃Imi. XRPD patterns of both these compounds confirmed that the frameworks were maintained. The amount of loaded imidazole was determined by TG analysis.

Proton conductivity measurement of 1⊃Im and 2⊃Im

Samples for conductivity measurements were prepared by sandwiching the respective powders **1**⊃Im and **2**⊃Im between two gold-coating electrodes (diameter 3 mm) and then tightly connecting the two electrodes, by means of springs, to ensure good contact between the sample and each electrode. Temperature-dependent conductivities of **1**⊃Im and **2**⊃Im were determined using alternative current (AC) impedance spectroscopy (Solartron SI 1260 Impedance/Gain-Phase analyzer), using a homemade cell over the frequency range 1 Hz – 10 MHz and with an input voltage amplitude of 100 mV. The measurement cell was filled with nitrogen at atmospheric pressure prior to recording the measurements. ZView software was utilized to extrapolate impedance data results via equivalent circuit simulation to complete the Nyquist plot and obtain the resistance values.

^{2}H solid-state NMR

Solid-state ^{2}H NMR spectra were recorded using a Varian Chemagnetics CMX-300 spectrometer, at 45.826 MHz, and a quadrupole echo pulse sequence. Simulated spectra were produced with FORTRAN programs written by us.

References

[1] Kreuer, K. D., Paddison, S. J., Spohr, E. and Schuster, M., Transport in Proton Conductors for Fuel-Cell Applications: Simulations, Elementary Reactions, and Phenomenology. *Chem. Rev.* **2004**, *104*, 4637.

[2] Martin F.H. Schuster and Meyer, W. H., Anhydrous Proton Conducting Polymers. *Annu. Rev. Mater. Res.* **2003**, *33*, 233.

[3] Jannasch, P., Recent developments in high-temperature proton conducting polymer electrolyte membranes. *Curr. Opin. Colloid Interface Sci.* **2003**, *8*, 96.

[4] Li, S. et al., Synthesis and properties of imidazole-grafted hybrid inorganic-organic polymer membranes. *Electrochim. Acta* **2006**, *51*, 1351.

[5] West, A. R., *Basic Solid State Chemistry*. (Wiley, 1999).

[6] Kawada, A., McGhie, A. R. and Labes, M. M., Protonic Conductivity in Imidazole Single Crystal. *J. Chem. Phys.* **1970**, *52*, 3121.

[7] Noro, S., Kitagawa, S., Kondo, M. and Seki, K., A New, Methane Adsorbent, Porous Coordination Polymer. *Angew. Chem. Int. Ed.* **2000**, *39*, 2081.

[8] Rowsell, J. L. and Yaghi, O. M., Strategies for hydrogen storage in metal-organic frameworks. *Angew. Chem. Int. Ed.* 2005, *44*, 4670.

[9] Ferey, G. et al., Hydrogen adsorption in the nanoporous metal-benzenedicarboxylate $M(OH)(O_2C\text{-}C_6H_4\text{-}CO_2)$($M = Al^{3+}$, Cr^{3+}), MIL-53. *Chem. Commun.* **2003**, 2976.

[10] Rosi, N. L.et al., Hydrogen Storage in Microporous Metal-Organic Frameworks. *Science* **2003**, *300*, 1127.

[11] Li, H., Eddaoudi, M., O'Keeffe, M. and Yaghi, O. M., Design and synthesis of an exceptionally stable and highly porous metal-organic framework. *Nature* **1999**

402, 276.

[12] Cychosz, K. A., Wong-Foy, A. G. and Matzger, A. J., Liquid Phase Adsorption by Microporous Coordination Polymers: Removal of Organosulfur Compounds. *J. Am. Chem. Soc.* **2008**, *130*, 6938.

[13] Finsy, V.et al., Pore-Filling-Dependent Selectivity Effects in the Vapor-Phase Separation of Xylene Isomers on the Metal-Organic Framework MIL-47. *J. Am. Chem. Soc.* **2008**, *130*, 7110.

[14] Bradshaw, D.et al., Permanent Microporosity and Enantioselective Sorption in a Chiral Open Framework. *J. Am. Chem. Soc.* **2004**, *126*, 6106.

[15] Dybtsev, D. N.et al., Microporous Manganese Formate: A Simple Metal-Organic Porous Material with High Framework Stability and Highly Selective Gas Sorption Properties. *J. Am. Chem. Soc.* **2004**, *126*, 32.

[16] Min, K. S. and Suh, M. P., Self-Assembly and Selective Guest Binding of Three-Dimensional Open-Framework Solids from a Macrocyclic Complex as a Trifunctional Metal Building Block. *Chem. Eur. J.* **2001**, *7*, 303.

[17] Wang, B.et al., Colossal cages in zeolitic imidazolate frameworks as selective carbon dioxide reservoirs. *Nature* **2008**, *207*, 453.

[18] Hasegawa, S.et al., Three-Dimensional Porous Coordination Polymer Functionalized with Amide Groups Based on Tridentate Ligand: Selective Sorption and Catalysis. *J. Am. Chem. Soc.* **2007**, *129*, 2607.

[19] Horike, S., Dinca, M., Tamaki, K. and Long, J. R., Size-Selective Lewis Acid Catalysis in a Microporous Metal-Organic Framework with Exposed Mn2+ Coordination Sites. *J. Am. Chem. Soc.* **2008**, *130*, 5854.

[20] Cho, S.-H.et al., A metal-organic framework material that functions as an

enantioselective catalyst for olefin epoxidation. *Chem. Commun.* **2006**, 2563.

[21] Horcajada, P.et al., Synthesis and catalytic properties of MIL-100(Fe), an iron(III) carboxylate with large pores. *Chem. Commun.* **2007**, 2820.

[22] Schroder, F.et al., Ruthenium Nanoparticles inside Porous $[Zn_4O(bdc)_3]$ by Hydrogenolysis of Adsorbed [Ru(cod)(cot)]: A Solid-State Reference System for Surfactant-Stabilized Ruthenium Colloids. *J. Am. Chem. Soc.* **2008**, 130, 6119.

[23] Ingleson, M. J.et al., Generation of a solid Bronsted acid site in a chiral framework. *Chem. Commun.* **2008**, 1287.

[24] Fujita, M., Kwon, Y. J., Washizu, S. and Ogura, K., Preparation, Clathration Ability, and Catalysis of a Two-Dimensional Square Network Material Composed of Cadmium(II) and 4,4'-Bipyridine. *J. Am. Chem. Soc.* **1994** *116*, 1151.

[25] Seo, J. S.et al., A homochiral metal-organic porous material for enantioselective separation and catalysis. *Nature* **2000**, *404*, 982.

[26] Evans, O. R., Ngo, H. L. and Lin, W., Chiral Porous Solids Based on Lamellar Lanthanide Phosphonates. *J. Am. Chem. Soc.* **2001**, *123*, 10395.

[27] Nagao, Y.et al., Preparation and proton transport property of N,N'-diethyldithiooxamidatocopper coordination polymer. *Synth. Met.* **2005**, *154*, 89.

[28] Ferey, G.et al., Mixed-Valence Li/Fe-Based Metal-Organic Frameworks with Both Reversible Redox and Sorption Properties13. *Angew. Chem. Int. Ed.* **2007**, 46, 3259.

[29] Uemura, T.et al., Radical polymerisation of styrene in porous coordination polymers. *Chem. Commun.* **2005**, 5968.

[30] Uemura, T.et al., Conformation and Molecular Dynamics of Single Polystyrene

Chain Confined in Coordination Nanospace. *J. Am. Chem. Soc.* **2008**, 130, 6781.

[31] Mulfort, K. L. and Hupp, J. T., Chemical Reduction of Metal-Organic Framework Materials as a Method to Enhance Gas Uptake and Binding. *J. Am. Chem. Soc.* **2007**, *129*, 9604.

[32] Muller, M.et al., Loading of MOF-5 with Cu and ZnO nanoparticles by gas-phase infiltration with organometallic precursors: Properties of Cu/ZnO@MOF-5 as catalyst for methanol synthesis. *Chem. Mater.* **2008**, *20*, 4576.

[33] Turner, S.et al., Direct Imaging of Loaded Metal-Organic Framework Materials (Metal@MOF-5). *Chem. Mater.* **2008,** *20*, 5622.

[34] Horcajada, P.et al., Flexible Porous Metal-Organic Frameworks for a Controlled Drug Delivery. *J. Am. Chem. Soc.* **2008,** *130*, 6774.

[35] Horcajada, P.et al., Metal-Organic Frameworks as Efficient Materials for Drug Delivery. *Angew. Chem. Int. Ed.* **2006**, *45*, 5974.

[36] Tanaka, D.et al., Anthracene array-type porous coordination polymer with host-guest charge transfer interactions in excited states. *Chem. Commun.* **2007**, 3142.

[37] Comotti, A.et al., Nanochannels of Two Distinct Cross-Sections in a Porous Al-Based Coordination Polymer. *J. Am. Chem. Soc.* **2008**.

[38] Loiseau, T.et al., A Rationale for the Large Breathing of the Porous Aluminum Terephthalate (MIL-53) Upon Hydration. *Chem. Eur. J.* **2004,** *10*, 1373.

[39] Serre, C.et al., An Explanation for the Very Large Breathing Effect of a Metal-Organic Framework during CO2 Adsorption. *Adv. Mater.* **2007**, 19, 2246 .

[40] Spek, A. L., Foundations of Crystallography. *Acta Crystallogr., Sect. A* **1990**,

A46, c34.

[41] Craven, B. M., McMullan, R. K., Bell, J. D. and Freeman, H. C., The crystal structure of imidazole by neutron diffraction at 20 oCand -150 oC. *Acta Crystallogr., Sect. B* **1977**, *33*, 2585.

[42] Horike, S.et al., Motion of methanol adsorbed in porous coordination polymer with paramagnetic metal ions. *Chem. Commun.* **2004**, 2152.

[43] Ueda, T.et al., Phase transition and molecular motion of cyclohexane confined in metal-organic framework, IRMOF-1, as studied by 2H NMR. *Chem. Phys. Lett.* **2007**, *443*, 293.

[44] Horike, S.et al., Dynamic Motion of Building Blocks in Porous Coordination Polymers13. *Angew. Chem. Int. Ed.* **2006**, *45*, 7226.

[45] Schmidt-Rohr, K. and Spiess, H. W., *Multidimensional Solid-State NMR and Polymers*. (Academic Press, London, 1994).

[46] Abragam, A., *Principles of Nuclear Magnetism* (Oxford University Press, Oxford, 1961).

[47] Bozkurt, A. and Meyer, W. H., Proton conducting blends of poly(4-vinylimidazole) with phosphoricacid. *Solid State Ionics* **2001** *138*, 259.

Chapter 2

Control of Interpenetration for Tuning Structural Dynamics Impacted on Sorption Property.

ABSTRACT: Based on the effect of solvent, the self-assembly of ZnII with 2,2'-bithiophene-5,5'-dicarboxylic acid and 4,4´-bipyridine produces the two different 3D porous coordination polymers with two-fold and three-fold interpenetrating, and consequently a control of porosity. On account of loose entanglement of two-fold interpenetrate compound, dynamics of framework could be observed

Introduction

Porous coordination polymers (PCPs)[1-6] have been developed to provide the nanometer-sized coordination space which is potentially applicable in gas storage[7-17], heterogeneous catalysis[18-21], and separation[22-27]. The synthesis of PCPs has been

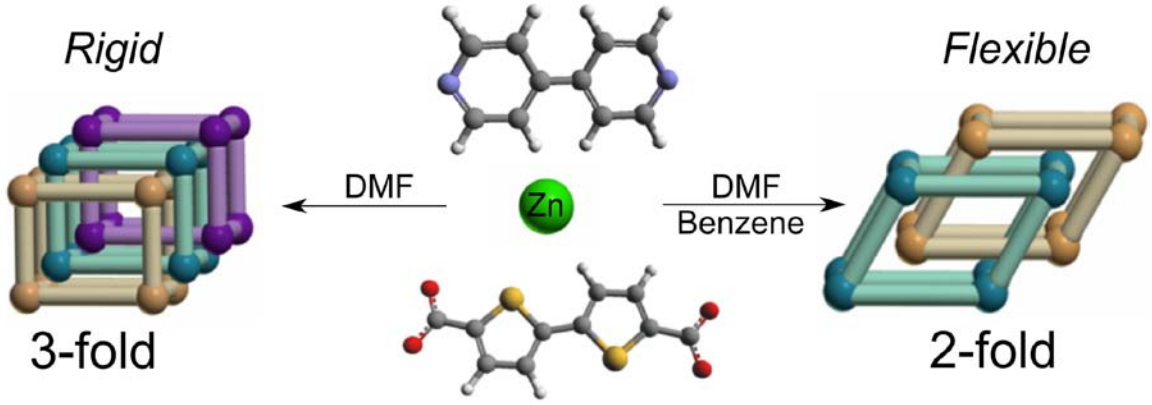

Scheme 1. Control of degree of interpenetration by using solvent molecule as template.

particularly profitable in terms of designability, because in principle we can design the structures and properties of these coordination networks which are obtained by the assembling of metal ions and bridging ligands. Interpenetration of frameworks in PCPs[28] has been seen as an undesirable feature due to a reduction of the working void volume. However, recent reports have demonstrated that interpenetrated frameworks can show improved gas uptake in PCPs thanks to an increase of internal surface area and/or pore space[29]. Moreover, observed structural transformations responding to a critical amount or specific characteristic of the accommodated guest molecules provide excellent case studies for the investigation of the dynamics of PCPs[30, 31]. Dynamical effects can arise either locally from flexible ligands or/and the flexibility of the coordination geometry of the metal ions[32-34], or from the global cooperative movement of the framework on a

periodic scale, such as the sliding of interpenetrated networks for example[35]. These two effects can occur simultaneously and contribute to one another. Usually, the thermal stability of flexible structures is less than that of rigid structures in single network; however, this problem can be overcome by the use of interpenetration. Indeed, as well as improving stability and rigidity, interpenatration does not impair on the flexible properties of the single network. Therefore, the control over the interpenatration degree in PCPs is of utmost importance. Recent synthetic reports have shown that can be achieved by liquid-phase epitaxial growth[36], using solvent molecules as template[37-39], or by changing the concentration of reagents[40].

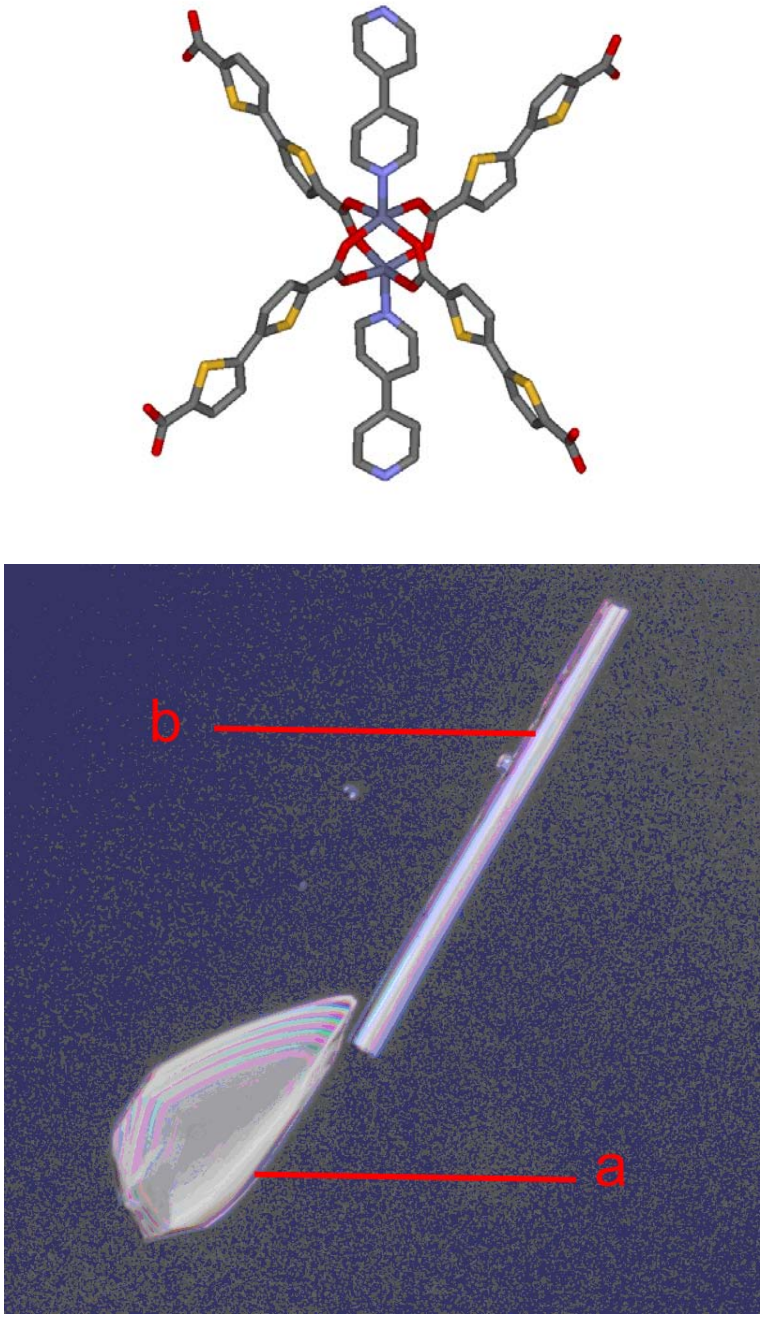

Figure 1. Upper: coordination environment of **1** and **2.** Zn, C, N, O and S atoms are shown as dark gray, gray, blue, red, and yellow, and H atoms are omitted. Lower: crystal images of **1** (a) and **2** (b).

Results and discussion

Crystal data reveal that asymmetric units of both are $[Zn_2(btdc)_2(bpy)]$ which is composed of two Zn atoms, two deprotonated btdc ligands, and one bpy. The btdc ligands are connected by paddle-wheel like $Zn_2(COO)_4$ building units, forming the distorted square-grid like 2D layers. The sulfur atoms of bithiophene unit point *trans* to each other. These 2D layers are further pillared by the bpy ligands, occupying the axial sites of Zn paddle-wheel to form 3D frameworks (Figure 2). Due to the extensive disorder, neither dmf nor benzene as the solvent molecules could not be located.

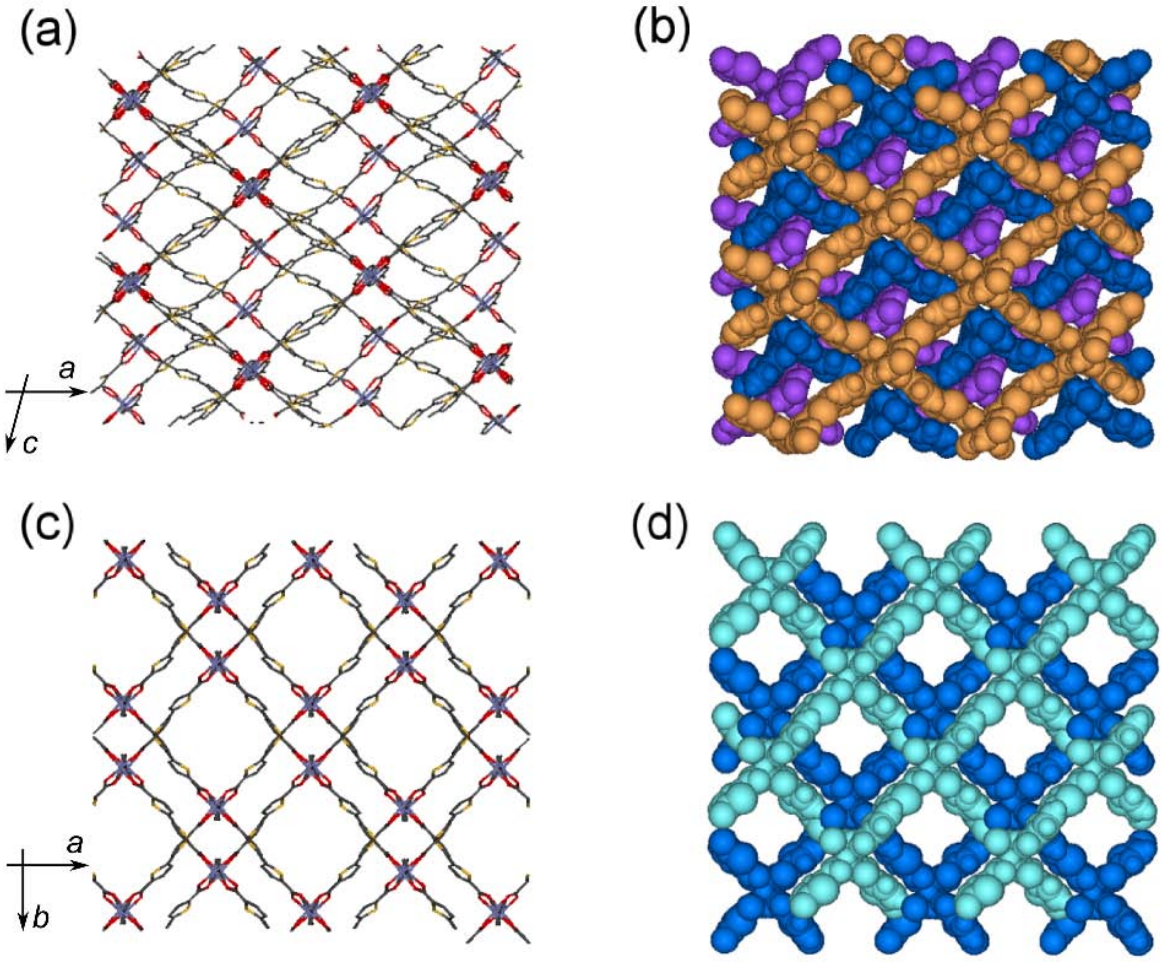

Figure 2. Crystal structures of **1** (and b) and **2** (c and d) viewing of 2D grid networks of $[Zn(btdc)]_n$ with 3-fold and 2-fold interpenetrating fashions, respectively.

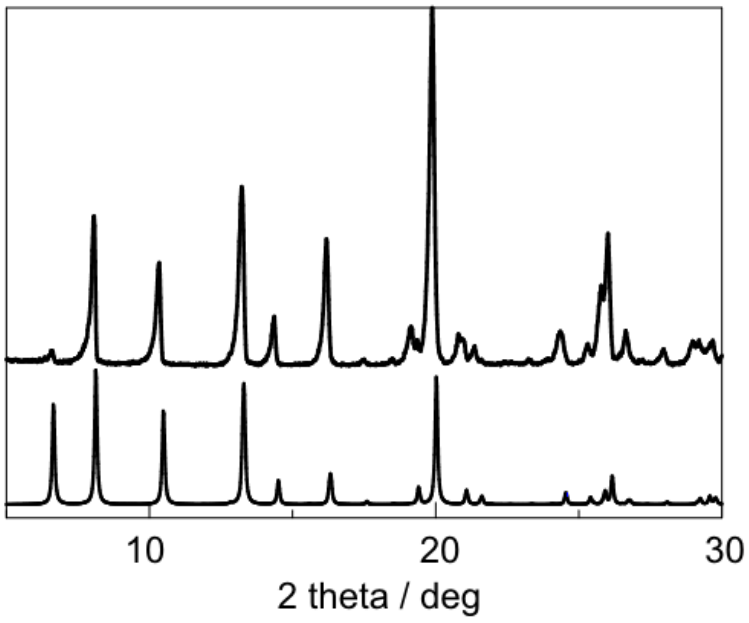

Figure 3. XRPD pattern of simulated **1** (upper) and as-synthesized **1** (lower)

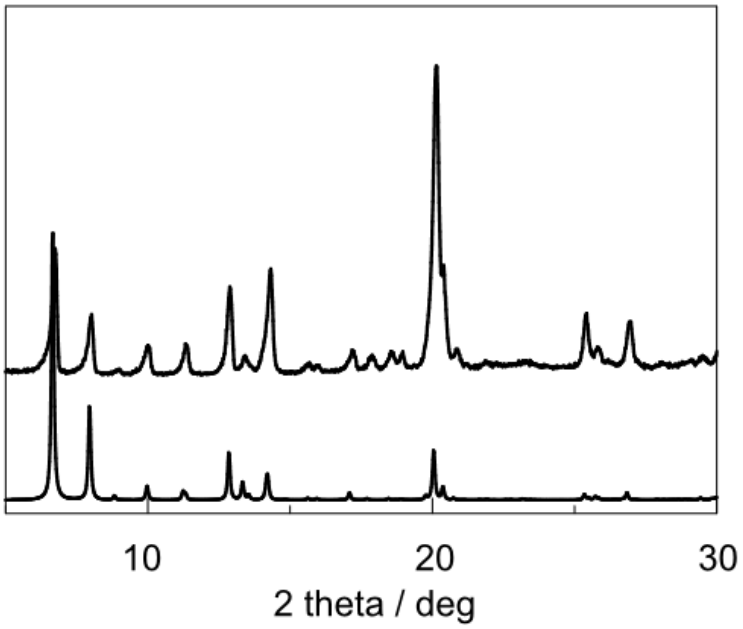

Figure 4. XRPD pattern of simulated **2** (upper) and as-synthesized **2** (lower)

Based on the crystallographic data and the van der Waals radii of atoms, the apohost **1** provides 1D channels with dimension of 3.8 × 3.8 $Å^2$ and 6.3× 6.3 $Å^2$ for apohost **2**, viewing along the *c* axis. The total potential solvent-accessible volume of the unit cell of **1** is 601 (17.1%) and of **2** is 2323.6 $Å^3$ (47.2%), calculated using the PLATON program. From a topological point of view, the conventional interpenetration of **1** is originated by the translation along the *c* axis which is not found in **2**. The interpenetration of **2** is explained by the symmetry element of space group.

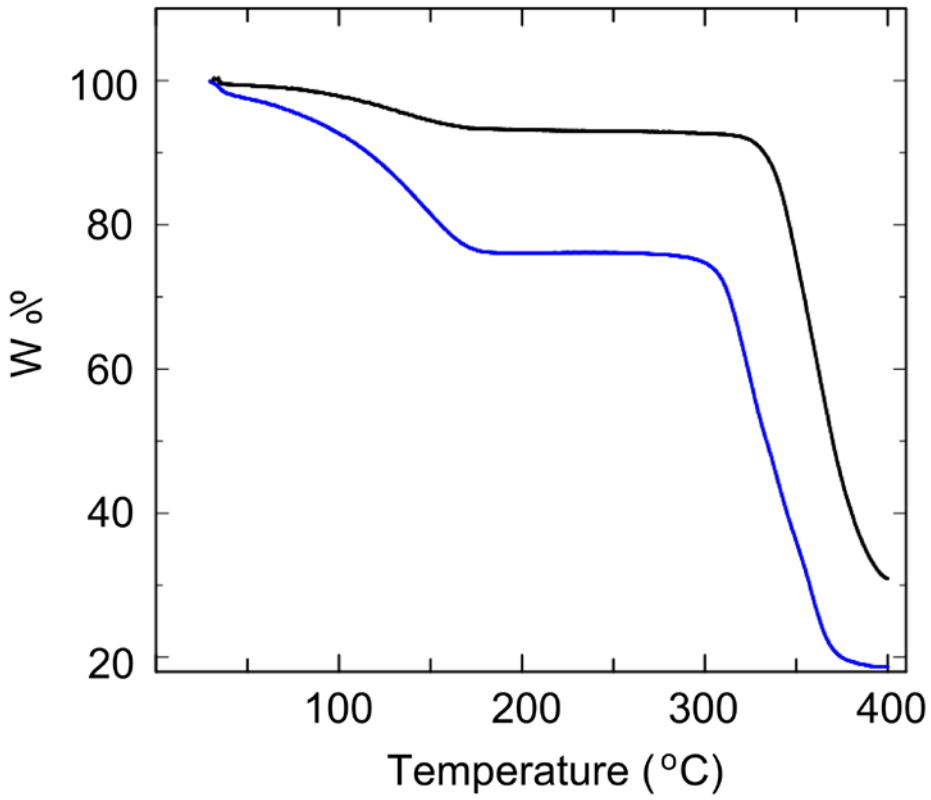

Figure 5. TGA profiles of as-synthesized **1**·*x*G (blue) and **2**·*y*G (black).

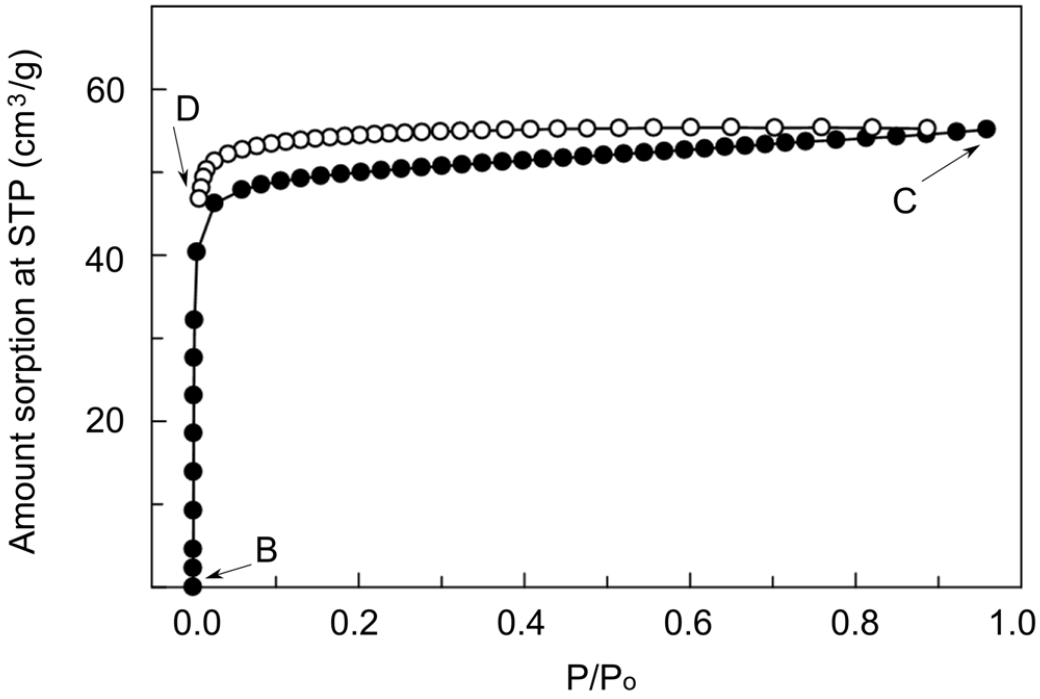

Figure 6. CO_2 adsorption (filled dots) and desorption (empty dots) profiles of **1** at 195 K.

The thermal stability of both compounds was examined by thermogravimetric analysis (TGA). 7% weight loss is observed in **1**·*x*S between room temperature to 170 °C and TGA profile platures until 330 °C, where **1** collapses (Figure 5). The TGA data of **2**·*y*S show a lose of solvent between 25 to 170 °C by 23%. As we expected, two-fold interpenetrated **2** has higher void volume than three-fold interpenetrated **1**. The guest-free framework **2** is stable until 270 °C, lower than **1**. This confirms the effect of interpenetration on the thermal stability of PCPs.

To explore the porosity and dynamics of both compounds, the CO_2 sorption properties on **1** and **2** at –78 ^{o}C (195 K) were investigated and we found that two compound showed contrasting sorption behaviours. Sorption isotherm (Figure 6), **1** with more densely packing exhibits the typical type I sorption behaviour. As defined by the

IUPAC classification, type I is indicative of a typical physisorption process of a microporous compound. To obtain batter understanding of the dynamics of this framework, the XRPD patterns were also measured during the sorption process. From XRPD patterns (Figure 7), roughly, the peaks patterns are almost unchanged. Only some peaks are slightly shifted and the intensities of some of the corresponding peaks are different. The main structure still maintains as it is. The difference in intensities is ascribed to the change caused by guest accommodation. The saturation adsorbed amount of CO_2 is ca. 55 $cm^3(STP)g^{-1}$, corresponds to one CO_2 per unit formula.

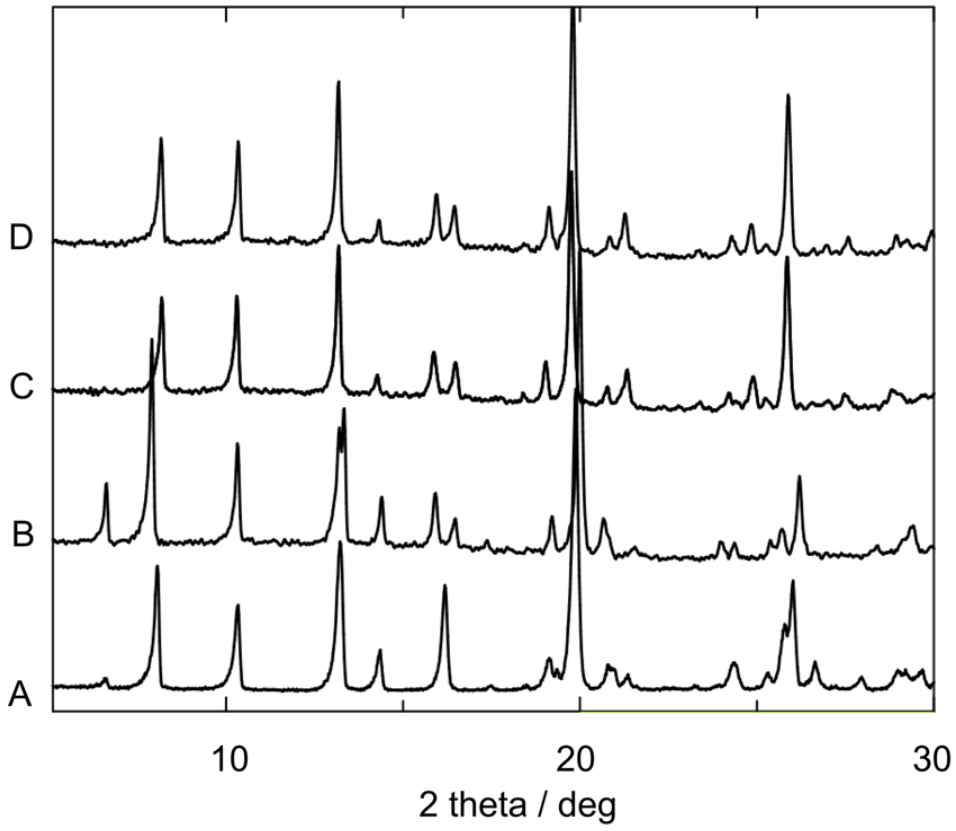

Figure 7. Pattern A is as-synthesized 1 measured at ambient temperature. The others are patterns of **1** at various pressure measured during sorption process.

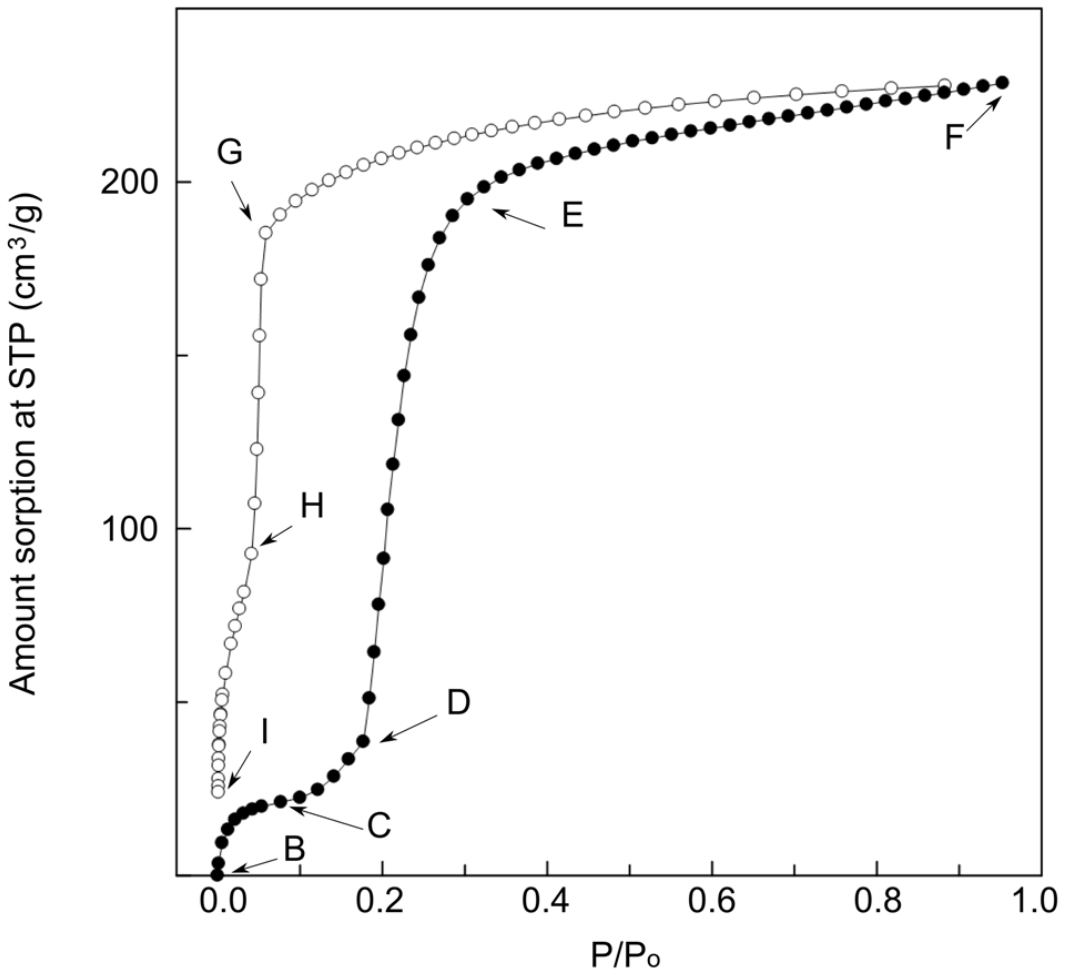

Figure 8. CO_2 adsorption (filled dots) and desorption (empty dots) profiles of **2** at 195 K.

On the other hand, owing to the lower degree of interpenetration and the absence of specific interactions between the two interpenetrated frameworks, **2** is expected to posses the dynamic feature involving framework transformations (sliding motion and/or shrinkage-expansion). To elucidate the structural change, the structure of guest free **2** is necessary. Unfortunately, after the degassing process, the crystals lost the crystallinity, they were not suitable for singly crystal analysis. However, flexibility of **2** can be clearly established. The structure of **2** changes significantly at lower temperature as shown by

Table 1. Summary of crystalographic data and refinement parameters for 2•xS

	2•*x*S	**2**•4(CO_2)
Crystal system	*monoclinic*	*monoclinic*
Space group	*C*2/*c*	*C*2/*c*
a (Å)	20.472(10)	19.3958(16)
b (Å)	19.400(8)	20.4502(17)
c (Å)	13.944(7)	13.8925(6)
β (°)	117.185(5)	116.697(5)
V (Å^3)	4926.21	4922.9(9)

XRPD pattern in Figure 9, pattern A (as-synthesized **2**·*y*S at ambient temperature) and pattern B (apohost **2** at 195 K) are different. Moreover, the step and hysteresis which are normally found in the flexible structure can be observed in the CO_2 sorption isotherm (Figure 8). The amount of adsorbed CO_2 at first uptake, point C (ca. 20 $cm^3(STP)g^{-1}$), is less than that of **1** which must serve lower void volume than **2** due to the crystallographic darta, implying the shrinkage of apohost **2** at low temperature (195 K). From point C to D, the amount of adsorbed CO_2 gradually increases, and according to XRPD pattern, framework **2** steadily expands because of the increase of relative pressure. The CO_2 uptake at $P/P_0 = 0.2$ increases abruptly and the saturation adsorbed amount of CO_2 (point F) is ca. 228 $cm^3(STP)g^{-1}$, corresponding to four CO_2 per unit formula, about four times higher than that of found in **1**. At this state the XRPD pattern of A and F are quite similar, probably indicating the similar architecture of both states. To confirm this, the space group and cell parameters were calculated by Dicvol and Rietica solftware[42]. The results show that at point F, frameworks is classified by a space group of *C*2/*c*, similar with that of A, and the cell parameters are close to those of as-synthesized **2**•*x*S (Table 1) [43].

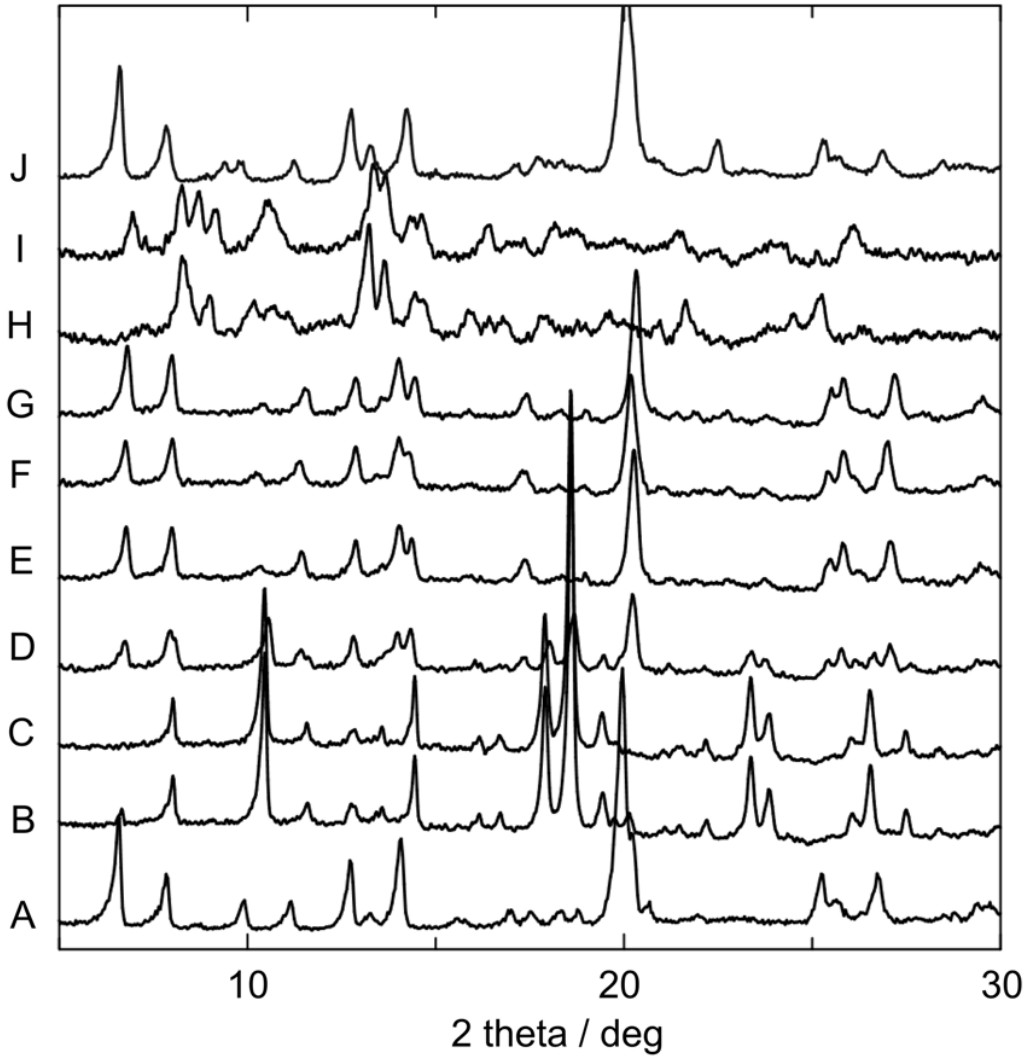

Figure 9. Pattern A is as-synthesized 1 measured at ambient temperature. The others are patterns of **2** at various pressure measured during sorption process.

e

reduced to P/Po = 0.05. The step can be observed again at point H with the change of XRPD patterns. After completely desorped the CO_2 from **2**, framework cannot recover as the initial state. The XRPD patterns at B and I are different. To re-activate **2** into the initial state, the treat by immerse in DMF is necessary. J is the XRPD pattern of re-activate **2** after directly immersed in DMF.

Conclusion

In conclusion, we succeeded in the selective synthesis of two PCPs with different interpenetration by taking an advantage of template effect. From this control, we can tune the porosity, stability and dynamics of PCP frameworks.

Experimental section

Mixture of two type of crystals were obtained from the reaction of $Zn(NO_3)_3 \cdot 6H_2O$, 2,2'-bithiophene-5,5'-dicarboxylic acid (btdc), and 4,4´-bipyridine (bpy) under the solvothermal synthesis. After the reaction finished, two types of crystal were collected. One is the yellow crystal of $[[Zn_2(btdc)_2(bpy)] \cdot xS]_n$ (**1**) (S = solvent) (Figure 1) which shows the three-fold interpenetrated fashion, while the other one is the pale yellow needle-like crystal of $[[Zn_2(btdc)_2(bpy)] \cdot yS]_n$ (**2**), possessing the two-fold fashion.

In the bulk synthesis, with the same condition as the single crystal synthesis, only the pure phase of **1** can be obtained, as confirmed by XRPD patterns (Figure 3 and 4). However, after the addition of benzene as the mixed solvent with dmf, surprisingly, pure phase of **2** could be obtained. Benzene should act as templates during the assembly process. Larger molecular size could prohibit the denser packing of frameworks. The difference between crystal and bulk synthesis might be the homogeniality of the reaction. **1** and **2** should have different reaction rates. In the crystal synthesis, different crystals can be obtained individually. However, in the bulk synthesis, the magnetic stirrer bar was put in the reaction mother liquor to achieve the homogeniality, thus, only one phase **1** which favors that condition could be obtained. On the other hand, by the addition of benzene, the template effect gives rise the other phase (**2**) which has lower degree of interpenetration.

References

[1] O. M. Yaghi, M. O'Keeffe, N. W. Ockwig, H. K. Chae, M. Eddaoudi, J. Kim, *Nature* **2003**, *423*, 705.

[2] G. Ferey, *Chem. Soc. Rev.* **2008**, *37*, 191.

[3] D. Bradshaw, J. B. Claridge, E. J. Cussen, T. J. Prior, M. J. Rosseinsky, *Acc. Chem. Res.* **2005**, *38*, 273.

[4] S. J. Dalgarno, N. P. Power, J. L. Atwood, *Coord. Chem. Rev.* **2008**, *252*, 825.

[5] M. P. Suh, Y. E. Cheon, E. Y. Lee, *Coord. Chem. Rev.* **2008**, *252*, 1007.

[6] S. Kitagawa, R. Kitaura, S.-i. Noro, *Angew. Chem., Int. Ed.* **2004**, *43*, 2334.

[7] S. Yang, X. Lin, A. J. Blake, G. S. Walker, P. Hubberstey, N. R. Champness, M. Schroeder, *Nat. Chem.* **2009**, *1*, 487.

[8] H. K. Chae, D. Y. Siberio-Perez, J. Kim, Y. B. Go, M. Eddaoudi, A. J. Matzger, M. O'Keeffe, O. M. Yaghi, *Nature* **2004**, *427*, 523.

[9] B. D. Chandler, G. D. Enright, K. A. Udachin, S. Pawsey, J. A. Ripmeester, D. T. Cramb, G. K. H. Shimizu, *Nat. Mater.* **2008**, *7*, 229.

[10] H. J. Choi, M. Dinca, J. R. Long, *J. Am. Chem. Soc.* **2008**, *130*, 7848.

[11] J. A. R. Navarro, E. Barea, A. Rodriguez-Dieguez, J. M. Salas, C. O. Ania, J. B. Parra, N. Masciocchi, S. Galli, A. Sironi, *J. Am. Chem. Soc.* **2008**, *130*, 3978.

[12] K. L. Mulfort, J. T. Hupp, *J. Am. Chem. Soc.* **2007**, *129*, 9604.

[13] C. D. Wood, B. Tan, A. Trewin, F. Su, M. J. Rosseinsky, D. Bradshaw, Y. Sun, L. Zhou, A. I. Cooper, *Adv. Mater.* **2008**, *20*, 1916.

[14] F. Nouar, J. F. Eubank, T. Bousquet, L. Wojtas, M. J. Zaworotko, M. Eddaoudi, *J. Am. Chem. Soc.* **2008**, *130*, 1833.

[15] J. L. Belof, A. C. Stern, M. Eddaoudi, B. Space, *J. Am. Chem. Soc.* **2007**, *129*, 15202.

[16] E. Y. Lee, S. Y. Jang, M. P. Suh, *J. Am. Chem. Soc.* **2005**, *127*, 6374.

[17] G. Ferey, C. Mellot-Draznieks, C. Serre, F. Millange, J. Dutour, S. Surble, I. Margiolaki, *Science***2005**, *309*, 2040.

[18] M. Fujita, J. Y. Kwon, S. Washizu, K. Ogura, *J. Am. Chem. Soc.* **1994**, *116*, 1151.

[19] S. Horike, M. Dinca, K. Tamaki, J. R. Long, *J. Am. Chem. Soc.* **2008**, *130*, 5854.

[20] J. S. Seo, D. Whang, H. Lee, S. I. Jun, J. Oh, Y. J. Jeon, K. Kim, *Nature* **2000**, *404*, 982.

[21] C.-D. Wu, W. Lin, *Angew. Chem., Int. Ed.* **2007**, *46*, 1075.

[22] R. Matsuda, R. Kitaura, S. Kitagawa, Y. Kubota, R. V. Belosludov, T. C. Kobayashi, H. Sakamoto, T. Chiba, M. Takata, Y. Kawazoe, Y. Mita, *Nature* **2005**, *436*, 238.

[23] B. Wang, A. P. Cote, H. Furukawa, M. O'Keeffe, O. M. Yaghi, *Nature* **2008**, *453*, 207.

[24] S. Ma, X.-S. Wang, D. Yuan, H.-C. Zhou, *Angew. Chem., Int. Ed.* **2008**, *47*, 4130.

[25] L. Pan, D. H. Olson, L. R. Ciemnolonski, R. Heddy, J. Li, *Angew. Chem., Int. Ed.* **2006**, *45*, 616.

[26] M. J. Horner, K. T. Holman, M. D. Ward, *J. Am. Chem. Soc.* **2007**, *129*, 14640.

[27] G. J. Halder, C. J. Kepert, B. Moubaraki, K. S. Murray, J. D. Cashion, *Science (Washington, DC, U. S.)* **2002**, *298*, 1762.

[28] R. Robson, *Dalton* **2000**, 3735.

[29] M. Dinca, A. Dailly, C. Tsay, J. R. Long, *Inorg. Chem. (Washington, DC, U. S.)* **2008**, *47*, 11.

[30] K. Seki, *Phys. Chem. Chem. Phys.* **2002**, *4*, 1968.

[31] R. Kitaura, K. Seki, G. Akiyama, S. Kitagawa, *Angew. Chem., Int. Ed.* **2003**, *42*, 428.

[32] R. Matsuda, R. Kitaura, S. Kitagawa, Y. Kubota, T. C. Kobayashi, S. Horike, M. Takata, *J. Am. Chem. Soc.* **2004**, *126*, 14063.

[33] D. Bradshaw, J. E. Warren, M. J. Rosseinsky, *Science***007**, *315*, 977.

[34] C. Serre, C. Mellot-Draznieks, S. Surble, N. Audebrand, Y. Filinchuk, G. Ferey, *Science* **2007**, *315*, 1828.

[35] T. K. Maji, R. Matsuda, S. Kitagawa, *Nat. Mater.* **2007**, *6*, 142.

[36] O. Shekhah, H. Wang, M. Paradinas, C. Ocal, B. Schuepbach, A. Terfort, D. Zacher, R. A. Fischer, C. Woell, *Nat. Mater.* **2009**, *8*, 481.

[37] E.-Y. Choi, K. Park, C.-M. Yang, H. Kim, J.-H. Son, S. W. Lee, Y. H. Lee, D. Min, Y.-U. Kwon, *Chem.--Eur. J.* **2004**, *10*, 5535.

[38] L. Ma, W. Lin, *J. Am. Chem. Soc.* **2008**, *130*, 13834.

[39] S. Ma, D. Sun, M. Ambrogio, J. A. Fillinger, S. Parkin, H.-C. Zhou, *J. Am. Chem. Soc.* **2007**, *129*, 1858.

[40] M. Eddaoudi, J. Kim, N. Rosi, D. Vodak, J. Wachter, M. O'Keeffe, O. M. Yaghi, *Science* **2002**, *295*, 469.

[41] A. L. Spek, *J. Appl. Crystallogr.* **2003**, *36*, 7.

[42] E. Nishibori, M. Takata, K. Kato, M. Sakata, Y. Kubota, S. Aoyagi, Y. Kuroiwa, M. Yamakata, N. Ikeda, *J. Phys. Chem. Solid* **2001**, *62*, 2095.

[43] B. LeBail, H. Duroy, J. L. Fourquet, *Mat. Res. Bull.* **1988**, *23*, 447.

Chapter 3

A Dynamic Isocyanurate-Functionalized Porous Coordination Polymer

ABSTRACT: Two isomorphous sponge-like flexible 3D porous frameworks providing the hydrophilic channel surface, by using a flexible ligand with the secondary functional group (C=O) were synthesized. The frameworks show size and affinity based selective sorption *via* dynamic structural transformation visualized by the single-crystal-to single-crystal structural analysis.

Introduction

Porous coordination polymers (PCPs) or metal‑organic frameworks (MOFs) have attracted much attention due to scientific interest in the creation of nanometer-sized spaces and for their potential application in molecular sieves, gas storage, and heterogeneous catalysis.[1 - 4] Besides porosity, stability, and pore shape and size, pore-surface functionalization and framework flexibility are currently considered to be key factors for the next generation of PCPs.[1b,3-4] Some PCPs exhibit dynamic behavior and thus can be developed into unique classes of materials, such as highly selective gas sensors and gas-separating materials, which could not be obtained with rigid porous materials. To functionalize the channel surface, two types of strategies are used: introduction of organic groups to provide guest-accessible functional organic sites (FOSs),[5] and immobilization of coordinatively unsaturated (open) metal sites (OMSs).[6] The use of OMSs for Lewis acid catalysis and specific gas adsorption has been widely explored in PCPs, but less attention has been devoted to FOSs despite their importance. This is because of the difficulty of producing guest-accessible FOSs on the pore surface, as organic groups tend to coordinate metal ions in a self-assembly process to give frameworks in which FOSs are completely blocked. In most cases framework flexibility results from coordinative bonds, H-bonds ,pi-electron stacking, and van der Waals interactions.[7] Ligands having a highly flexible component are another possibility which has not been commonly used to prepare three-dimensional (3D) PCPs.[6a] Here we report the synthesis, structure ,and selective (stepwise) sorption properties of two isomorphous 3D LnIII frameworks, synthesized from a tripodal symmetrical ligand with a highly flexible arms (CH_2CH_2) and secondary functional groups (C=O),which shows spongelike dynamic behavior, directly visualized by single crystal to single crystal

transformations (Scheme 1).

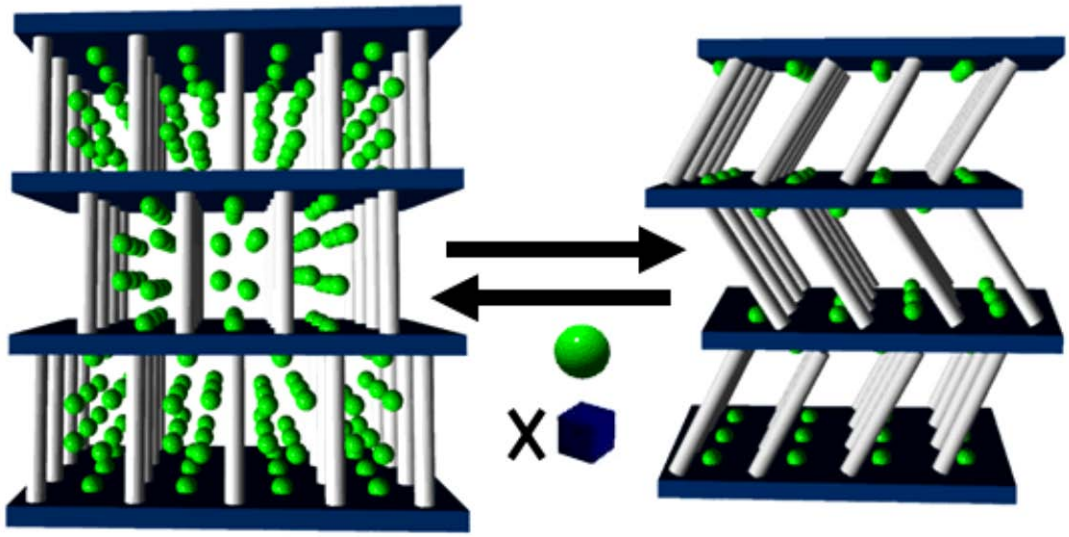

Scheme 1. Representation of the selective guest sorption of a soft coordination polymer by dynamic structural transformation.

Results and discussion

*Structures of **1** and **2***

Two isomorphous three-dimentional (3D) porous coordination polymer $\{[Ce(tci).H_2O]\ 4H_2O\}_n$ (**1**) and $\{[Gd(tci).H_2O]\ 4H_2O\}_n$ (**2**) [$tciH_3$ = tris(2-carboxyethyl) isocyanurate] were prepared from $Ln(NO_3)_3.xH_2O$ and $tciH_3$ by hydrothermal technique. Both the compounds are stable in air and insoluble in common organic. As both **1** and **2** have an identical structure, only the structure of **1** is and ninth coordination is occupied by one coordinated water molecule. All three carboxylate groups of the tci^{3-} unit are making bidentate chelating bond with Ln(III), where two of them are also making bridge with another Ln(III) to extend the framework. These bridging bonds are extending metal centers to make metal-carboxylate chain along *c*-axis. Three arms of the ligand are bridging three such metal-carboxylate chains and this continuous network forming the assembled 3D structure. To understand the structure very simple way we can assume that, the metal-carboxlylate chains bridged by the two arm of the tripodal ligand forming a 2D sheet structure and these 2D sheets are bridged by the third arm of the ligand making a porous 3D structure. The resultant three dimensional frameworks contain one dimensional channel along the crystallographic *a*-axis occupied by four water molecules, which are H-bonded with the coordinated water molecule as well as with the carboxylate oxygen atoms. The water molecules inside the channel are highly disorder. The channel dimensions are 2.85 x 2.74 $Å^2$ (the channel size is measured by considering van der Walls radii for constituting atoms), which provide a void space composed of 21.1% of the total crystal volume. After determining the structure, simulated powder x-ray diffraction (PXRD) has been matched with the as-synthesized compounds **1** and **2**.

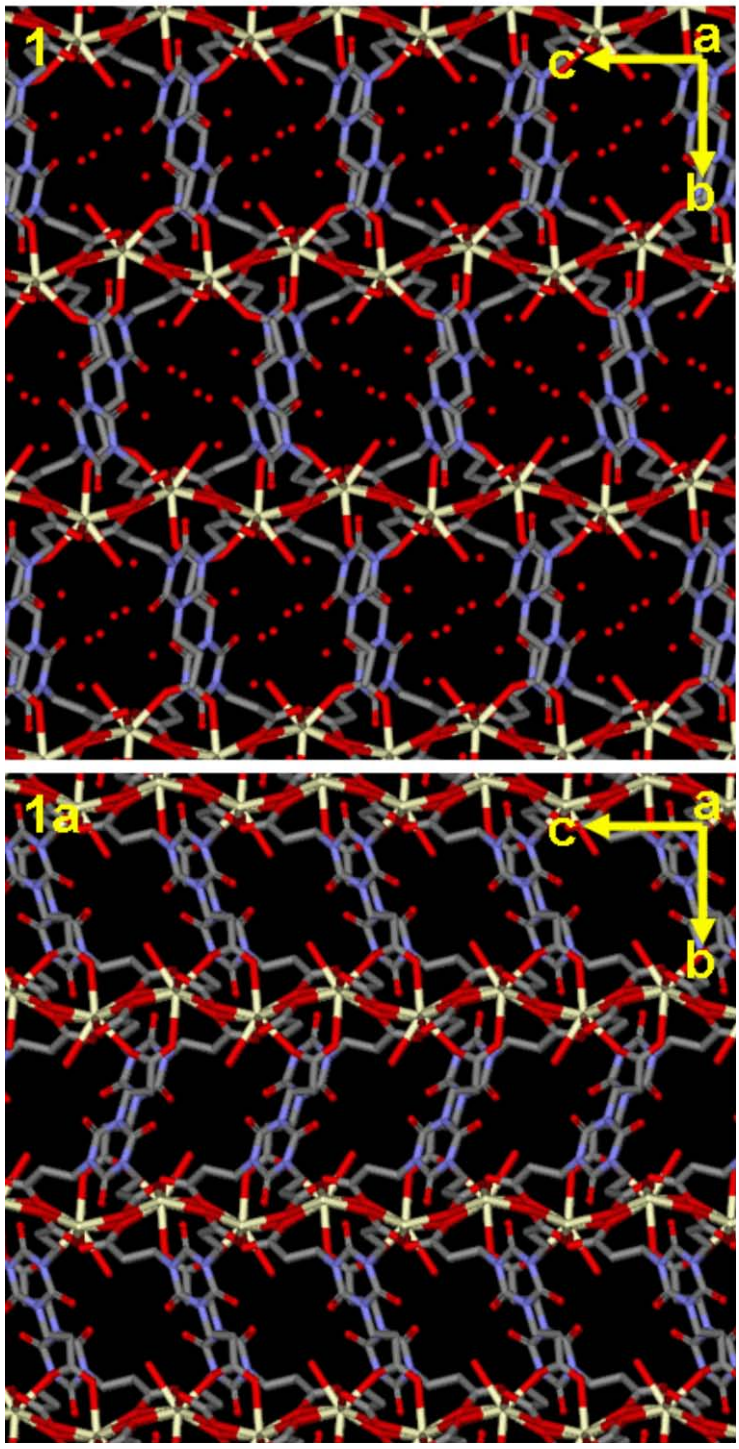

Figure 1. Perspective view of the 3D dynamic frameworks of : (a) as-synthesized compound **1** containing a water filled 1D-channel along *a* axis (above) and (b) partially dehydrated (only uncoordinated water molecules) framework **1a** (bottom).

Thermal Properties of 1 and 2

Thermogravetric analysis for both the compounds were carried out in a N_2 atmosphere and 1 atm pressure. The stepwise thermogravemetric curve of **1** indicated that the four guest water molecules are released at less then 100 ºC and one coordinated water molecule is released at around 150 ºC. The compound is stable upto ~ 300 ºC and after

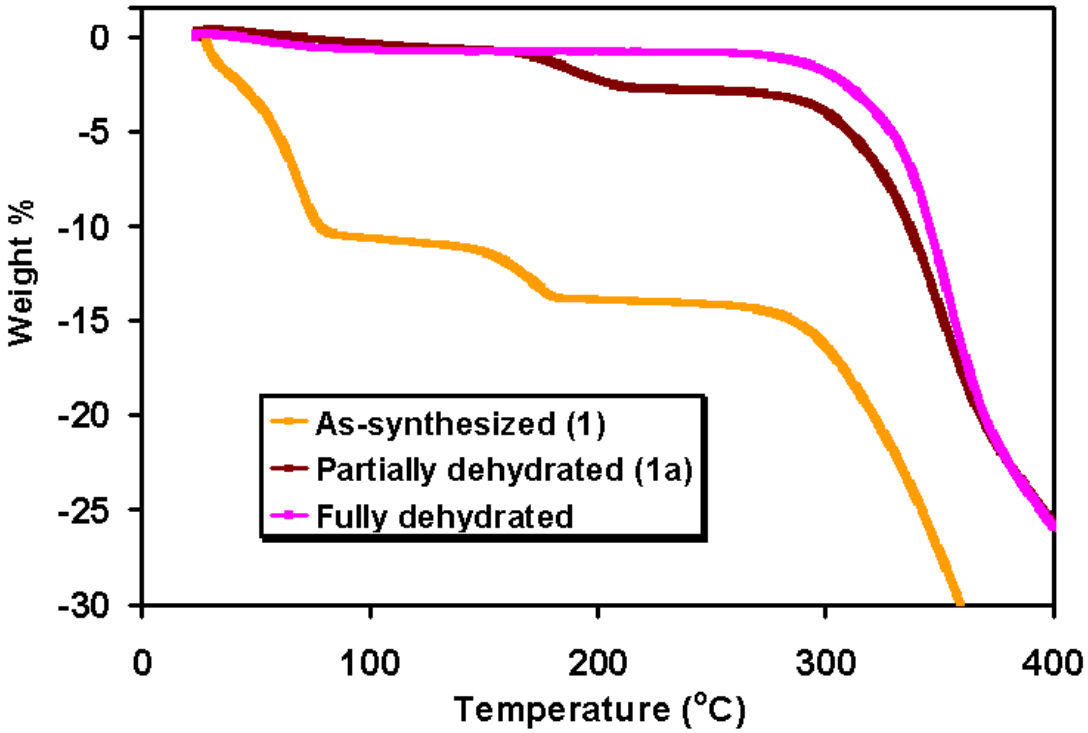

Figure 2. Thermogravimetric analysis pattern of as-synthesized compound (**1**), partially dehydrated compound (**1a**) and fully dehydrated compound.

that it decompose continiously, possibly breaking of the ligands occuring after that tempurature. Therefore, partially (with one coordinated water) dehydrated phase (**1a**) can be accomplished by heating at the temperature below 100 ºC and fully dehydrated compound at just above 150 ºC. Powder XRD pattern of the partially dehydrated compound (**1a**) indicates that it maintaining good crystallinity but the fully dehydrated

compound is like amorphous, indicating that the 3D frakework is not maintaining after removal of the coordinated water molecules.

As compound **1** and **2** are isostructural, only compound **1** is considered for detail structural changes and other studies. It is notworthy that compound **1** retains its single crystallinity even after the removal of the guest water molecules by heating the crystal at 70 ºC for ~7 hours under an Ar atmosphere. The single crysytal X-ray structure of the partially dehydrated crystal (**1a**) indicated that compound has been shrinked largely along *b*-axis but crystal symmetry remain same. Due to the very flexible ($-CH_2CH_2-$) part of the the ligand the framework can easly make changes along all directions with the available free space to the required structure. The one dimentional channel dimensions are now shrinked to 2.52 X 1.30 $Å^2$ from 2.85 X 2.74 $Å^2$ and now void space in compound **1a** composed of 13.2% comparative to 21.1% in compound **1**. Structural changes leads to the change of channels position from parallel in compound **1 t**o zig-zag in **1a** along *b*-axis, which also provide a different look in the overall view of the framework (Figure 1). The structural changes is mainly created by the movements of the flexible arms of the ligands. When the dehydraeted single crystal of **1a** was exposed to the ambiant atmosphere for 1-2 days, from single crystal cell measurement it shows that it returns to the original structure **1**.

*Sorption Properties of **1** and **2***

Since the completely dehydrated phase framework is not stable, so based on the well defined structure of partially dehydrated phase, we carried out the sorption measurements

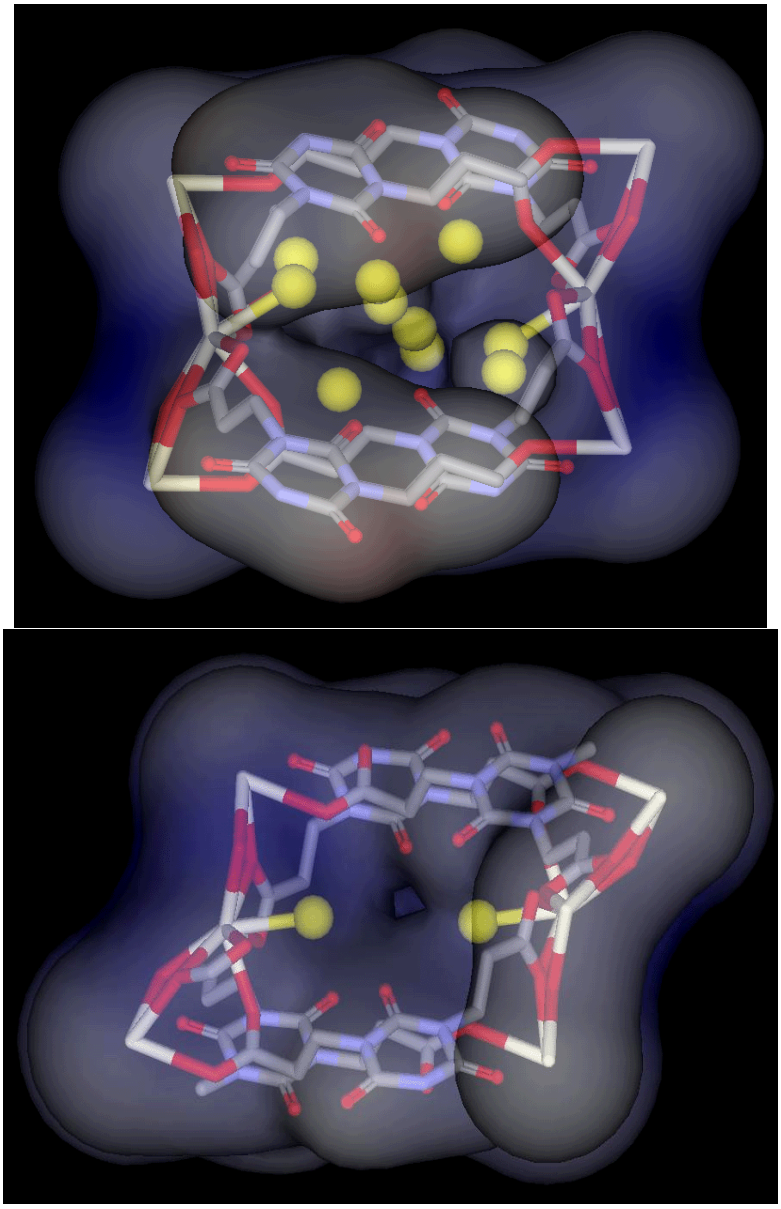

Figure 3. Close view of the pore of compound **1** (top) and **1a** (bottom) along the *a* axis.

of compound **1a**. CO_2 adsorption at 195K and N_2/O_2 adsorption at 77K shows only surface adsorption, indicates that these molecules cannnot diffuse into the micropores, which is chiefly associated with the smaller channel dimensions (Figure 3).

Interesting phenomenons were observed in the solvent sorption experiments at 298K as shown in figure 3. The isotherms show selective and stepwise sorptions with hysteresis. In the case of H_2O as a guest, the copound **1a** adsorp four water molecules correspond to eight water molecules per unit pore, which is also the same amount present in compound **1**. The adsorption profile shows very unusual pattern, upto P/P_o (relative solvent vapour pressure) ~ 0.06 the isotherm slowly increase, then it sharply increase unto 0.2 and then with increasing pressure it very slowly increase upto P/P_o = 1. The value at 0.06 corresponding to the one H_2O molecule per unit pore, which means the pore size is not enough to enter the guest water molecules and with its small aperture (dimension 2.52 X 1.30 $Å^2$) it slowly interact with the surface of the pore by making H-bonding and after entering one water molecule the pore partially open, which help the surface of the channel to interact with other water molecules to easily enter and so isotherm increse sharply until P/P_o = 0.2 that correspond to six water molecules per unit pore. This is possibile only because of the sponge-like highly flexible framework, which can easily expand the structure depending upon the amount of guests. This is also strongly supported by the H-bonding of the guest H_2O molecules with the inside hydrophilic surface of the pore containing -C=O group and coordinated water molecules as well as carboxylate oxygens to interact rapidly and so become easy to enter into the pore. After entering six water molecules the pore size become saturated at that pressure and with increasing pressure value the pore size also expand slowly to uptake two more water molecules and so it show very slow increase of the isotherm. Once water molecules enter into the pore they strongly interact with the surface of the pore and so desorption become difficult which results into the hystereses profile. The sorption profile of methanol (MeOH) is very similar to H_2O, but only two MeOH molcules can enter into the pore, which is because of

the large size of MeOH compared to H_2O molecules. In case of MeOH also the profile first slowly increase upto P/P_o = ~ 0.05 which corrsponds to one MeOH molecule per unit pore, after that profile increase shraply comparative to the lower region and become saturated at P/P_o value < 0.1 correspond to the two methanol molecules per unit pore. After P/P_o = 0.1 the profile is completely flat upto P/P_o ~ 0.9 indicates no adsorption on that pressure region, but at very high pressure (P/P_o ~ 0.9) profile further start to increase sharply until P/P_o = 1. Like water molecules, MeOH molecules (dimension 3.80 X 4.70 $Å^2$) also can not easily enter into the small aperture of the channel (dimension 2.52 X 1.30 $Å^2$), and after slowly entering one molecule of MeOH, the channel size expand and another MeOH molecule easily enter by expanding the soft framework with the supporting of strong H-bonding force with the hydrofilic channel suface. After entering

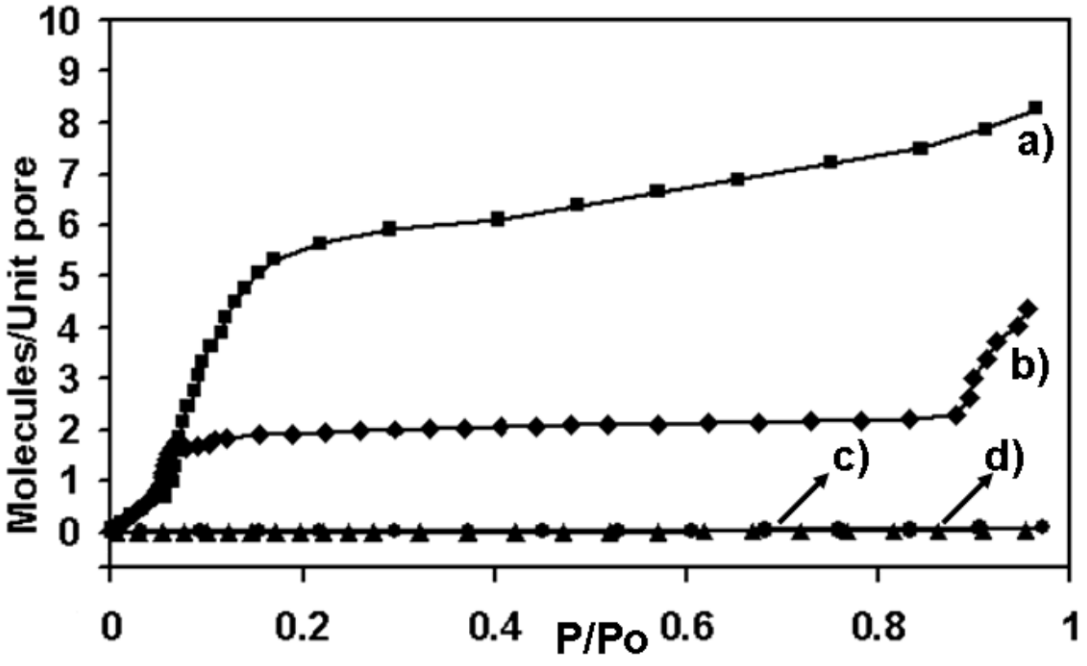

Figure 4. Adsorption profile of a) H_2O (square), b) MeOH (diamond), c) MeCN (circle) and d) EtOH (triangle) of compound **1a** at 298K.

two MeOH molecules the channel become saturated and so no more inclusion of MeOH molecules takes place. But at high pressure (P/P_o ~ 0.9) the profile shows another sharp increase, which is due to the adsorption between the particales of the compound. MeOH also strongly interact with the surface (-C=O group) as well as with the carboxylate oxygens, so become very difficult to desorp easily and show hystereses profile. Interestingly instead of the comparative size of acetonitrile (dimension 3.80 X 5.49 $Å^2$) to MeOH, it can not enter into the channel, which may be due to the fact that, MeOH can make strong H-bonds with the hydrophilic pore surface which help to enter into the pore but since MeCN can not make strong H-bonding it fail to enter into the pore. Then as expected from the very big molecules comparative to the channel aperture size like EtOH (dimension 4.72 X 5.96 $Å^2$), THF and Me_2CO are not adsrobed, it is clear that selectivity arises from the very small size of the channels window comparative to the size of the adsorbates.

Conclusion

We have synthesized two isomorphous sponge-like soft flexible 3D porous frameworks with hydrophilic channel surface, by rationally choosing a flexible ligand with secondary functional group. The framework shows size and affinity based selective sorption *via* dynamic structural transformation visualized by the single-crystal-to single-crystal structural analysis.

Experimental section

Materials. Tris(2-carboxyethyl) Isocyanurate, $Ce(NO_3)_3.6H_2O$ and $Gd(NO_3)_3.6H_2O$ and all solvents(dehydrated) were obtained from Wako and used without further purification.

Synthesis of $\{[Ce(tci)(H_2O)].4H_2O\}_n$ (1). Single crystal of **1** was prepared by reacting 1 mmol of $Ce(NO_3)_3.6H_2O$ and 1 mmol of tris(2-carboxyethyl) Isocyanurate ($tciH_3$) in 15 mL of water by the hydrothermal technique, in a Teflon-lined autoclave. The autoclave was heated under autogenous pressure to 150 °C for 3 days and then cooled to RT for 24 h period. Upon cooling to RT, the desired product appeared as long colorless rectangular parallelepipeds in ~ 40% yield.

Synthesis of $\{[Gd(tci)(H_2O)].4H_2O\}_n$ (2). Compound **2** was synthesized using the same method like compound **1** here $Gd(NO_3)_3.6H_2O$ has been used instead of $Ce(NO_3)_3.6H_2O$. Yield ~ 45%.

Physical Measurements: X-ray powder diffraction was carried out on a Rigaku RINT-2000 Ultima diffractometer with Cu Kα radiation. Thermogravimetric analyses were recorded on a Rigaku Thermo plus TG 8120 apparatus in the temperature range between 300 and 800 K under a nitrogen atmosphere at a heating rate of 1 K min^{-1}. The adsorption isotherms of H_2O and MeOH at 298 K were measured with BELSORP18 volumetric adsorption equipment from Bel Japan and the low temperature adsorption isotherm for gases was measured with Quantachrome AUTOSORB-1.

X-ray Crystal Analysis. Single crystal X-ray diffraction data collection was carried out on a Rigaku mercury diffractometer with a graphite monochromic MoKα radiation (γ = 0.71069 Å) and a CCD detector. The structure was solved by the direct method using SHELXTL and was refined on F^2 by full-matrix least-squares technique using the

SHELXL-97 program package. Non-hydrogen atoms were refined anisotropically. All hydrogen atoms except water molecules were positioned geometrically, and they were treated as riding atoms using SHELXL default parameters.

References

[1] a) G. Ferey, C. Mellot-Draznieks, C. Serre, F. Millange, *Acc. Chem. Res.* **2005**, *38*, 217 – 225; b) S. Kitagawa, R. Kitaura, I. S. Noro, *Angew. Chem. Int. Ed.* **2004**, *116* ,2388 – 2430; *Angew. Chem. Int. Ed.* **2004**, *43*, 2334 – 2375; c) C. N. R. Rao, S. Natarajan, R. Vaidhyanaathan, *Angew. Chem.* **2004**, *116*, 1490 – 1521; *Angew. Chem. Int. Ed.* **2004**, *43*, 1466 – 1496; d) O. M. Yaghi, M. O'Keeffe, N. W. Ockwig, H. Chae, M. Eddaoudi, J. Kim, *Nature* **2003**, *423*, 705 – 714; e) G. S. Papaefstathiou, L. R. MacGillivary, *Coord. Chem. Rev.* **2003**, *246*, 169 – 184; f) O. R. Evans,W . Lin, *Acc. Chem. Res.* **2002**, *35*, 511 – 512.

[2] a) Y. Liu, J. F. Eubank, A. J. Cairns, J. Eckert, V. C. Kravtsov, R. Luebke, M. Eddaoudi, *Angew. Chem.* 2007, 119, 3342 – 3347; *Angew. Chem. Int. Ed.* **2007**, *46*, 3278 - 3283; b) K. L. Mulfort, J. T. Hupp, *J. Am. Chem. Soc.* **2007**, *129*, 9604 - 9605; c) M. Dinca, A. F. Yu, J. R. Long, *J. Am. Chem. Soc.* **2006**, *128*, 8904 - 8913; d) X. Lin, A. J. Blake, C . Wilson, X. Z. Sun, N . R. Champness, M. W. George, P . Hubberstey, R. Mokaya, M. Schroder, *J. Am. Chem. Soc.* **2006**, *128*, 10745 - 10753; e) E. Y. Lee, M. P. Suh, *Angew. Chem. Int. Ed*. **2004**, *116*, 2858 - 2861; *Angew. Chem. Int. Ed*. **2004**, *43*, 2798 - 2801.

[3] a) G. Ferey, *Chem. Soc. Rev.* **2008**, DOI : 10.1039/b618320b; b) S. Kitagawa, R. Matsuda, *Coord. Chem. Rev.* **2007**, *251*, 2490 - 2509; c) C. J. Kepert, *Chem. Commun.* **2006**, 696 - 700; d) A. J. Fletcher, K. M. Thomas, M. J. Rosseinsky, *J. Solid State Chem.* **2005**, *178*, 2491 - 2510; e) S. Kitagawa, K. Uemura, *Chem. Soc. Rev.* **2005**, *34*, 109 - 119; f) D. Bradshaw, J . B. Claridhe, E. J. Cussen,T . J. Prior, M. J. Rosseinsky, *Acc. Chem. Res.* **2005**, 38, 273 - 282.

[4] a) S. K. Ghosh, J. P. Zhang, S Kitagawa, *Angew. Chem. Int. Ed.* **2007**, *119*, 8111 - 8114; *Angew. Chem. Int. Ed.* **2007**, *46*, 7965 - 7968; b) C. Serre, C. Mellot-Draznieks, S . Surble, N . Audebrand, Y. Filinchuk, G . Ferey, *Science* **2007**, *315*,1828 - 1831; c) Y. Kubota, M. Takata, R. Matsuda, R. Kitaura, S. Kitagawa, T. C. Kobayashi, *Angew. Chem. Int. Ed.* **2006**, *118*, 5054 - 5058; *Angew. Chem. Int. Ed.* **2006**, *45*, 4932 - 4936; d) Y. E. Lee, S . Y. Jang, M. P. Suh, *J. Am. Chem. Soc.* **2005**, *127*, 6374 - 6381; e) R. Matsuda, R. Kitaura,S . Kitagawa,Y . Kubota,R. V. Belosludov, T. C. Kobayashi, H. Sakamoto, T. Chiba, M. Takata, Y. Kawazoe, Y. Mita, *Nature* **2005**, *436*, 238 - 241; f) R. Matsuda, R. Kitaura, S. Kitagawa, Y . Kubota, T . C. Kobayashi, S . Horike, M. Takata, *J. Am. Chem. Soc.* **2004**, *126*, 14063 - 14070.

[5] a) S. Horike, S. Bureekaew, S. Kitagawa, *Chem. Commun.* **2008**, DOI: 10.1039/b715481j; b) S. Hasegawa, S . Horike, R. Matsuda, S. Furukawa, K. Mochizuki, Y. Kinoshita, S . Kitagawa, *J. Am. Chem. Soc.* **2007**, *129*, 2607 - 2614.

[6] a) S. H. Cho, B . Ma, S. T. Nguyen, J. T. Hupp, T . E. Albrecht-Schmitt, *Chem. Commun.* **2006**, 2563 - 2565; b) J. P. Zhang, S. Horike, S . Kitagawa, *Angew. Chem. Int. Ed.* **2007**, *119*, 907 - 910; *Angew. Chem. Int. Ed*. **2007**, *46*, 889 - 892; c) B. Chen, N. W. Ockwig, A. R. Millward, D . S. Contreras, O. M. Yaghi, *Angew. Chem. Int. Ed.* **2005**, *117*, 4823 - 4827; *Angew. Chem. Int. Ed.* **2005**, *44*, 4745 - 4749.

[7] a) T. K. Maji, G . Mostafa, R. Matsuda, S. Kitagawa, *J. Am. Chem. Soc.* **2005**, *127*, 17152 - 17153; b) A. J. Fletcher, E. J. Cussen, D. Bradshaw, M. J. Rosseinsky, K. M. Thomas, *J. Am. Chem. Soc.* **2004**, *126*, 9750 - 9759; c) K.

Seki, *Phys. Chem. Chem. Phys.* **2002**, *4*, 1968 - 1971.

[8] A. L. Spek, *Acta Crystallogr. Sect. A* **1990**, *46*, C34.

[9] G. M. Sheldrick,SHELX-97,Program for crystal structure solution, University of Gottingen, Germany, 1997.

[10] G. M. Sheldrick, SHELX-97,Program for crystal structure refinement, University of GSttingen, Germany, 1997.

Chapter 4

Thermal Conductivity of Porous Coordination Polymers

ABSTRACT: The thermal conductivities of polycrystalline porous coordination polymers $[Cu_2(R)_2(dabco)]_n$ with and without guest molecules are reported. These compounds could be categorized into two groups based on their thermal conductivity. The ligands with different dynamic motion, give rise in the difference thermal conductivity and. The contribution of structural dynamic property of host and guest also affects on the heat transferring process.

Introduction

Heat transport in a system is governed by the motion of free particles which try to restore thermodynamic equilibrium in the system subjected to a temperature gradient. Heat energy can be transmitted through solid materials via electrical carriers (electrons or holes), lattice wave (phonons), electromagnetic waves, or other excitations. In metal, electrical carriers carry the majority of the heat, while insulators, lattice vibrations are the dominant heat transporter. Materials with both very high and very low thermal conductivities are technologically important. High thermal conductivity insulators, like diamond or silicon, have been extensively studied because of their potential application in thermal management of electronic devices. Low thermal conductive materials such skutterudites, clathrates, chalogenides and oxides are focused for the high-efficiency thermoelectric materials.[1]

In insulator, heat can flow from hotter part to cooler part by the vibration of each atomic lattice. Every harmonic vibration can be decomposed in the elementary vibrations called phonons which are the quantized modes of vibration in rigid lattice. The total number of phonons in a system that vibrates (e.g. crystal) is related to the temperature of the system. At higher temperatures, vibration of an object is stronger and the number of phonons larger. Every phonon carries a quantum of vibrational energy, this means that the internal energy of the object is also larger. The thermal conductivity is defined by analog with the kinetic theory of gas, as follows:

$$\lambda = C_v \cdot \nu \cdot l$$

where λ is the thermal conductivity ($Wm^{-1}K^{-1}$), C_v the specific heat capacity ($J{\cdot}g^{-1}K^{-1}$), ν the sound velocity (ms^{-1}) and l is the mean free path of phonon (m). The materials provide a high C_v and l would give a high λ, while the scattering of phonon enhances

the thermal resistivity, decreasing the heat-transferring rate. At very high temperatures (much above the Debye temperature, θ_D), the heat capacity is governed by the temperature dependence of the phonon mean free path, which increases as the temperature increases due to increased probability of phonon-phonon collisions (so called 'Umklapp' processes to indicate that they turn back the heat flux) which cause resistance to heat flow.[2]

On the other hand, the porous coordination polymers (PCPs) have been regarded as a new class of porous materials. They contain notable advantages such as high crystallinity, high regularity and high designability. Recently we reported the dynamic behavior of PCPs in guest adsorption/desorption processes. The study of thermal property of PCPs is significantly less, but still important to their developments and applications.[3-9]

The thermal expansion of PCPs is one of thermal property which has been studied. The experimental and theoretical study of $[Zn_4O(bdc)_3]_n$ (bdc = 1,4-benzene dicarboxilate), so-called MOF-5 has been revealed that this porous compound possesses negative thermal expansion (NTE). The rigid-unit vibration mode, described as the ZnO_4 tetrahedral and the benzene ring unit serve as rigid units while the carboxyl groups serve as the bridge. The large amplitude transverse vibration of the bridge results in the negative thermal expansion. Because the PCPs do not contain the free electron, heat can transfer only by the vibrational process. Porosity in PCPs, similar with typical point defect, enhances the scattering of phonon, thus PCPs generally are the low thermal conductor. In this study, the thermal conductivities of PCPs with similar structures but different ligands have been measured under guest-free and guest-containing conditions. Thermal conductivity is one important property of PCPs because it affects on their

applications, for example, in gas storage application, the heat gate opening phenomenon resulting from structural change or the adsorption and desorption processes are correlate with heat in term of both heat in the framework itself and heat communication between host and guest. In the application of PCPs as nano-vessel for chemical reaction, the heat transferring characteristic of PCPs might be one of the origins of the difference in reaction in such nano-vessel and in bulk-phase reaction.

Results and discussion

Crystal structures.

The paddle-wheel type three dimensional (3D) structural PCPs were employed in the present study. This structure is suitable to study the relationship between the heat transferring and ligands by varying the organic bridging ligands. Five Cu(II) compounds, $[Cu_2R_2(dabco)]_n$ (**1**, R = 1,4-naphthalene dicarboxylate; **2**, R = 2,5-dimethylterephthalate; **3**, R = 1,4-benzene dicarboxylate; **4**, R = 2,6-naphthalene dicarboxylate; **5**, R = biphenyl-4,4'-dicarboxylate; dabco = diazobicyclo[2.2.2]octane) were prepared for this studied. The single crystals of these Cu compounds could not been prepared, however, their structures could be investigated from the characterization of single crystal of zinc compounds, $[Zn_2R_2(dabco)]_n$ which provide similar structure of those Cu complexes. All materials have similar structures with difference bridging ligands, R as shown in Figure 1.

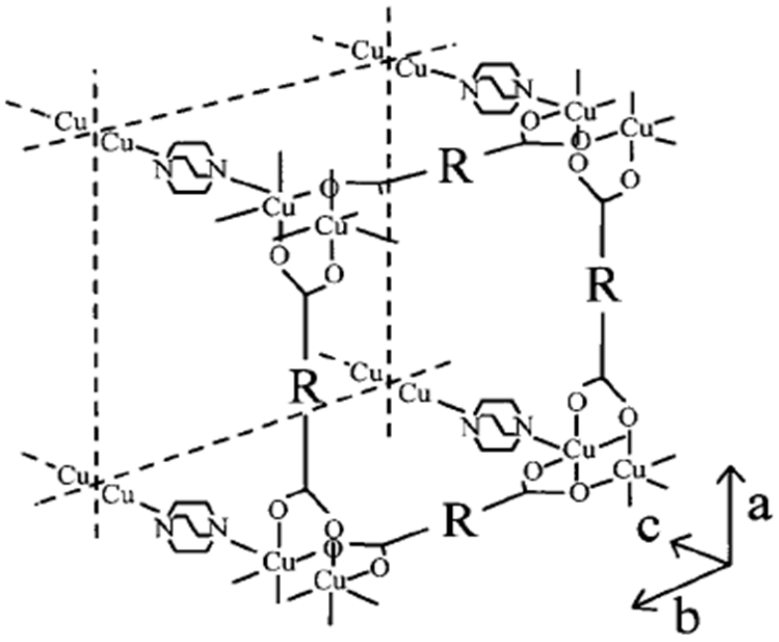

Figure 1. The 3D structure of $[Cu_2R_2(dabco)]_n$.

Thermal conductivity of $[Cu_2R_2(dabco)]_n$

The measurements of thermal conductivity were carried out at ambient temperature. The conductivities of $[Cu_2R_2(dabco)]_n$ are reported in Table 1. According to their thermal conductivity, we can classify $[Cu_2R_2(dabco)]_n$ compound series into two groups: (1) lower thermal conductivity (**1** and **2**) with the value about 0.10 – 0.15 $W \cdot m^{-1} \cdot K^{-1}$, and (2) higher thermal conductivity (**3**, **4**, and **5**) with the value about 0.20 – 0.25 $W \cdot m^{-1} \cdot K^{-1}$.

The difference in thermal conductivity of these $[Cu_2R_2(dabco)]_n$ compound series should be caused by the difference in the R ligands. Because of the free volume in these PCPs and flexibility which is the unique property of PCPs, the dynamic motion (rotation) of some linkage ligands could be observed. In the case of **1**, **3**, and **5**, the

ligands could rotate freely around the C1-C4 axis, confirmed by solid state NMR and from the conformation disorder in crystal structures.[9] On the other hand, in the case of **4**, a naphthalene ring cannot rotate because of the lacking of molecular axis into support the rotation.

Theoretically, heat can transfer by the motion of free particles. In crystal with *n* atoms per unit call, there are 3*n* degrees of freedom which can be divided into acoustic and optical modes. Three modes would be acoustic phonon which are predominant hear carriers in insulators and the rest are optical modes. However, if *n* is large, some of optical mode might couple with acoustic phonon leading to the resistivity. Solid nitrogen is an interesting system to examine for its thermal conductivity because it exhibits two solid phases, one ordered and one disordered.[2] Thermal conductivity of solid N_2 in the orientationally disordered β-phase (cubic) is about 20% less than in the ordered α-phase (hexagonal).[10] This is attributed to the interaction of heat-carrying phonon with fluctuations associated with orientationally disorder of N_2 molecules.

From the study influence of the rotation of fragments of molecules on the thermal conductivity of methyl-substituted benzenes: methylbenzene (toluene), 1,2-dimethylbenzene (orthoxylene), 1,3-dimethylbenzene (metaxylene) 1,4-dimethylbenzene (paraxylene), and 1,3,5- trimethylbenzene (mesitylene) in the temperature range 80–270 K. It was found that at high temperatures the rotation of the methyl groups with respect to C-C bonds becomes thermally activated. From the presence of this rotation, strong translational-orientational interaction makes for a significant contribution from molecular librations to the thermal resistance of the crystal. This phenomenon is also found in the case of molar crystal of solid ethane.

Table 1. Thermal conductivity of $[Cu_2L_2(dabco)]_n$ with and without guest molecule (dmf)

Framework	Thermal conductivity ($W \cdot m^{-1} \cdot K^{-1}$)	
	without guest	dmf
1,4-ndc	0.12	0.15
Met-bdc	0.15	0.16
bdc	0.24	0.18
2,6-ndc	0.25	0.27
bpdc	0.25	0.26

In PCPs with lower thermal conductivity (**1** and **2**), the rotation of ligand brings about the conformational disorder of framework (Figure 2). From the crystal structure of $[Zn_2(1,4\text{-ndc})_2(bdc)]_n$, the four-fold conformational disorder of naphthalene ring could be observed. Moreover the ^2H solid state NMR also support this four-cite flipping with the angle of 0°, 70°, 180° and 250° (Figure 3).[5] Each flipping of naphthalene rings give

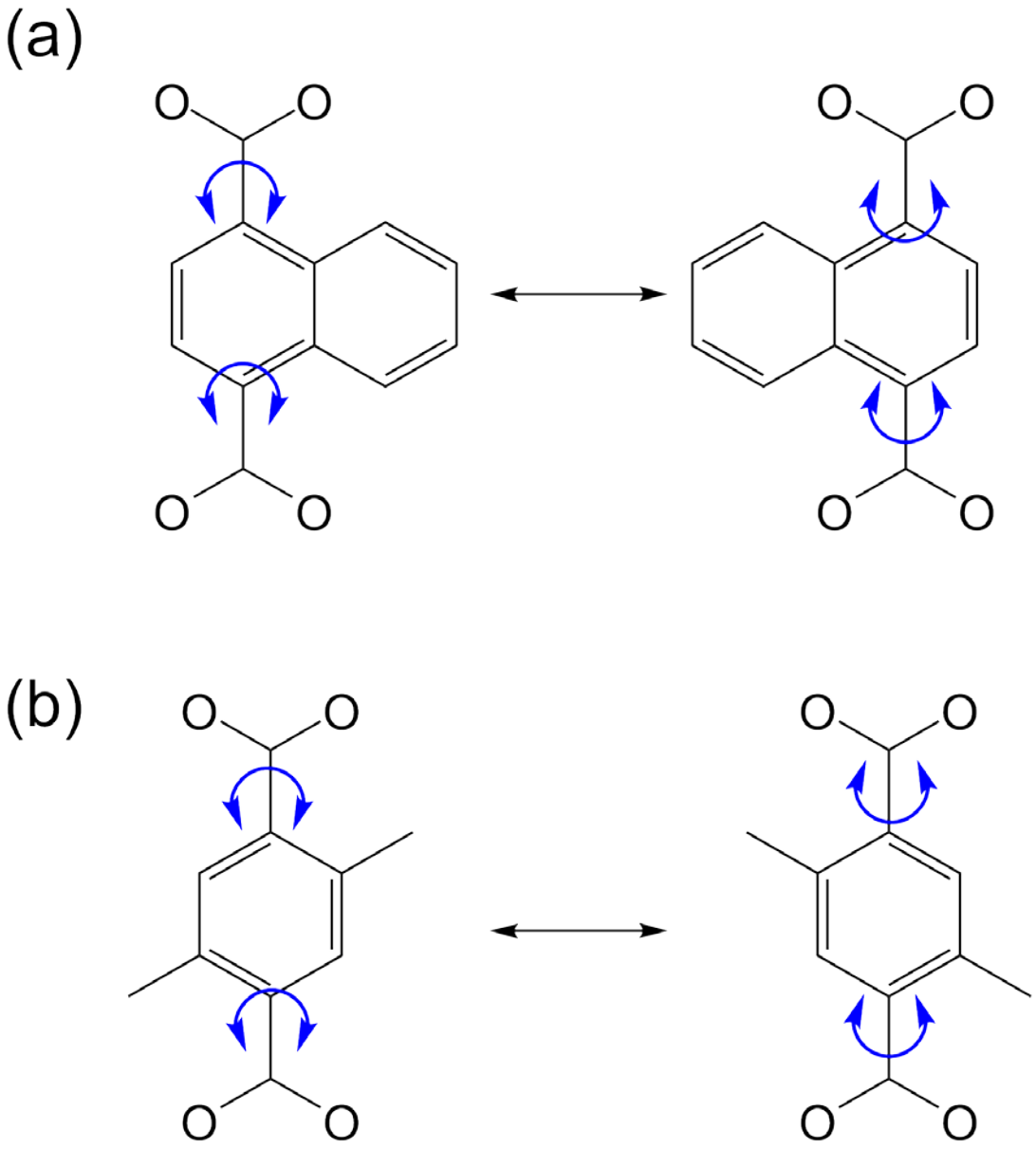

Figure 2. Schematic of conformational disorder during the rotation of ligand in **1** and **2**.

rise in the different conformations. This orientationally disorder might interact with acoustic phonon and consequence of the retardation of heat conduction, similar with the observation in solid N_2 and methyl-substituted benzenes.

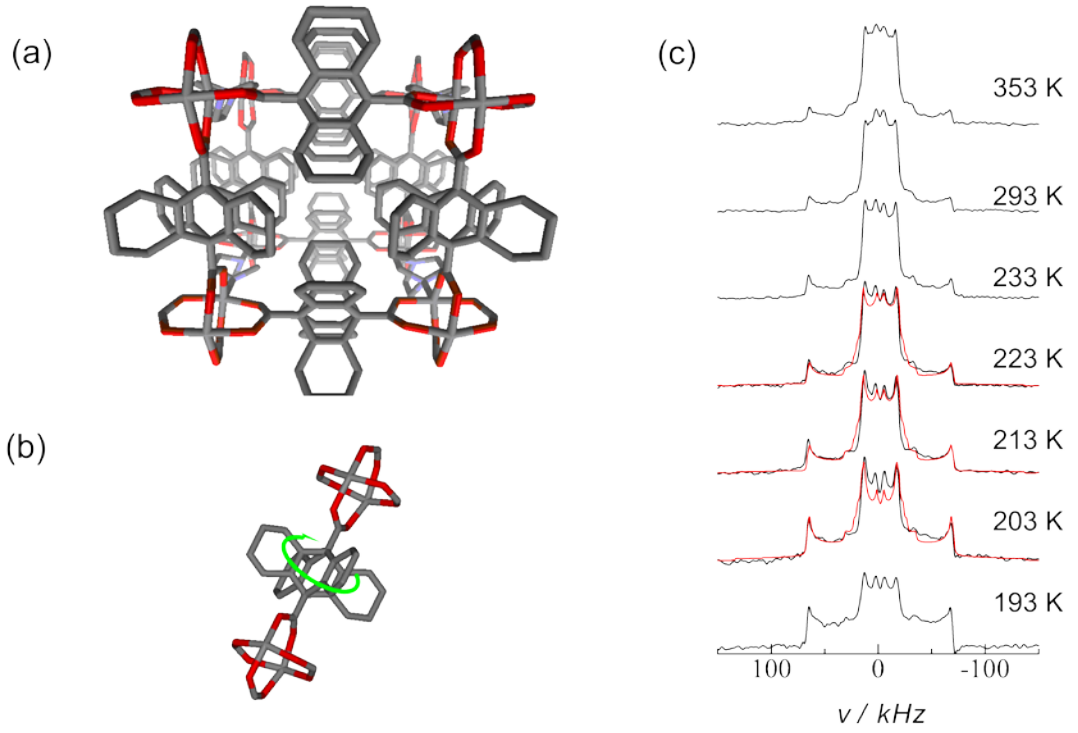

Figure 3. (a) View of crystal structure of $[Cu_2(1,4\text{-ndc})_2(dabco)]_n$. The four-fold conformational disorder has been observed (b). The spectra of ^2H solid state NMR also show the four-cite flipping mode of naphthalene ring(c).

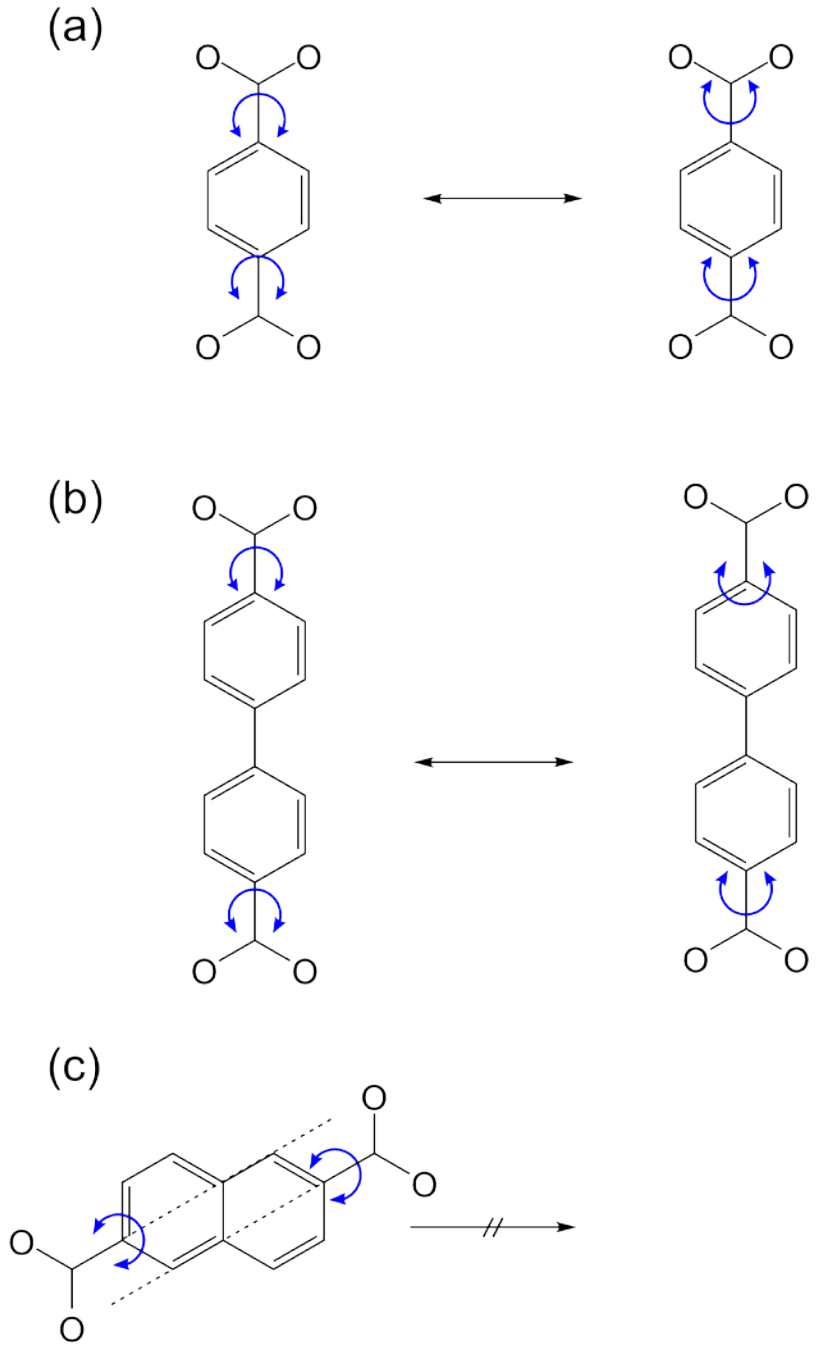

Figure 4. Schematic of rotation of ligand of **3** (a) and **4** (b). The rotation does not give rise the change of conformation of ligand. Ligand in **5** cannot rotate due to the lacking of rotational axis (c). The two C–COO axes do not superimpose each other, prohibiting the rotation of ligand.

However, in the case of **3** and **4**, although by considering the symmetry, the benzene and naphthalene ring could rotate freely, they possess higher thermal conductivity rather than that of **1** and **2** (Figure 4). From crystal structure of **3** and **4**, the conformational disorder of benzene and biphenyl could not be observed, even though we can observe the 2-site flipping of benzene ring in **3** by using ^{2}H solid state NMR (Figure 5). The rotations of benzene and phenylene rings do not affect on the conformational disorder, thus interaction of acoustic phonon with the orientational disorder is less than in the case of **1** and **2.** Thermal conductivities of PCPs with guest molecule (dmf), especially in the case of **1** and 3, are significantly different from the guest-free networks. In the cause of using benzene as guest molecule accommodated into 1,4-ndc, even though there is no evidence from XRPD for the structural change after addition of dmf into framework, the ^{2}H solid state NMR spectra reveal that the four-cite flipping dynamic motion of the naphthalene ring disappeared.[5] This is because this rotation requires free space which is diminished by the accommodation of guest molecule. Thus, the conformational disorder is removed, and thermal resistivity decreases.

In the case of clathrate crystal, for example Ge clathrates (doped with Sr and/or Eu) exhibit lattice thermal conductivities typical of amorphous materials.[11] The low-thermal conductivity of these compounds at low temperatures is attributable to the disorder introduced by the dynamic ‘‘rattling’’ introduced by these ‘‘guest’’ atoms inside the polyhedra.[8] Dianin’s clathrate crystal, The host molecules form hexamers held together by hydrogen bonding through the phenolic oxygens, giving cages 11 Å high and 6.3 Å at the widest spot. Each cage can hold, for example, two ethanol molecules or one CCl_4 molecule. Thermal conductivity measurements show that ethanol guests, which are dynamically disordered, give more thermal resistance than CCl_4 guests, which only

librate slightly and therefore do not increase the thermal resistivity beyond what is observed in the empty host lattice.[2] In the case of **3**, thermal conductivity decreases when guest molecules occupy in void space. From these observation in above clathrates, we can explain the decrease of thermal conductivity of bdc with guest molecule by the interaction between the heat-carrying phonon and optic modes associated with dynamical disorder induced by the dynamic motion of guest molecules in the host framework that is usually found in PCPs can shorten the mean free path, consequently the low thermal conductivity.

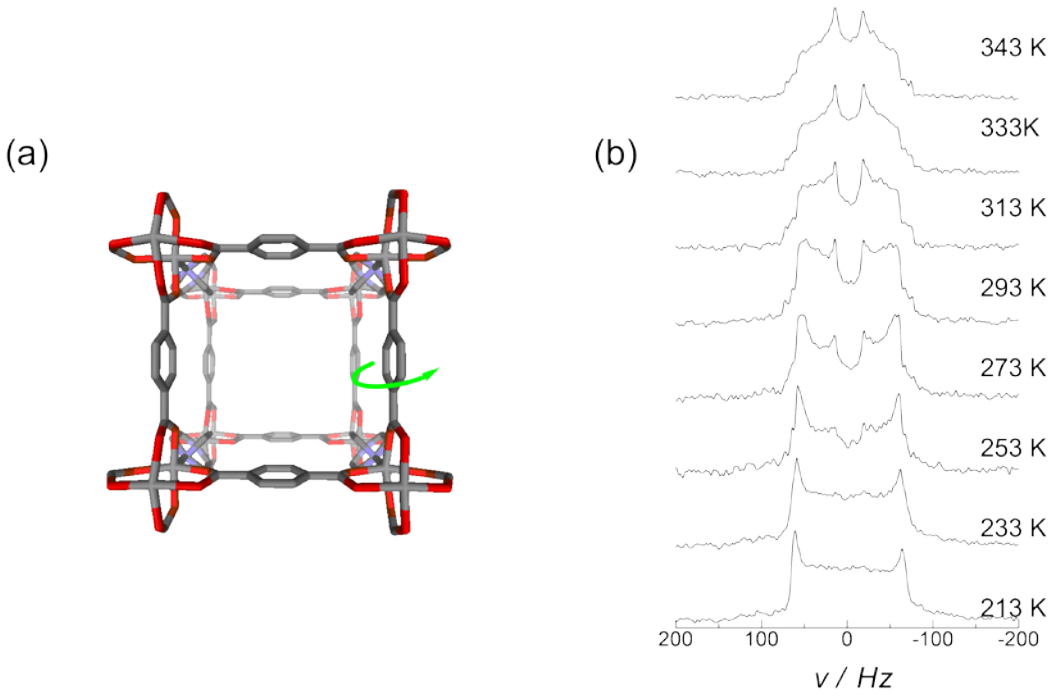

Figure 5. (a) View of crystal structure of $[Cu_2(bdc)_2(dabco)]_n$. The conformational disorder has not been observed, however, the spectra of ^2H solid state NMR show the two-cite flipping mode of benzene ring of bdc ligands (b).

Experimental section

Material synthesis

$[Cu_2L_2(dabco)]_n$ (bdc, L = 1,4-benzene dicarboxylate; 1,4-ndc, L = 1,4-naphthalene dicarboxylate; 2,6-ndc, L = 2,6-naphthalene dicarboxylate; phdc, L = biphenyl-4,4'-dicarboxylate; Met-bdc, L = 2,5-dimethylterephthalate; andc, L = 9,10-anthacene dicarboxylate, dabco = diazobicyclo[2.2.2]octane) were prepared for this studied.

Measurement of thermal conductivity

Thermal diffusivity was estimated by the Transient Plane Source (TPS) technique under ambient conditions using TPS 2500. With the TPS technique, the probe comprises a flat sensor with a continuous double-spiral of electrically-conducting Nickel (Ni) metal. The sensor is normally placed between the surfaces of two pieces of the sample to be measured. During measurement, a current passes through the Nickel and creates an increase in temperature. The heat generated dissipates through the sample on either side at a rate dependent on the thermal transport characteristics of the material. By recording the temperature versus time response in the sensor, these characteristics can accurately be calculated. The measurements were carried out at ambient temperature.

References

[1]. T. M. Tritt, *Thermal conductivity: Theory, properties, and application*, springer, 2004.

[2]. M. White, *J. Therm.l Anal. Calorie*, 1999, **57**, 765-771.

[3]. S. Bureekaew, S. Shimomura and S. Kitagawa, *STAM*, 2008, **9**.

[4]. K. W. Chapman, G. J. Halder and P. J. Chupas, *J. Am. Chem. Soc.*, 2008

[5]. S. Horike, R. Matsuda, R. Kitaura, S. Kitagawa, T. Iijima, K. Endo, Y. Kubota and M. Takata, *Chem.Commun.*, 2004, 2152-2153

[6]. C. Serre, S. Bourrelly, A. Vimont, N. A. Ramsahye, G. Maurin, P. L. Llewellyn, M. Daturi, Y. Filinchuk, O. Leynaud, P. Barnes and G. Ferey, *Adv. Mater.*, 2007, **19**, 2246-2251

[7]. J. L. C. Rowsell and O. M. Yaghi, *Microporous and Mesoporous Mater.*, 2004, **73**, 3-14

[8]. N. L. Rosi, J. Eckert, M. Eddaoudi, D. T. Vodak, J. Kim, M. O'Keeffe and O. M. Yaghi, *Science*, 2003, **300**, 1127-1129.

[9]. S. Horike, R. Matsuda, D. Tanaka, S. Matsubara, M. Mizuno, K. Endo and S. Kitagawa, *Angew. Chem. Int. Ed.*, 2006, **45**, 7226-7230.

[10]. P. Stachowiak, V. V. Sumarokov, J. Mucha and A. Jeowski, *Phys. Rev. B*, 1994, **50**, 543.

[11]. J. L. Cohn, G. S. Nolas, V. Fessatidis, T. H. Metcalf and G. A. Slack, *Phys. Rev. Lett.*, 1999, **82**, 779.

[12]. G. S. Nolas, T. J. R. Weakley, J. L. Cohn and R. Sharma, *Phys. Rev. B*, 2000, **61**, 3845.

Chapter 5

SAC-CI theoretical study on the excited states of lumiflavin: Structure, excitation spectrum, and solvation effect

ABSTRACT: The excited states of a flavin-related compound, lumiflavin, were studied by the symmetry-adapted cluster (SAC)-configuration interaction (CI) method. The absorption peaks observed in the experimental spectrum were theoretically assigned. Transition energy of some low-lying n-π* states were obtained. The energy minimum structures of the first singlet and triplet excited states were calculated by the SAC-CI method. The structural changes upon excitation were at most 0.05 Å. The solvation effect on the absorption energy in aqueous solution was investigated using polarizable continuum model (PCM) and by including water molecules into the computational model. The solvatochromic shift of the second peak (3^1A' state) originates from both microscopic (hydrogen bonding) and macroscopic (electronic polarization of solvent) solvation effects.

Introduction

Flavins are well-known redox-active chromophores that are widely found in enzymes and photoreceptors[1]. These compounds contain a heterocyclic isoalloxazine ring (7,8-dimethyl benzo[g]pteridine-2,4(3H,10H)-dione) that exhibits electrontransfer capability. Riboflavin is found in various types of foods in the human diet. A lack of riboflavin causes growth disturbance, skin disease, and hair loss. Flavin adenine dinucleotide (FAD) works as a redox-active light-harvesting chromophore in DNA photolyase, blue-light-using FAD (BLUF), and crytochrome. Flavin mononucleotide (FMN) exhibits redox-active properties in respiratory complex I in mitochondria and other electron-transfer systems. FMN also functions as a blue light photoreceptor in phototropin. Since flavins play important roles in a very wide range of biological processes in which both ground and excited states of theses molecules are involved, their photophysical and photochemical properties have been studied from various points of view[2–11]. Lumiflavin (LF), which is shown in Figure 1a, is one of the simplest flavin compounds. In ongoing efforts to study photoexcitation and electron-transfer reactions in flavin-type compounds, LF has been used as a representative molecule. Several studies on electronic excitation of LF have been published, involving both experimental research[2,4,7–11] and theoretical calculations[3,5–11]. Theoretical studies using configuration interaction-singles (CIS)[6], time-dependent density functional theory (TDDFT)[6,8–10] and DFT-multireference (MR) CI[6] have been reported. These studies mainly focused on the excitation spectrum. A complete active space self-consistent field method with second-order perturbation theory (CASPT2) study[3] on the excited states of isoalloxazine has recently been published. This study reported the ground-state absorption spectrum and the potential energy surface of the low-lying singlet and triplet states.

Photochemical events in the gas phase were interpreted using a quantitative correlated method. Since LF is a trimethyl-isoalloxazine, important problems regarding the excited states of LF in the gas phase might have been solved. However, these studies on LF failed to reproduce the excitation energy for the second peak, and its maximum error reached 0.5 eV [6]. One of the remaining problems is to clarify the reason why the absorption energy of the second peak has never been reproduced quantitatively, even though modern correlated methods have been employed. One of the main reasons is the solvation effect on the excitation energy. In general, the absorption energy of the π–π* transition does not strongly depend on the solvent. However, the second peak shifts by approximately 0.4 eV by the solvation effect. The above-mentioned studies did not include the solvation effect in their computations. In this study, we applied the symmetry-adapted cluster

(SAC)[12] /SAC-configuration interaction (CI) [13–15] method [16,17]. The SAC/SAC-CI method is established as an accurate electron-correlation method for studying ground, excited, ionized and electron-attached states. As numerous applications have shown, the SAC-CI method is a reliable tool for calculating the excitation energy and properties of excited states of molecules[16,17]. In the present report, we first show SACCI results for the excited states of LF in the gas phase. The optimized structures are explained in some details for ground, singlet, and triplet excited states at the SAC/SAC-CI level. Next we investigated the solvation effect in the excited states. As a previous experimental study showed [8], the excitation energy of the second peak remarkably depends on the solvent, even though the absorption was assigned to a π–π* transition. We applied the polarizable continuum model (PCM) [18–20] to the SAC-CI calculations to capture the solvation effect. With these calculations, we succeeded in explaining the solvent

dependent excitation energy observed in the second peak.

Computational details

The computational models for LF are shown in Figure1. The isolated model (Figure 1a) was used for the gas-phase calculations. The second model with five water molecules (Figure1b) was used to investigate the effect of hydrogen bondings in water solution. The geometry of LF in the gas phase was optimized by density functional theory (DFT) [21-23] using the B3LYP[24,25] functional. The structure of LF with five water molecules was also optimized using DFT calculations. The optimized geometries were confirmed to be the energy-minimum by performing frequency analysis. The optimized structure has Cs symmetry, which agrees with previous studies[3,26]. The 6-31G(d)[27,28] basis sets were used for both LF and water molecules. We also performed geometry optimization for the ground (S0) the first singlet (S1), and triplet (T1) excited states by using the SAC/SAC-CI method with D95V(d) basis functions [29]. We performed the SAC-CI optimization within the Cs symmetry. To date, the second derivative of the SAC-CI energy has not yet been developed. We referred to recently published complete active space self-consistent field method (CASSCF) structures for the S1 and T1 states, which are found to be planar (Cs-symmetry) in both cases [3]. The solvation effect in water solution was included using the PCM[18-20]. The dielectric constant of water (ε = 78.39) was used. For the model with five water molecules, the rest of the solvation effect was treated using the PCM. The self-consistent reaction field calculation was performed at the ground-state Hartree-Fock (HF) level, and the orbitals and one-electron operators were transferred to the SAC/SAC-CI calculation. For the SAC/SAC-CI calculations, we employed the D95V(d) sets. The 1s orbitals of C, N, and O atoms were

treated as frozen-core orbitals. The active orbitals were comprised of 48 occupied orbitals and 223 virtual orbitals. All the single and selected double excitation operators were included in the SAC/SAC-CI wave functions. Perturbation selection[30] was performed to select the important doubles. The energy thresholds for the perturbation selection procedure were $5.0 \times 10{-}6$ and $5.0 \times 10{-}7$ a.u. for the ground and excited states, respectively. The oscillator strengths reported in this paper were calculated in dipole length representation. All computations were carried out using the Gaussian 03 quantum chemistry program package[31].

(a)

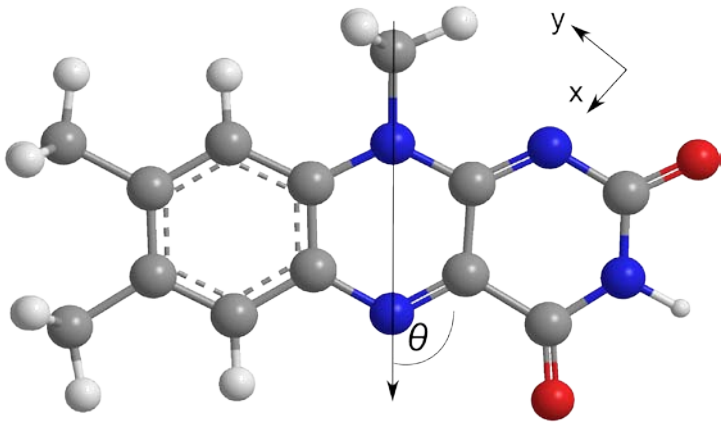

(b)

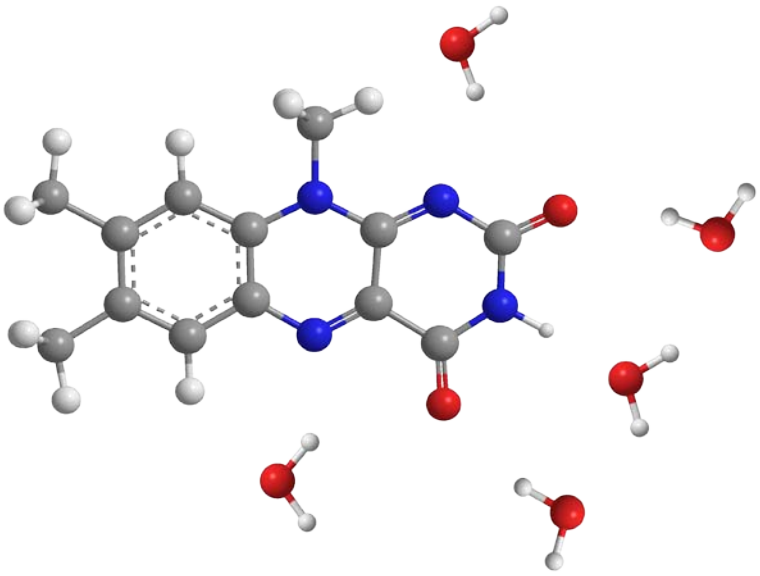

Figure 1. Computational models for (a) lumiflavin (LF) and (b) lumiflavin with five explicit water molecules directly solvating the charged atoms. The arrays in (a) show the definition of the angle (θ) of the transition dipole moment vector.

Results and discussion

Electronic excitation of lumiflavin in the gas phase

We begin with the electronic excitation spectrum for the ground state of LF in the gas phase. The SAC-CI results are summarized in Table 1. Unfortunately, there is no experimental gas-phase spectrum available for comparison. In solution, LF shows the first band centered at 2.77–2.81 eV, depending on the solvent [8]. On the low-energy side of the absorption peak, there is also a strong shoulder at 2.6 eV. In the SAC-CI result,

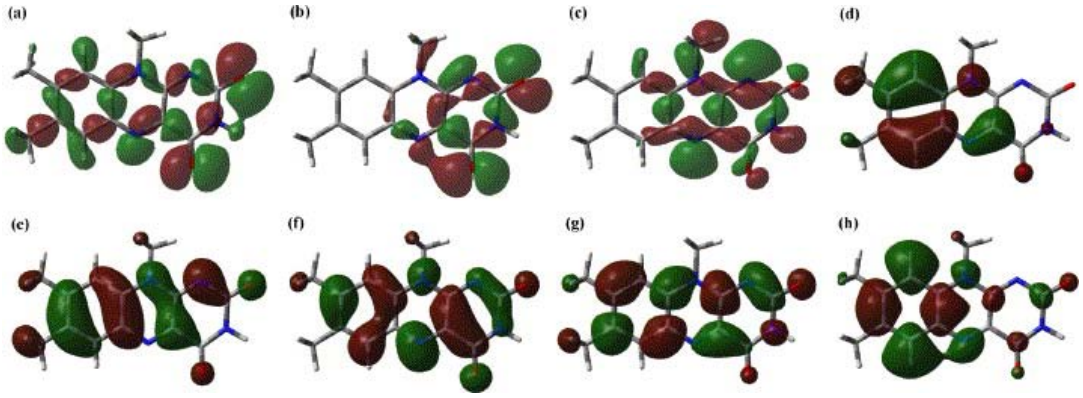

Figure. 2. Hartree-Fock molecular orbitals of lumiflavin in the gas phase. These orbitals are relevant to the low-lying excited states: (a) 60th MO (n+π, HOMO-7);(b) 62th MO (n+π, HOMO-5); (c) 63th MO (n+π, HOMO-4); (d) 66th MO (π, HOMO-1); (e) 67th MO (π, HOMO); (f) 68th MO (π, LUMO); (g) 69th MO (π,LUMO+1); (h) 70th MO (π, LUMO+2).

the first singlet excited state (2^1A') was calculated at 2.46 eV. There is a deviation of 0.14 eV from the shoulder and of 0.31–0.35 eV from the peak center. Since there is no other excited state in this energy region of the spectrum, the 2^1A' state is assigned to the first band. The S1 state is characterized as a π–π* transition dominated by

HOMO-LUMO transition. Figure 2 shows some important MOs. Both HOMO and LUMO are delocalized over the π skeleton of the ring. Using linear dichroism (LD) spectroscopy, the angle of the transition dipole moment in FMN[32,33] was measured. The definition of the angle (θ) is indicated in Figure 1a. Johansson et al.[33] and Eaton et al.[32] reported θ =58° ±4° and 75°, respectively. The present SAC-CI result is 72°, which is very close to the CASPT2 result for isoalloxane (75°) [3]. The theoretical results thus support the latter experiment. There are two (n +π)-π* states around 3.2-3.6 eV. The 1^1A" and 2^1A" states calculated at 3.18 and 3.59 eV are transitions from HOMO-4 to LUMO and from HOMO-5 to LUMO, respectively. The n+π orbitals HOMO-4 and HOMO-5 are characterized as mixed π and lone-pair O (nO) and N (nN) orbitals. HOMO-4 has a relatively larger orbital amplitude at the nitrogen atoms, while that of HOMO-5 is at the oxygen atoms. The second π-π* transition, the 3^1A' state, is at 3.84 eV in the SAC-CI result for the gas phase. The corresponding experimental peak position ranges from 3.73 to 3.38 eV, depending on the solvent [3]. The most non-polar and aprotic solvent used in the experiment was 1,4-dioxane. In this solution, the peak was observed at 3.73 eV. The main configuration of the state is a transition from HOMO-1 to LUMO. As observed in Figure 2d, HOMO-1 has a population around the left ring. Table 2 summarizes the calculated dipole moments of the ground and low-lying π-π* states. The total dipole moment of the 3^1A' state is 13.2 Debye, which is greater than those of the ground and 2^1A' states by 3.6 and 2.0 Debye, respectively. Compared to the ground state, the Cartesian components μx and μy increase by 1.8 and 3.3 Debye, respectively. This change is related to the main configuration of the state. Owing to the localized character of HOMO-1, the charger-transfer character of the 3^1A' state is greater than that of the 2^1A' state. As mentioned later, this property becomes

important for interpreting the solvent dependence of the absorption peak. The angle of the transition dipole moment was calculated to be 85.0°. The experimental values obtained by LD spectroscopy were 97° ±3° by Johansson et al.[33] and 95° by Eaton et al. [32], which are in reasonable agreement with the present value and the CASPT2 result [3] (100°). For the third and fourth π-π* transitions, the 4^1A' and 5^1A' states were calculated at 4.55 and 4.86 eV, respectively, in the resent SAC-CI result. The main configurations of the 4^1A' and 51A' states are transitions from HOMO to LUMO+1 and from HOMO to LUMO+2, respectively. In the experimental spectrum, there is a broad absorption peak centered at approximately 4.5 eV. Considering the absorption coefficient in the experimental spectrum, both the 4^1A' and 5^1A' states would contribute to this absorption. The angle of the transition dipole moment calculated is 108.0° and 125.0° for these states, respectively. On the other hand, the experimental value for the peak is 119°±2.[33] Therefore, the angle averaged for the two states is close to the experimental value.

Structure of LF in the lowest singlet and triplet excited states (S1 and T1)

The structures of LF in the S1 (2^1A') and T1 (1^3A') states in the gas phase were determined by the SAC-CI method. The optimized bond lengths are summarized in Figure 3. The result for the ground state (S0) is also shown in Figure 3a. Both states were characterized as a HOMO (π) to LUMO (π*) transition. As shown in Figure 3, the transitions cause no significant change in the bond lengths. The maximum change is at most 0.05 Å, observed for the C8 C9, C4 C5, and C4 C7 bonds. The reason can be found in the nature of the HOMO and LUMO. There is no clear bonding to anti-bonding

Table 1. Excited states of lumiflavin calculated by the SAC-CI method

State	SAC-CI						Exptl.[c]					
	Nature	Main configuration	Eex(Osc.)[a]			LD[b]	Eex[a]					LD[b]
			In gas phase	In water solution		θ (o)	in Dx[e] ε = 4.03	in DCE[f] ε = 10.36	in MeOH[g] ε = 32.63	in Acn[h] ε = 36.64	in H_2O[i] ε =78.39	θ (o)
				PCM	$5H_2O$[d]							
$2^1A'$	π-π*	67→68	2.46	2.42	2.40	72.0	(-/2.81)	(-/2.77)	2.6/2.80	2.6/2.80	2.6/2.79	58±4.75
$1^1A''$	n-π*	63→68	3.18	3.18	3.28	-						
2A''	n-π*	62→68	3.59	3.59	4.05	-						
$3^1A'$	π-π*	66→68	3.84	3.84	3.54	85.0	3.73	3.59	3.53	3.62	3.38, 3.35	97±3.95
$4^1A'$	π-π*	67→69	4.55	4.55	4.56	108.0			4.65	4.65	4.59	119±2
$5^1A'$	π-π*	67→70	4.86	4.86	4.95	125.0						

a Excitation energy in eV. Numbers in parentheses are the oscillator strength in atomic units.

b Angle of the transition dipole moment from LD data. The definition of the angle is

c Experimental absorption energy. The data (x/y) for the 21A□state denotes that the strong shoulder is at “x” eV and the pe

d Effect of the explicit hydrogen bonds using the 5H2O model was taken into account. Correction to the SAC-CI excitation energy was obtained by the ONIOM like procedure at CIS level.

e In 1,4-dioxane solution.

f In dichloroethane solution.

g In methanol solutio

h In acetonitrile solut

i In water solution.

j Ref. [8].

k Ref. [6].

transition in the HOMO-LUMO excited state. The transition is mostly from the bonding to non-bonding orbitals and from the anti-bonding to non-bonding orbitals. The changes in the bond lengths reflect the character of the HOMO and LUMO. For example, the C4 C5 bond has bonding character in the HOMO, while it changes to non-bonding in the LUMO. The C4 C5 bond lengthens in the first excited state. The C8 C11 bond shortens in both the S1 and T1 states, because the LUMO shows bonding character for the C8 C11 bond, which is stronger than that of the HOMO.

Table 2. Dipole moment of griund, 2^1A' and 3^1A' states in the gas phase calculated by SAC-CI method

State	Dipole moment (Debye)			
	μ_x	μ_y	μ_z	μ_{total}
X^1A' (ground state)	3.0	9.1	0.0	9.6
2^1A' (HOMO →LUMO)	2.6	10.9	0.0	11.2
3^1A' (HOMO-1 →LUMO)	4.8	12.4	0.0	13.3

Solvation effect on the excitation energy of the singlet states

The present gas-phase result shows reasonable agreement to the experimental absorption energy in 1,4-dioxane solution[8], which is the most non-polar and aprotic solvent of those used in experiments. Since previous theoretical studies were on the excited states of LF in the gas phase[3,6,8,9,11], one of the problems to be solved is the absorption energy in polar and protic solution. In particular, the absorption energy of the

second peak strongly depends on the solvent, even though it is a π-π* excitation. As shown in Table 1, the absorption energy in 1,4-dioxane is 3.73 eV, while that in water solution is 3.38-3.35 eV. On the other hand, other absorption peaks are almost insensitive to the solvent. Considering the properties of the solvents, there are two reasons for the red shift. The first is the dielectric polarization of the solvent due to the charge distribution of the solute. Table 1 also shows the dielectric constant of the solvent. The magnitude of the red shift tends to be greater if the dielectric constant of the solvent is larger. The second reason is hydrogen bonding between LF and the solvent. In protic solvents as H_2O and MeOH, the absorption maximum shifts to lower energy. We estimated the absorption energy in water solution as follows. In the first step, we performed the SAC-CI calculation using PCM. In the next step, the effects of the explicit solvent molecules were estimated using an ONIOM[34] -like approach. For this purpose, two types of CIS calculations were performed: one with PCM and the other with five explicit water molecules (Figure 1b) and PCM. The change in excitation energy accounts for the correction introduced by the explicit solvent molecules, and is used as an energy correction to the SAC-CI +PCM excitation energy. The PCM calculation correctly reproduced the solvation effect in the π-π* transition. The explicit water model was therefore expected to improve the description of the n-π* transitions in water solution. The water molecules were placed at the protic part of LF, where the hydrogen bondings take place. The rest of the solvation effect was taken into account by PCM. To reduce the computing time and resources, the structure of the LF-water complex was kept to Cs symmetry. Since the hydrogen bonding effect is mainly electrostatic[35], this approximated model would be qualitatively correct enough to describe hydrogen bonding to the lone-pair electrons of the O and N atoms in LF. The

results are summarized in Table 1. The excitation energy of the 3^1A' state changes to 3.54 eV, which is a red shift of 0.30 eV compared to the gas-phase result. The deviation from the experimental peak position changes to 0.16-0.19 eV. On the other hand, the solvation effect on the 2^1A' state was estimated to be a red shift of only 0.06 eV, which agrees with the trend in the experiment [8]. The 4^1A' and 5^1A' states also show only small solvatochromism. The solvation effects in the n-π* transitions tend to be greater than that in the π-π* transitions. The excitation energies of the 1^1A" and 2^1A" states in water solution were estimated to be 3.28 and 4.05 eV, respectively. These results involve a blue shift of 0.10 and 0.46 eV, respectively, compared to the gas-phase result. In particular, the 2^1A" state showed marked blue shift. One reason is in the orbital distribution of the 62th MO. The wave function of the 2^1A" state is one electron transition from 62th MO to 68th MO. As clearly seen in Figure 2, the 62th MO distributes over the right hand of the molecule. On the other hand, the 3^1A' state shows red shift in water solution and is one electron transition from 66th MO. The distribution of the 66th MO is in the left side of LF. Since directions of the dipole moments of the two states were opposite, the solvatochromic shift of the 2^1A' state is also opposite to that of the 3^1A' state. To qualitatively analyze the solvatochromic shift, we performed a series of CI-Singles calculations using different environments. First, the shift due to direct hydrogen bonding was estimated by the excitation energy difference between the explicit solvation model (W) and the gas phase model (*G*), which are listed in the "*E*ex(W)−*E*ex(G)" column in Table 3. Second, the dielectric polarization effect of the solvent was estimated by the excitation energy difference between the W plus PCM model and the W model, which are summarized in the "*E*ex(W+P)−*E*ex(W)" column. The total solvatochromism shift, *E*ex(W+P)−*E*ex(G), is also listed. As shown in Table 3,

the explicit solvation effect and the dielectric polarization of the solution contribute almost equally to the total solvatochromic shift in the $3^1A'$ state. This result could be interpreted in terms of the MO populations. The $3^1A'$ state arises from a transition from HOMO-1 to LUMO. HOMO-1 has a population localized in the left ring. Consequently, the dipole moment of the state increases more than those of the ground and the $2^1A'$ states, as shown in Table 2. This increase in the solute dipole causes dielectric stabilization of the solvent. In HOMO-1, there is little amplitude in the N14 and O16 atoms, which are supposed to be the hydrogen bond acceptors. Since negative charges on the N14 and O16 atoms increase upon excitation, direct hydrogen bonds contribute to the red shift of the excitation energy. In the excited states of LF, direct hydrogen bonds and dielectric polarization of solution contribute equally to the total solvatochromic shift. Therefore, both the explicit solvating molecules and PCM are necessary to quantitatively describe the solvation effect of water. If we only use PCM (“P” in Table 3), the result for the π-π* state is very close to that for the W+ P model. In the PCM model, charges relevant to the electron density of the solute are generated on the surface of the cavity[18]. These surface charges might help the PCM to describe the microscopic solvation effect. However, this P model gives deviations of 0.10 and 0.07 eV in the n-π* states.

Conclusion

The excited states of LF were studied by the SAC-CI method. Considering the solvation effect on the absorption peaks, we obtained theoretical assignment for the experimental absorption peaks below 5 eV. Transition energies of two n-π* states were calculated at 3.3 and 4.1 eV. The molecular structures of the first singlet and triplet excited states were optimized using the SAC-CI method. The structural changes observed upon transitions were at most 0.05 Å. The solvation effect on the absorption energy was investigated by PCM and by including explicit water molecules. The characteristic solvatochromism observed for the second π-π* transition was analyzed. Both direct hydrogen bonding and dielectric polarization effects are responsible for the red shift in the 3^1A' state. Both effects were equally important in all the states investigated. If the solvation effect is described only by the PCM (P model), the absorption energies calculated for π-π* states were very close to those obtained with the PCM plus explicit water molecules model (the W+ P model). However, in the case of the n-π* states, the results were overestimated by 0.07-0.10 eV. This indicates that the results would be more reliable to include hydrogen bonding effect in addition to the PCM.

References

[1] D. Voet, J. Voet, Biochemistry, 2nd ed., John Wiley & Sons, New York, **1995**.

[2] M. Sun, P.S. Song, *Biochemistry 12*, **1973**, 4663.

[3] T. Climent, R. Gonzalez-Luque, M. Merchan, L. Serrano-Andres, *J. Phys. Chem. A 110* , **2006**, 13584.

[4] A.M. Edwards, C. Bueno, A. Saldano, E. Silva, K. Kasssab, L. Polo, G. Jori, *J. Photochem. Photobiol. 48* ,**1999**, 36.

[5] M. Meyer, H. Hartwig, D. Schomburg, *J. Mol. Struct. (THEOCHEM) 364*, **1996**, 139.

[6] C. Neiss, P. Saalfrank, M. Parac, S. Grimme, *J. Phys. Chem. A 107* ,**2003**, 140.

[7] M. Sikorski, E. Sikorska, A. Koziolowa, R.G. Moreno, J.L. Bourdelande, R.P. Steer, F.J. Wilkison, *Photochem. Photobiol. B: Biol. 60*, **2001**, 114.

[8] E. Sikorska, I.V. Khmelinskii, W. Prukala, S.L. Williams, M. Patel, D.R. Worrall, J. K. Bourdelande, J. Koput, M. Sikiorski, *J. Phys. Chem. A 108* ,**2004**, 1501.

[9] E. Sikorska, I. Khemelinskii, J. Koput, M. Sikorski, *J. Mol. Struct. (THEOCHEM) 155* **2004**.

[10] E. Sikorska, I. Khemelinskii, A. Komasa, J. Koput, L. F. V. Ferreira, J. R. Herance, J. L. Bourdelande, S.L.Williams, D. R.Worrall, M. Insinska-Rak, M. Sikorski, *Chem. Phys. 314*, **2005**, 239.

[11] E. Sikorska, J. R. Herance, J. L. Bourdelande, I. V. Khmelinskii, S. L Williams, D. R. Worrall, G. Nowacka, A. Komosa, M. Sikiorski, *J. Photochem. Photobiol. A: Chem. 170*, **2005**, 267.

[12] H. Nakatsuji, K. Hirao, *J. Chem. Phys. 68* ,**1978**, 2053.

[13] H. Nakatsuji, *Chem. Phys. Lett. 59* ,**1978**, 362.

[14] H. Nakatsuji, *Chem. Phys. Lett. 67* ,**1979**, 329.

[15] H. Nakatsuji, *Chem. Phys. Lett. 67*, **1979,** 334.

[16] H. Nakatsuji, in: J. Leszczynski (Ed.), Computational Chemistry−Reviews of Current Trends, vol. 2, World Scientific, Singapore, **1997**, p. 62.

[17] M. Ehara, J. Hasegawa, H. Nakatsuji, in: C. Dykstra, G. Frenking, K. Kim, G. Scuseria (Eds.), Theory and Applications of Computational Chemistry: The First Forty Years, Elsevier Science, **2005**.

[18] J. Tomasi, M. Persico, *Chem. Rev. 94* **1994**.

[19] J. Tomasi, R. Cammi, B. Mennucci, *Int. J. Quant. Chem. 75* ,**1999**, 783.

[20] V. Barone, M. Cossi, J. Tomasi, *J. Comp. Chem. 19*, **1998**, 404.

[21] P. Hohenberg, W. Kohn, *Phys. Rev. 136*, **1964**, B864.

[22] W. Kohn, L. J. Sham, *Phys. Rev. 140* ,**1965**, A1133.

[23] R.G. Parr, W. Yang, Density-Functional Theory of Atoms and Molecules, Oxford Univ. Press, Oxford, **1989.**

[24] C. Lee, W. Yang, R.G. Parr, *Phys. Rev. B,37,***1988** 785.

[25] A.D. Becke, *J. Chem. Phys. 98,* **193**,5648.

[26] J. Rodrıguez-Otero, M.-N.E.A. Pena-Gallego, S. A.Vazquez, *J. Org. Chem. 67*, **2002**, 6347.

[27] W. J. Hehre, R. Ditchfield, J. A. Pople, *J. Chem. Phys. 56*, **1972**, 2257.

[28] P. C. Hariharan, J. A. Pople, *Theor. Chim. Acta 28* **1973**), 213.

[29] T. H. Dunning JR, P. J. Hay, H. F. Schaefer, Methods of Electronic Structure Theory, Prenum Press, New York, **1977**.

[30] H. Nakatsuji, *Chem. Phys. 75*, **1983,** 425.

[31] M. J. Frisch, G.W. Trucks, H. B. Schlegel, G.E. Scuseria, M. A. Robb, J. R. Cheeseman, J. J. A. Montgomery, T. Vreven, K. N. Kudin, J. C. Burant, J. M. Millam, S. S. Iyengar, J. Tomasi, V. Barone, B. Mennucci, M. Cossi, G. Scalmani, N. Rega, G. A. Petersson, H. Nakatsuji, M. Hada, M. Ehara, K. Toyota, R. Fukuda, J. Hasegawa, M. Ishida, T. Nakajima, Y. Honda, O. Kitao, H. Nakai, M. Klene, X. Li, J. E. Knox, H. P. Hratchian, J. B. Cross, C. Adamo, J. Jaramillo, R. Gomperts, R.E. Stratmann, O. Yazyev, A. J. Austin, R. Cammi, C. Pomelli, J. W. Ochterski, P. Y. Ayala, K. Morokuma, G. A. Voth, P. Salvador, J. J. Dannenberg, V. G. Zakrzewski, S. Dapprich, A. D. Daniels, M. C. Strain, O. Farkas, D. K. Malick, A. D. Rabuck, K. Raghavachari, J. B. Foresman, J. V. Ortiz, Q. Cui, A.G. Baboul, S. Clifford, J. Cioslowski, B B. Stefanov, G. Liu, A. Liashenko, P. Piskorz, I. Komaromi, R. L. Martin, D. J. Fox, T. Keith, M. A. Al-Laham, C. Y. Peng, A. Nanayakkara, M. Challacombe, P. M. W. Gill, B. Johnson,W. Chen, M. W. Wong, C. Gonzalez, J. A. Pople, Gaussian Development Version, Revision B. 04., Gaussian, Inc., Pittsburgh, PA, **2003**.

[32] W. A. Eaton, J. Hofrichter, M. W. Makinen, R.D. Andersen, M. L. Ludwig, *Biochemistry 14*, **1975**, 2146.

[33] L. B. A. Johansson, A. Davidsson, G. Lindblom, K. R. Naqvi, *Biochemistry 18*, **1979**, 4249.

[34] F. Maseras, K. Morokuma, *J. Comp. Chem. 16* **1995**, 1170.

[35] K. Morokuma, *Acc. Chem. Res. 10*, **1977**, 294.

List of Publications

Chapter 1

One-Dimensional Imidazole Aggregate in Aluminum Porous Coordination Polymers with High Proton Conductivity
Sareeya Bureekaew, Satoshi Horike, Masakazu Higuchi, Motohiro Mizuno, Takashi Kawamura, Daisuke Tanaka, Nobuhiro Yanai, Susumu Kitagawa
Nat. Mater. **2009**, *in press.*

Chapter 2

Control of Interpenetration for Tuning Structural Dynamics Impacted on Sorption Property.
Sareeya Bureekaew, Hiroshi Sato, Ryotaro Matsuda, Yoshiki Kubota, Jungeun Kim, Masaki Takata, Susumu Kitagawa
Angew. Chem. Int. Ed. submitted.

Chapter 3

A Dynamic Isocyanurate-Functionalized Porous Coordination Polymer
Sujit K. Ghosh, Sareeya Bureekaew, Susumu Kitagawa
Angew. Chem. Int. Ed. **2008**, *47*, 3403.

Chapter 4

Thermal Conductivity of Porous Coordination Polymers
Sareeya Bureekaew, Satoshi Horike, Susumu Kitagawa
in preparation.

Chapter 5

SAC-CI Theoretical Study on the Excited States of Lumiflavin: Structure, Excitation Spectrum, and Solvation Effect
Jun-ya Hasegawa, Sareeya Bureekaew and Hiroshi Nakatsuji
J. Photochem. and Photobio. A: Chem. **2007**, *189*, 205.

Other Publications

Electronic Circular Dichroism Spectrum of Uridine Studied by the SAC-CI Method
Sareeya Bureekaew, Jun-ya Hasegawa and Hiroshi Nakatsuji
Chem. Phys. Lett., **2006**, *425*, 367.

Coordination Pillared-layer Type Compounds Having Pore Surface Functionalization by Anionic Sulfonate Groups
Satoshi Horike, Sareeya Bureekaew and Susumu Kitagawa
Chem. Commun., **2008**, *8*, 471.

A Porous Coordination Polymer with Accessible Metal Site and Its Complementary Coordination Action
Hirotoshi Sakamoto, Ryotaro Matsuda, Sareeya Bureekaew, Daisuke Tanaka, Susumu Kitagawa
Chem. -Eur. J. **2009**, *15*, 4985.